Constraining modified gravitational wave propagation with the black hole mass gap

by

Edwin Genoud-Prachex

Thesis

submitted in partial fulfillment
of the requirements for the degree of
Master of Science in Physics

at the
University of Geneva
July 2021

Under the supervision of:

Prof. Michele Maggiore
and
Dr Michele Mancarella

UNIVERSITÉ
DE GENÈVE

FACULTY OF SCIENCE
Department of Theoretical Physics

Contents

Preface

This thesis was written to complete a Master in Physics at the University of Geneva. I worked on this project from September 2020 to July 2021, that contributes to ref. [1].

This master's project was my first real experience with research in physics. I discovered a really exciting and fascinating domain that I enjoy a lot. Physics is amazing and I hope I will have the possibility to pursue my studies as far as possible.

I would like to thank several people without whom this year and my studies of physics in Geneva would have been very different. Of course it is hard to quote everyone and so this list is not exhaustive! First of all, I thank my supervisors, Prof. Michele Maggiore who enthusiastically proposed me this wonderful topic of research and who always answered my questions, and also Dr Michele Mancarella, who explained me the topic, methods and who answered many questions. I also acknowledge Michele's and Michele's proofreading and comments of the present thesis. However any remaining mistake is mine.

I also want to thank my mother, Dominique, and my sister, Maëliss, for their great support and time. This year would have been highly different without my fellow students and friends, especially Sergio Ricossa, Louis-Philippe Ghanadian and Jonathan Pham. Also big thanks to Camille Criado.

Edwin Genoud-Prachex,
Genève, 12 July 2021
edwin.genoud-prachex@protonmail.ch

Abstract

Gravitational waves emitted by a compact binary give a direct measurement of the gravitational wave luminosity distance $d_{\mathrm{L}}^{\mathrm{GW}}$ between the source and the observer. This property is the reason why coalescing black holes at a cosmological distance are called *standard sirens*. If the redshift z of the binary is also known, the standard siren gives a test of cosmology.

In this work, we explore the possibility to statistically estimate redshifts of gravitational waves sources using the cosmological redshift of masses: $m^z = m^0(1+z)$, where m^z is the source mass in the detector-frame and m^0 the source mass in the source-frame, and using the source-frame mass population of binary black holes.

We test the possibility to constrain the values of cosmological parameters such as H_0 and $\Omega_{\mathrm{m},0}$ using only detections of gravitational waves and we also test the possibility to measure modified gravitational waves propagation by constraining the values of the (Ξ_0, n) parametrisation of the ratio $d_{\mathrm{L}}^{\mathrm{GW}}/d_{\mathrm{L}}^{\mathrm{EM}} = \Xi_0 + (1-\Xi_0)/(1+z)^n$ [$d_{\mathrm{L}}^{\mathrm{EM}}$ being the electromagnetic luminosity distance].

Data is analysed by applying Bayesian hierarchical inference and using a Markov chain Monte Carlo method.

This method is working: on mock data that simulates 5 years of advLIGO observation, we are able to constrain the value of Ξ_0 at $\sim 30\%$. By analysing the BBHs detections of catalogs GWTC-1 and GWTC-2 we obtain $\Xi_0 = 0.66^{+1.20}_{-0.42}$, and if we neglect GW190521, we obtain $\Xi_0 = 1.93^{+4.44}_{-1.43}$ (both values at 68% C.L. for a flat prior on $(0.1, 10)$). The value without GW190521 is in accordance with previous results and in particular is compatible with GR ($\Xi_0 = 1$) and with the largest prediction by available cosmological model ($\Xi_0 \approx 1.8$).

Keywords: Standard sirens – Black hole mass gap – Modified gravity – Modified gravitational waves propagation – Bayesian hierarchical inference – MCMC.

Introduction

Gravitational waves provide an amazing possibility to test physical theories. Since the first detection of a gravitational wave (GW) in September 2015 [2], more than fifty other events have been detected [3, 4]. A famous example of test of cosmology by using GWs is given by the constraint on the value of the Hubble constant using the events GW170817 (a gravitational wave observation) and GRB 170817A (a gamma-ray burst) [5]. GW170817 was caused by two neutron stars (NS) of $1.46^{+0.12}_{-0.10}$ $\mathrm{M}_\odot$ and 1.27 ± 0.09 $\mathrm{M}_\odot$ that merged at 40^{+7}_{-15} Mpc from us [3]. The gamma-ray burst GRB 170817A was the electromagnetic (EM) counterpart of this gravitational wave [6]. From the amplitude of the GW, it is possible to measure the luminosity distance d_L between the source and the observer, while the cosmological redshift, z, is measurable from the electromagnetic counterpart. At nearby distance, the Hubble constant is given by:

$$H_0 = \frac{cz}{d_\mathrm{L}},$$

and for GW170817 and GRB 170817A used together, one gets: $H_0 = 70.0^{+12.0}_{-8.0}$ km s^{-1} Mpc^{-1} [5].

The credible intervals on this value are large (*i.e.* the accuracy on the measurement is pretty bad), but that measurement was done on a single observation. With the next generation of GW detectors, expected in the mid-2030s, there will have $\mathcal{O}(10^2)$ NS–NS GWs with EM counterpart detections over a few years of observation [7]. The accuracy of the measurement of the Hubble constant by using GWs are going to be quickly improved. In a short term it could become precise enough to decide in the Hubble tension between standard candles and CMB measurements.
In analogy with the standard candle, merging compact binaries are called *standard sirens*.

In addition to the measurement of H_0, standard sirens can be used to test modified GW propagation and consequently modified gravity theories. In general relativity (GR), the distance that is measured from GWs, d_L^GW, (the *gravitational wave luminosity distance*) is equal to the classical definition of the luminosity distance d_L^EM (see *e.g.* ref. [8]). However in modified gravity theories, these two distances can be different (see *e.g.* ref. [9]). The ratio between these distances is parametrisable as [9]:

$$\frac{d_\mathrm{L}^\mathrm{GW}}{d_\mathrm{L}^\mathrm{EM}} = \Xi_0 + \frac{1-\Xi_0}{(1+z)^n}$$

where Ξ_0 is the most important parameter, since n gives the shape of the ratio while Ξ_0 gives its maximal amplitude. Since GR predicts $d_\mathrm{L}^\mathrm{GW} = d_\mathrm{L}^\mathrm{EM}$, it predicts $\Xi_0 = 1$.

When a GW does not have any EM counterpart, it is impossible to measure the redshift of its source and it is called a *dark siren*. However there exist a few techniques to statistically estimate the redshift. A first technique consists in using a galaxy catalog (that gives the redshift of the galaxies) and correlate the origin of the GW with a galaxy in the catalog. This technique was used *e.g.* in ref. [10]. Another technique uses the cosmological redshift of the masses to estimate the redshift of the GW source [11]. In other words, the detected mass is not the source-frame mass m^0 but rather the detector-frame mass $m^z = m^0(1+z)$. By using the mass population of binary black holes, we can statistically estimate the redshifts of GW sources. This method was used *e.g.* in refs [11, 12], and it is this second method we use in this master's project.

The statistical analyses are performed by using the framework of Bayesian probability and more especially Bayesian hierarchical inference, the calculations being made with a Markov chain Monte Carlo method.

This thesis is composed of three chapters. In chapter 1, we start from GR and show how it predicts GWs, how they can be created by astrophysical binaries and how we detect them with ground-based interferometers. We then recall some basics of cosmology and in particular the ΛCDM and wCDM models. It is then possible to look at propagation of GWs in an expanding Friedmann–Lemaître–Robertson–Walker Universe and how standard sirens work. We then dedicate a section to the introduction of modified gravity theories and modified GWs propagation. The chapter ends with a review of binary black holes mass populations.

In chapter 2, we first introduce Bayesian interpretation of probability, that is necessary to perform Bayesian inference. More precisely, we are interested in performing *hierarchical Bayesian inference with a selection bias* [13], a method introduced just after an example of Bayesian inference to better understand it. At the end of the chapter, we explain in details the specific inference we use in order to constrain modified gravitational waves propagation with the black hole mass gap.

Chapter 3 presents the main results we obtain by applying our method, first on mock data and then on the real GW data of advLIGO and advVirgo [3, 4].

The thesis ends with two appendices: in appendix A we present the working of Markov chain Monte Carlo methods and in particular the algorithm we use. Appendix B gives more information on the selection bias of the GWs detections.

Chapter 1

Theory

Contents

In the present chapter, we first present *some* properties of *Gravitational Waves* (GWs), especially the properties we are interested in for this master's project. Then there is a short introduction to cosmology and to the cosmological models we use. After a small presentation of standard sirens, we discuss some modified gravity theories and particularly modified gravitational wave propagation. The chapter ends with a presentation of the binary black holes population models we use.

1.1 Basics of Gravitational waves

The existence of gravitational waves is one of the main consequences of the theory of General Relativity. One can find an introduction (and more) to gravitational-wave physics in number of textbooks or lecture notes about gravitation, *e.g.* refs [14–20]. Refs [8, 21] are focused more especially on gravitational waves, and we mostly use them for this section.

1.1.1 How General Relativity predicts gravitational waves

Gravitational waves can emerge in GR with different approaches. Here we expose the most straightforward way to find GWs, using *linearized theory* (one expands the GR metric g around the flat Minkowski metric $\boldsymbol{\eta}$). But exact gravitational wave solutions are possible (see *e.g.* ref. [19], sect. 2.4), and a field-theoretical approach to GWs is also possible (see *e.g.* ref. [8], chap. 2).

If the metric is (at least locally) nearly flat, one can expand it at the first order:

$$g_{\mu\nu} = \eta_{\mu\nu} + h_{\mu\nu} \quad \text{with } h_{\mu\nu} = h_{\nu\mu} \text{ and } |h_{\mu\nu}| \ll 1, \tag{1.1}$$

where $\eta_{\mu\nu}$ is the Minkowski spacetime metric and where $h_{\mu\nu}$ is the (first order) perturbation: for example in the Solar System (the Sun being approximately the total mass), we have $|h_{\mu\nu}| \sim |\phi|/c^2 \lesssim (G\ \mathrm{M}_\odot)/(c^2\ \mathrm{R}_\odot) \sim 10^{-6}$ [14].

The goal is now to compute the Einstein's equations (with $c = 1$):

$$G_{\mu\nu} \equiv R_{\mu\nu} - \frac{1}{2} g_{\mu\nu} R = 8\pi G\ T_{\mu\nu}, \tag{1.2}$$

with the metric of eq. (1.1). Since h is small, we can write the Ricci tensor as:

$$R_{\mu\nu} = \partial_\lambda \Gamma^\lambda{}_{\mu\nu} - \partial_\nu \Gamma^\lambda{}_{\lambda\mu} + \mathcal{O}(hh), \tag{1.3}$$

where the Christoffel symbols are linearized:

$$\Gamma^\alpha{}_{\mu\nu} = \frac{1}{2} \eta^{\alpha\beta} \left(\partial_\nu h_{\nu\beta} + \partial_\mu h_{\beta\nu} - \partial_\beta h_{\nu\mu} \right). \tag{1.4}$$

(We raise or lower the indices with the flat metric $\boldsymbol{\eta}$. It is as if $h_{\mu\nu}$ were a tensorial field on the flat Minkowski spacetime.) In eq. (1.3), we can neglect terms of order h^2: for example, in the Solar System $h^2 \sim 10^{-12} \ll h$. The Ricci tensor (eq. (1.3)) is then:

$$R_{\mu\nu} = \frac{1}{2} \left(h^\lambda{}_{\mu,\lambda\nu} - \Box h_{\mu\nu} - h^\lambda{}_{\lambda,\mu\nu} + h^\lambda{}_{\nu,\lambda\mu} \right), \tag{1.5}$$

and the Ricci scalar is:

$$R = h^{\lambda\sigma}{}_{,\lambda\sigma} - \Box h, \tag{1.6}$$

where h is the trace of the perturbation: $h \equiv h^\nu{}_\nu = \eta^{\mu\nu} h_{\mu\nu}$, $\Box$ is the flat space d'Alembertian operator: $\Box \equiv \partial_\mu \partial^\mu = \eta_{\mu\nu} \partial^\mu \partial^\nu$, and the comma indicates a partial derivative ∂.

At this approximation, the Einstein's equations (eq. (1.2)) give the *linearized field equations*:

$$\Box h_{\mu\nu} + h_{,\mu\nu} - h^{\lambda}{}_{\mu,\lambda\nu} - h^{\lambda}{}_{\nu,\lambda\mu} - \eta_{\mu\nu}\Box h + \eta_{\mu\nu}h^{\lambda\sigma}{}_{,\lambda\sigma} = -16\pi G T_{\mu\nu}. \tag{1.7}$$

To obtain a shorter expression, we define the *trace reversed perturbation* as:

$$\bar{h}_{\mu\nu} = h_{\mu\nu} - \frac{1}{2}\eta_{\mu\nu}h, \tag{1.8}$$

($\bar{h}_{\mu\nu}$ is also often written $\gamma_{\mu\nu}$ or $H_{\mu\nu}$) and eq. (1.7) becomes:

$$\Box\bar{h}_{\mu\nu} + \eta_{\mu\nu}\bar{h}_{\rho\sigma}{}^{,\rho\sigma} - \bar{h}_{\mu\rho,\nu}{}^{,\rho} - \bar{h}_{\nu\rho,\mu}{}^{,\rho} = -16\pi G T_{\mu\nu}, \tag{1.9}$$

this equation is still complicated but it can be simplified by a gauge transformation.

Let us consider an infinitesimal coordinate transformation:

$$x'^{\alpha} \equiv x^{\alpha} + \xi^{\alpha}, \quad \text{where } \xi^{\alpha} = \xi^{\alpha}(t, \boldsymbol{x}) \text{ and } |\xi^{\alpha}| \ll 1, \tag{1.10}$$

that induces:

$$g_{\mu\nu}(x) = \frac{\partial x'^{\sigma}}{\partial x^{\mu}}\frac{\partial x'^{\rho}}{\partial x^{\nu}}\, g'_{\sigma\rho}(x') \tag{1.11}$$

$$= g'_{\mu\nu}(x') + g'_{\sigma\nu}(x')\,\xi^{\sigma}{}_{,\mu} + g'_{\mu\sigma}(x')\,\xi^{\sigma}{}_{,\nu}, \tag{1.12}$$

and at first order in ξ^{α} and $h_{\mu\nu}$, one gets:

$$h'_{\mu\nu}(x') = h_{\mu\nu}(x) - \xi_{\mu,\nu} - \xi_{\nu,\mu} \tag{1.13}$$

$$\Rightarrow \bar{h}'_{\mu\nu} = \bar{h}_{\mu\nu} - \xi_{\mu,\nu} - \xi_{\nu,\mu} + \eta_{\mu\nu}\xi^{\rho}{}_{,\rho}. \tag{1.14}$$

Such a coordinate transformation lets the Riemann tensor invariant (at the order we are interested in):

$$R'_{\alpha\beta\mu\nu} = R_{\alpha\beta\mu\nu}, \tag{1.15}$$

then, if $h_{\mu\nu}$ satisfies the Einstein's equations (eq. (1.2)) then also does $h'_{\mu\nu}$. If we know a small (trace reversed) perturbation $h_{\mu\nu}$ ($\bar{h}_{\mu\nu}$) that is solution of the Einstein's equations, then we can transform it in a small (trace reversed) perturbation $h'_{\mu\nu}$ ($\bar{h}'_{\mu\nu}$) that also satisfies the Einstein's equations. In particular, we can choose $\bar{h}_{\mu\nu}$ satisfying the *Lorenz gauge* (also called *Hilbert gauge* or *harmonic gauge*):

$$\partial^{\nu}\bar{h}_{\mu\nu} = 0. \tag{1.16}$$

In this gauge, the three last terms of equation (1.9) vanish, and we get:

$$\Box\bar{h}_{\mu\nu} = -16\pi G T_{\mu\nu}. \tag{1.17}$$

Since the d'Alembertian operator is invertible, eq. (1.17) always admits a solution. Its retarded solution being:

$$\bar{h}_{\mu\nu} = 4G\int\frac{T_{\mu\nu}(x^0 - |\boldsymbol{x}-\boldsymbol{x}'|, \boldsymbol{x}')}{|\boldsymbol{x}-\boldsymbol{x}'|}\,\mathrm{d}^3x'. \tag{1.18}$$

If we are in vacuum (so outside the source, where $T_{\mu\nu} = 0$), eq. (1.17) becomes:

$$\Box\bar{h}_{\mu\nu} = 0, \tag{1.19}$$

so we have plane waves solutions, with the ansatz:

$$\bar{h}_{\mu\nu} = \varepsilon_{\mu\nu} \cos(k_\alpha x^\alpha). \tag{1.20}$$

The trace reversed perturbation $\bar{h}_{\mu\nu}$ is then a plane wave with undulations in the plane perpendicular to the propagation direction $\boldsymbol{k}$, with a velocity $v = \omega/k$. The Einstein's equations imply $k^2 = 0$, then $v = 1$ (remember we use units with $c = 1$). Thus gravitational waves propagate with the velocity of light. The matrix $\varepsilon_{\mu\nu}$ is called the *polarisation tensor*. By symmetry $\bar{h}_{\mu\nu}$ has ten independent components. By imposing the Lorenz gauge (eq. (1.16)), it has six degrees of freedom left.

Let us now consider another coordinates transformation $x^\mu \mapsto x'^\mu = x^\mu + \xi^\mu$, with $\Box \xi_\mu = 0$, then

$$\Box \left(\xi_{\mu,\nu} + \xi_{\nu,\mu} - \eta_{\mu\nu} \xi^\rho{}_{,\rho} \right) = 0. \tag{1.21}$$

From eq. (1.14), we see that to the six independent components of $\bar{h}_{\mu\nu}$ we can impose four conditions by choosing carefully the four functions ξ^μ. In particular, one can choose ξ^0 such that the trace $\bar{h}^\sigma{}_\sigma$ vanishes. One then has: $\bar{h}_{\mu\nu} = h_{\mu\nu}$, thus the metric perturbation $h_{\mu\nu}$ and the trace reversed perturbation $\bar{h}_{\mu\nu}$ (that follows the wave equation) are the same. The three other functions ξ^i can be chosen such that $h^{0i} = 0$.

Since $h_{\mu\nu} = \bar{h}_{\mu\nu}$, the Lorenz gauge eq. (1.16), for $\nu = 0$ is:

$$\partial^0 h_{00} + \partial^0 h_{0i} = 0 \tag{1.22}$$

$$\Rightarrow \partial^0 h_{00} = 0, \tag{1.23}$$

where the second equation comes from the gauge choice $h^{0i} = 0$. A time-independent h_{00} corresponds to the Newtonian potential of the source that generated the wave. Therefore if the potential does not vary in time as the wave propagates, it means that it is zero. Hence $h_{00} = 0$.

To summarise, we have a gauge in which:

$$h^{0\mu} = 0 \quad \text{(transverse)}, \tag{1.24}$$

$$h^i{}_i = 0 \quad \text{(traceless)}. \tag{1.25}$$

This gauge is then called the *transverse-traceless gauge* (or TT gauge) and we denote a metric perturbation in the TT gauge by $h^{\mathrm{TT}}_{\mu\nu}$.

Let us use a plane wave that propagates in the $\hat{z}$-direction as standard example. We then have: $k_\sigma = (-\omega, 0, 0, \omega)$. With the TT and Lorenz gauges we have that $\varepsilon_{t\mu} = \varepsilon_{z\nu} = 0$ and $\varepsilon_{xx} = -\varepsilon_{yy}$. The only non-vanishing components are then:

$$\varepsilon_{xy} = \varepsilon_{yx} \equiv \varepsilon_\times \tag{1.26}$$

$$\varepsilon_{xx} = -\varepsilon_{yy} \equiv \varepsilon_+. \tag{1.27}$$

Thus, in the TT gauge, a plane gravitational wave is the linear combination of two types of solutions:

$$\varepsilon_{\mu\nu} = \varepsilon_+ \begin{pmatrix} 0 & 0 & 0 & 0 \\ 0 & 1 & 0 & 0 \\ 0 & 0 & -1 & 0 \\ 0 & 0 & 0 & 0 \end{pmatrix} + \varepsilon_\times \begin{pmatrix} 0 & 0 & 0 & 0 \\ 0 & 0 & 1 & 0 \\ 0 & 1 & 0 & 0 \\ 0 & 0 & 0 & 0 \end{pmatrix}, \tag{1.28}$$

and the perturbation is:

$$h_{ij}^{\mathrm{TT}}(t,z) = \begin{pmatrix} h_+ & h_\times & 0 \\ h_\times & -h_+ & 0 \\ 0 & 0 & 0 \end{pmatrix}_{ij}, \tag{1.29}$$

also written:

$$h_{ab}^{\mathrm{TT}}(t,z) = \begin{pmatrix} h_+ & h_\times \\ h_\times & -h_+ \end{pmatrix}_{ab}, \tag{1.30}$$

where $a, b = 1, 2$ are indices in the transverse (x, y) plane and where $h_{+,\times} = \varepsilon_{+,\times} \cos(k_\alpha x^\alpha)$. The tensors ε_+ and $\varepsilon_\times$ are respectively called the "plus" and "cross" polarisations of the GW.

1.1.2 Generation of gravitational waves from a binary system

In this subsection we discuss some results about generation of gravitational waves by a binary system of massive compact objects. The equations we present (and many more) are proved in ref. [8], chapters 3 & 4.

Two bodies in gravitational interaction emit gravitational waves. This process is highly non linear: the dynamics of the binary system is described by GR (which is itself non linear), the system emits GWs, then the waves have a back-reaction on the system, etc. The general technique is to use a multipolar expansion of the mass distribution of the system (and also of its spin distribution).

We only consider here the easiest case where the velocity of the bodies is small: $(v/c) \ll 1$. This approximation is not always good: just before the coalescence of two black holes, their radial velocity is $v/c \sim 0.6$ (see *e.g.* ref. [2] and particularly their fig. 2, that is reproduced in fig. 1.1 below), so one needs to take into account higher order terms. In this first approximation, the amplitude of GWs is given by the change of the mass quadrupole moment (hence $l = m = 2$ in a multipole expansion) and has order $(v/c)^2$. When the expansion is stopped after the v^2 term, we get the *Post Newtonian approximation* (1PN) and the cut after the v^n term gives the $(n/2)$PN approximation. At higher order, higher mass multipole moments and spins have effects. The (highly complicated, but amazing) multipolar expansion using the Blanchet–Damour approach is explained in the lectures ref. [22] (by Thibault Damour himself) and in chapter 5 of ref. [8].

On the historical aspect, the 1PN approximation is known from the beginning of GWs (by Einstein, Lorentz and others), while the 2PN approximation dates from the early 1980s and the 4PN from 2014 [22]. Since ∼2005, numerical relativity (NR) is also another possibility to compute h. In practice multiple techniques are used to compute precise waveforms. To have a precise template of the GW, in general, the amplitude of the wave can be computed at 1PN, while its phase is computed at much higher order (see last paragraph of the present subsection). Let us see the main equations of the 1PN approximation, keeping c explicit.

We saw in eq. (1.18) that GWs always admit a solution that is a function of the stress-energy tensor $T_{\mu\nu}$. If we are far away from the source, we can take the approximations:

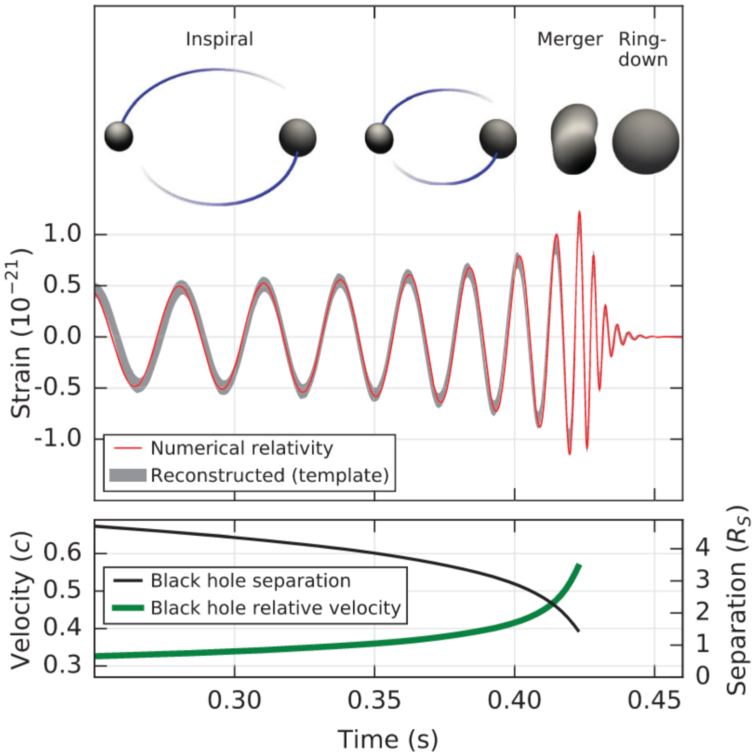

Figure 1.1: Top: *Estimated gravitational-wave strain amplitude from GW150914 projected onto H1. This shows the full bandwidth of the waveforms, without the filtering. The inset images show numerical relativity models of the black hole horizons as the black holes coalesce.* Bottom: *The Keplerian effective black hole separation in units of Schwarzschild radii ($R_S = 2GM/c^2$) and the effective relative velocity given by the post-Newtonian parameter $v = (GM\pi f/c^3)^{1/3}$, where f is the gravitational-wave frequency calculated with numerical relativity and M is the total mass. This figure (and its caption) is fig. 2 of Abbott* et al.*, ref. [2].*

$$|\boldsymbol{x}| \approx r, \tag{1.31}$$

$$t - |\boldsymbol{x} - \boldsymbol{x}'| \approx t - \frac{r}{c} + \frac{\boldsymbol{x} \cdot \hat{\boldsymbol{x}}}{c}, \tag{1.32}$$

where $\hat{\boldsymbol{x}}$ is the unit vector $\boldsymbol{x}/|\boldsymbol{x}|$. The metric perturbation h_{ij}^{TT} can be rewritten as:

$$h_{ij}^{\mathrm{TT}} = \frac{1}{r}\frac{4G}{c^4}\Lambda_{ij,kl}(\hat{\boldsymbol{x}}) \int T_{kl}\left(t - \frac{r}{c} + \frac{\boldsymbol{x} \cdot \hat{\boldsymbol{x}}}{c}, \hat{\boldsymbol{x}}\right)\,\mathrm{d}^3x', \tag{1.33}$$

where the projection operator $\Lambda_{ij,kl}$ is defined as:

$$\Lambda_{ij,kl}(\hat{\boldsymbol{x}}) = P_{ik}P_{jl} - \frac{1}{2}P_{ij}P_{kl} \tag{1.34}$$

$$\text{with } P_{ij}(\hat{\boldsymbol{x}}) = \delta_{ij} - x_i x_j. \tag{1.35}$$

With some work (see *e.g.* ref. [8], chap. 3), one can find that:

$$h_{ij}^{\mathrm{TT}}(t, \boldsymbol{x}) = \frac{1}{r}\,\frac{4G}{c^4}\Lambda_{ij,kl}(\hat{\boldsymbol{x}}) \times \left[S^{kl} + \frac{1}{c}x_m\dot{S}^{kl,m} + \frac{1}{2c^2}x_m x_p \ddot{S}^{kl,mp} + \cdots\right], \tag{1.36}$$

where:

$$S^{ij}(t) = \int T^{ij}(t, \boldsymbol{x})\ \mathrm{d}^3x \tag{1.37}$$

$$S^{ij,k}(t) = \int T^{ij}(t, \boldsymbol{x})\ x^k\ \mathrm{d}^3x \tag{1.38}$$

$$S^{ij,kl}(t) = \int T^{ij}(t, \boldsymbol{x})\ x^k x^l\ \mathrm{d}^3x \tag{1.39}$$

$$\vdots$$

and we define $M = S^{00}$, $M^i = S^{00,i}$, $M^{ij} = S^{00,ij}$, etc. Let us note that M is the ADM mass (Richard Arnowitt, Stanley Deser and Charles W. Misner): the total mass measured by an observer at infinity, in an asymptotically flat spacetime. It is the definition of the mass we use in the equations below. The leading term in eq. (1.36) gives:

$$\left[h_{ij}^{\mathrm{TT}}(t, \boldsymbol{x})\right]_{\mathrm{quad}} = \frac{1}{r}\ \frac{2G}{c^4} \Lambda_{ij,kl}(\hat{\boldsymbol{x}}) \ddot{M}^{kl}\left(t - \frac{r}{c}\right). \tag{1.40}$$

The mass term $\ddot{M}^{kl}$ can always be decomposed in two irreducible representations:

$$M^{kl} = \left(M^{kl} - \frac{1}{3}\delta^{kl} M_{ii}\right) + \frac{1}{3}\delta^{kl} M_{ii} \tag{1.41}$$

$$\equiv Q^{kl} + \frac{1}{3}\delta^{kl} M_{ii}, \tag{1.42}$$

thus one gets:

$$\left[h_{ij}^{\mathrm{TT}}(t, \boldsymbol{x})\right]_{\mathrm{quad}} = \frac{1}{r}\ \frac{2G}{c^4} \Lambda_{ij,kl}(\hat{\boldsymbol{x}}) \ddot{Q}_{kl}(t - r/c) \tag{1.43}$$

$$\equiv \frac{1}{r}\ \frac{2G}{c^4} \ddot{Q}_{kl}^{\mathrm{TT}}(t - r/c). \tag{1.44}$$

The power radiated by the GW, per solid angle $\mathrm{d}\Omega$ is given by

$$\left(\frac{\mathrm{d}P}{\mathrm{d}\Omega}\right)_{\mathrm{quad}} = \frac{r^2 c^3}{32\pi G}\left\langle \dot{h}_{ij}^{\mathrm{TT}} \dot{h}_{ij}^{\mathrm{TT}} \right\rangle, \tag{1.45}$$

and the total radiated power (also called the total gravitational luminosity $\mathcal{L}$) of the source is:

$$P_{\mathrm{quad}} = \frac{G}{5c^5}\left\langle \dddot{Q}_{ij} \dddot{Q}_{ij} \right\rangle. \tag{1.46}$$

This is the famous *Einstein's quadrupole formula.*

Before using these formulae in an explicit example, let us have a few comments. In the wave form (see *e.g.* eqs (1.33) or (1.44)), we see that $h \propto 1/r$, where r is the distance between the source and the observer. This is a classical property of spherical waves' amplitudes, and we will use this property in the following (see sect. 1.4). At the first order, a GW is sourced by the change of the mass quadrupole. In analogy with other waves (such as electromagnetic (EM) waves) we could have guessed that a gravitational wave come from the time variation of a mass multipole. Indeed, EM waves come from the variation of an electric charge dipole and the equivalent of the electric charge in gravity is the mass, while the main multipole must be different from the EM case, because of the transformation of the field under an infinitesimal coordinate transformation (see eq. (1.13)) that is different in the case of gravity than in the case of electromagnetism. Last comment, the factor 1/5 in the Einstein's quadrupole formula, eq.

(1.46), comes from the fact that GWs have spin 2 ($2s+1=5$) [22].

Let us now apply the above equations in the simple case of a binary system in circular orbit, with masses m_1 and m_2 (we suppose w.l.o.g. $m_1 \geq m_2$). We define the total mass of the system: $M = m_1 + m_2$; the reduced mass: $\mu = m_1 m_2/(m_1+m_2)$; the mass ratio: $q = m_2/m_1$ and the *symmetric mass ratio*: $\eta = \nu = \mu/M = m_1 m_2/(m_1+m_2)^2$ from which we define the *chirp mass*:

$$M_{\mathrm{c}} = \mu^{3/5} M^{2/5} = \eta^{3/5} M = \frac{(m_1 m_2)^{3/5}}{(m_1+m_2)^{1/5}}. \tag{1.47}$$

The waveforms produced by such a binary system is given by (see eq. (4.3) of ref. [8]):

$$\begin{aligned} h_+(t) &= \frac{4}{r}\left(\frac{GM_{\mathrm{c}}}{c^2}\right)^{5/3}\left(\frac{\pi f_{\mathrm{GW}}}{c}\right)^{2/3}\frac{1+\cos^2\theta}{2}\cos\left(2\pi f_{\mathrm{GW}} t_{\mathrm{ret}} + 2\phi\right) \\ h_\times(t) &= \frac{4}{r}\left(\frac{GM_{\mathrm{c}}}{c^2}\right)^{5/3}\left(\frac{\pi f_{\mathrm{GW}}}{c}\right)^{2/3}\cos\theta\sin\left(2\pi f_{\mathrm{GW}} t_{\mathrm{ret}} + 2\phi\right), \end{aligned} \tag{1.48}$$

where we introduce the frequency of the gravitational wave f_{GW}, the retarded time t_{ret} and the coordinates (θ, ϕ) to go from the observer to the source-frame. The frequency of the GW in term of $\tau \equiv t - t_{\mathrm{coal}}$, *i.e.* the time before the coalescing time t_{coal}, is given by:

$$f_{\mathrm{GW}}(\tau) = \frac{1}{\pi}\left(\frac{5}{256}\frac{1}{\tau}\right)^{3/8}\left(\frac{GM_{\mathrm{c}}}{c^3}\right)^{-5/8}, \tag{1.49}$$

we have numerically:

$$f_{\mathrm{GW}}(\tau) \approx 134\ \mathrm{Hz}\ \left(\frac{1.21\ \mathrm{M}_\odot}{M_{\mathrm{c}}}\right)^{5/8}\left(\frac{1\ \mathrm{s}}{\tau}\right)^{3/8}. \tag{1.50}$$

In the case of an elliptic orbit with semi-major axis a and eccentricity e, the total radiated power is given (exactly) by (Philip Carl Peters and Jon Matthews, 1963):

$$P = \frac{32 G^4 \mu^2 M^3}{5 c^5 a^5}\ f(e), \tag{1.51}$$

with

$$f(e) = \frac{1}{(1-e^2)^{7/2}}\left(1 + \frac{73}{24}e^2 + \frac{37}{96}e^4\right). \tag{1.52}$$

And it is possible to express the change in time of the semi-major axis and of the eccentricity as differential equations:

$$\frac{\mathrm{d}a}{\mathrm{d}t} = -\frac{64}{5}\ \frac{G^3 \mu M^2}{c^5 a^3}\ f(e) \tag{1.53}$$

$$\frac{\mathrm{d}e}{\mathrm{d}t} = -\frac{304}{15}\ \frac{G^3 \mu M^2}{c^5 a^4}\ \frac{e}{(1-e^2)^{5/2}}\left(1 + \frac{121}{304}e^2\right), \tag{1.54}$$

despite the unusual coefficients, these equations are exact. The evolutions of the semi-major axis and of the eccentricity say that from any elliptic orbit, the GWs emission first circularise the orbit (the eccentricity goes to zero) then the orbit decreases in size, until the merger of the two bodies (remember that at the merger, the 1PN approximation we use here does not hold anymore). Equation (1.53) has already been checked to be exact long before the first detection of a GW (15 September 2015 [2]) by looking at the change on the orbital period of the binary pulsar PSR B1913+16, also known as “Hulse–Taylor binary” (see fig. 1.2).

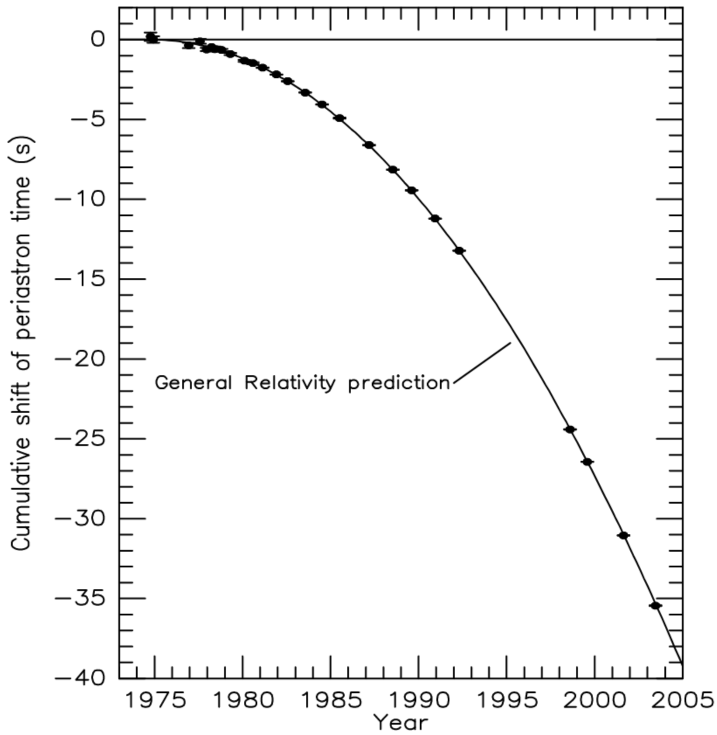

Figure 1.2: *Orbital decay of PSR B1913+16. The data points indicate the observed change in the epoch of periastron with date while the parabola illustrates the theoretically expected change in epoch for a system emitting gravitational radiation, according to general relativity (see eq. (1.53)). This figure (and the caption) is fig. 1 of Weisberg & Taylor, 2004, ref. [23].*

The change in the orbits can be understood in (at least) two ways: the orbit loses mechanical energy by emitting GWs, or since the GW has a finite velocity ($= c$), the information of the mass position takes a certain time to go from one body to the other, time during which the first body has moved, this delay continuously modifying the orbit.

What is the minimum accuracy that should be used to compute the waveforms? As we will see in subsection 1.1.3, very accurate waveforms are used in experiments to distinguish a GW signal from the noise background. This model of waveform has to be precise enough to match the real GW signal. For the amplitude of h, a very high precision is not needed, 1PN can be enough in a first approximation. But for the phase, it is different. The number of cycles $\mathcal{N}(f)$ that a wave of frequency f spent in the detector bandwidth can be written as (see subsection 5.6.1 of ref. [8] for the derivation):

$$\mathcal{N}(f) \equiv \frac{1}{32\pi^{8/3}} \left(\frac{GM_{\mathrm{c}}}{c^3}\right)^{-5/3} f^{-5/3}, \tag{1.55}$$

with the PN corrections given by:

$$\mathcal{N}(x) = \frac{x^{-5/2}}{32\pi\eta} \left[1 + \mathcal{O}(x) + \mathcal{O}(x^{3/2}) + \mathcal{O}(x^2) + \mathcal{O}(x^{5/2}) + \cdots\right], \tag{1.56}$$

where η is the symmetric mass ratio, and $x \equiv \left(GM\omega_{\mathrm{s}}/c^3\right)^{2/3}$, for ω_{s} the orbital frequency of the source and for M the total mass of the source. The goal is to have a template of the wave to a precision of at least $\mathcal{O}(1)$. From eq. (1.56), we can see that we need corrections of at least $\mathcal{O}(x^{5/2})$ on the phase of the GW to have $\mathcal{N}(x) \sim \mathcal{O}(1)$. Hence we need to use at least a 2.5PN approximation of the phase to construct waveform models. In fact it is even not

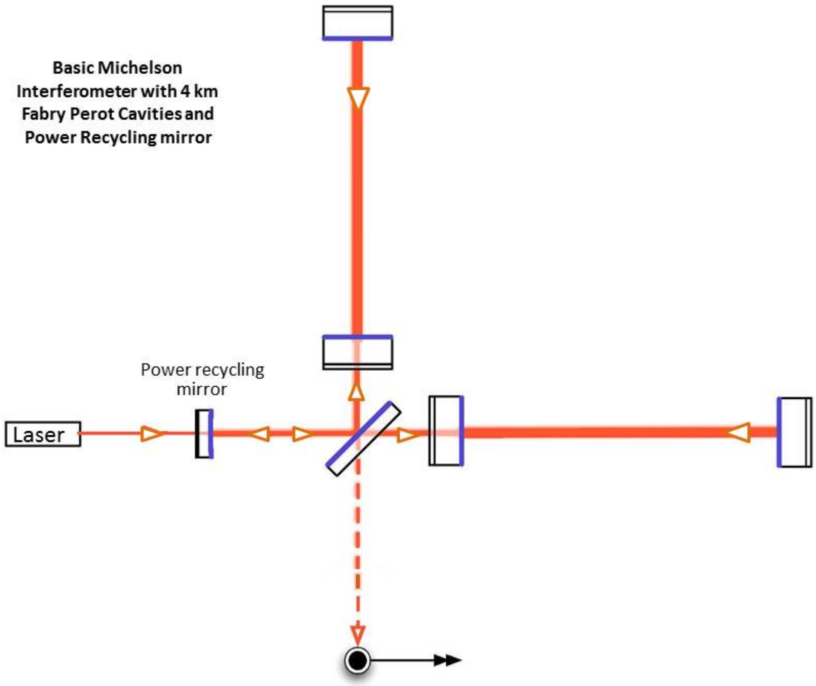

Figure 1.3: *Basic Michelson with Fabry–Perot cavities and Power Recycling mirror. LIGO's interferometers actually use multiple power recycling mirrors but for simplicity only one is shown in the diagram. This figure and its caption are taken from ref. [28].*

enough: an error of $\mathcal{O}(1)$ on the number of cycles would totally put the template out of phase with the GW signal (an error of $\mathcal{O}(1)$ on a function changes greatly the cosine of the function). So in general, for ground-based detectors (the only we have yet), one needs waveforms of at least 3PN level or even 3.5PN level for the phase (see refs [8, 22, 24]). Taking the 1PN expansion for the amplitude and higher order expansion for the phase is called a *restricted PN expansion*.

1.1.3 Detection of gravitational waves

Gravitational waves are currently detected by ground-based detectors (such that advanced LIGO [25], advanced Virgo [26] and KAGRA [27]) that are *Dual Recycled, Fabry–Perot Michelson interferometers*. It is basically a Michelson interferometer with arm's length $L \sim 3 - 4$ km. In addition to the Michelson interferometer, Fabry–Perot cavities are used in order to artificially increase the traveled distance by the lasers: the lasers go back and forth around 300 times in the arms, so the effective arm's length is $\sim 1\,000$ km. Power Recycling mirrors are also used in order to increase the laser power from 40 W to 750 kW [28]. A sketch of a Dual Recycled, Fabry–Perot Michelson interferometer is shown on fig. 1.3.

A detected signal is given by the ratio:

$$\frac{\delta L(t)}{L} = h^{\text{obs}}(t), \tag{1.57}$$

of the change in length δL (function of time) by the length L of the arms. The detected signal is composed of the gravitational wave plus a noise:

$$h^{\text{obs}}(t) = n(t) + h^{\text{signal}}(t), \tag{1.58}$$

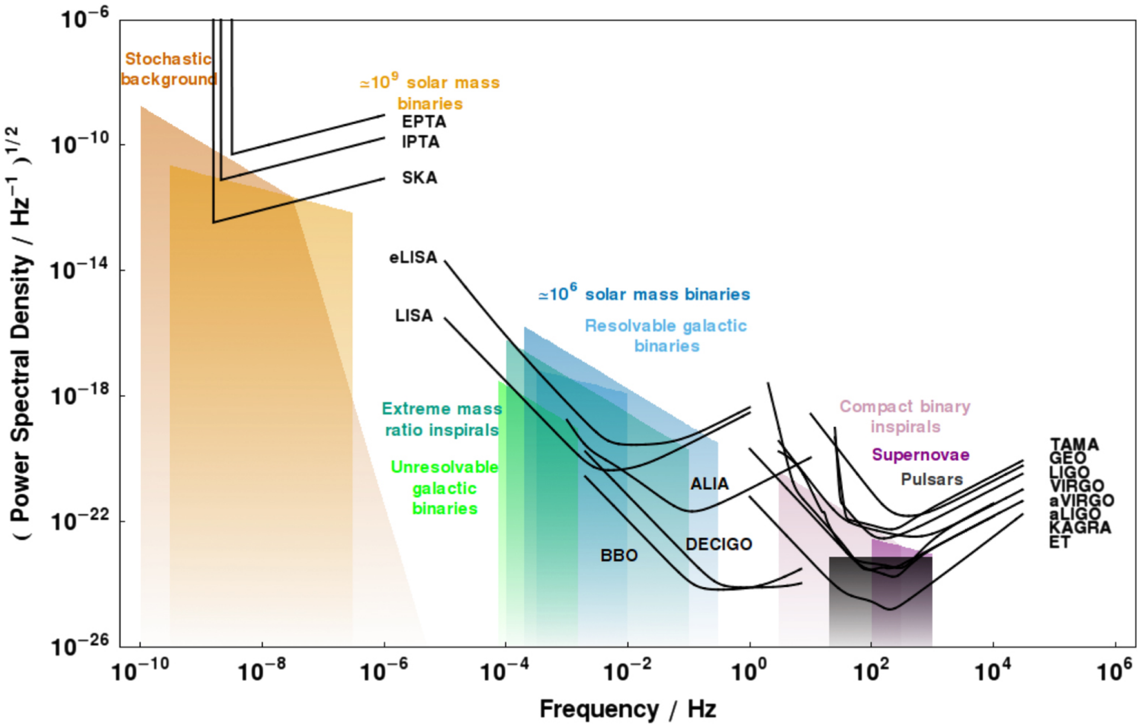

Figure 1.4: *Plots of power spectrum densities (PSD) for some current and future GWs detectors. We can see that the maximum of sensitivity for current detectors (such as aLIGO, aVIRGO and KAGRA) is of about 300 Hz. This figure is fig. A2 of Moore* et al.*, 2014, ref. [29].*

with $|n(t)| \sim 5 \times 10^{-19} \gg |h^{\text{signal}}| \sim 10^{-21}$ [24]. Hence the gravitational wave signal is lost in the noise, and if one does not filter the detected data, then the signal cannot be seen.

The noise $n(t)$ is a colored noise (*i.e.* it has correlations in time), it is then possible to define the correlation of the noise, at two different times t_1 and t_2, as:

$$\overline{n(t_1)\ n(t_2)} = \int \mathrm{e}^{\mathrm{i}2\pi(t_2-t_1)f} S_n(f)\ \mathrm{d}f, \tag{1.59}$$

where $S_n(f)$, the noise spectral density, is mathematically the Fourier transform of the correlation noise, and experimentally is measured by the signal that a detector sees when there is no gravitational wave passing through ($S_n(f)$ then depends of the detector). Typical $\sqrt{S_n}(f)$ are plotted in fig. 1.4.

To extract the signal from data, a *Wiener filter* (or *matched filter*) is used. (The notations we use here closely follow those of ref. [22], lecture 4. For a deeper introduction, see *e.g.* ref. [8], sect. 7.3. and ref. [29]) To do this, we introduce a Hilbert space structure on the space of real functions h's, with the (Wiener) scalar product:

$$\langle h_1(t), h_2(t)\rangle = \int \frac{\tilde{h}_1(f)\ \tilde{h}_2^*(f)}{S_n(f)}\ \mathrm{d}f, \tag{1.60}$$

where $\tilde{h}_i(f)$ is the Fourier transform of the signal $h_i(t)$ ($\tilde{h}_i^*(f)$ being the complex conjugate of $\tilde{h}_i(f)$).

A Wiener filter consists in computing the scalar product eq. (1.60) between the *observed* data $h^{\text{obs}}(t)$ and the *expected* signal $h_\theta(t)$ normalised by the norm of the expected signal:

$$\frac{\langle h^{\text{obs}}(t), h_\theta(t)\rangle}{\sqrt{\langle h_\theta(t), h_\theta(t)\rangle}} = \frac{\langle h^{\text{signal}}(t), h_\theta(t)\rangle}{\sqrt{\langle h_\theta(t), h_\theta(t)\rangle}} + \frac{\langle n(t), h_\theta(t)\rangle}{\sqrt{\langle h_\theta(t), h_\theta(t)\rangle}}. \tag{1.61}$$

The expected signal $h_\theta(t)$ is the waveform of a gravitational wave generated by a binary system with parameters $\theta = \{m_1, m_2, d_\text{L}, \cdots\}$. A lot of expected signals with different parameters θ are computed and the normalised scalar product between the data and these $h_\theta(t)$ (*i.e.* the filters) is evaluated. In general, the scalar product looks random, but when $h_\theta(t)$ matches the gravitational wave signal $h^{\text{signal}}(t)$, then it takes a large value.

Since the noise $n(t)$ is the Fourier transform of the noise spectral density that is used in the Wiener scalar product, eq. (1.60), then $\langle n(t), h_\theta(t)\rangle \cdot (\langle h_\theta(t), h_\theta(t)\rangle)^{-1/2}$ is a random variable. And if the noise is Gaussian, then it is a Gaussian random variable, that can be defined such that $\sigma^2 = 1$. So if eq. (1.61) is much larger than 1, one can neglect the noise contribution in the scalar product.

We can thus define the *signal-to-noise ratio* (written SNR, S/N or ρ), as:

$$\rho^2 \equiv \frac{|\langle h^{\text{signal}}(t), h_\theta(t)\rangle|^2}{\langle h_\theta(t), h_\theta(t)\rangle}, \tag{1.62}$$

and if $h^{\text{signal}}(t) = h_\theta(t) \equiv h(t)$, then we have the maximum SNR:

$$\rho^2_{\text{max}} = \langle h(t), h(t)\rangle = \int \frac{|\tilde{h}(f)|^2}{S_n(f)}\, \mathrm{d}f. \tag{1.63}$$

The Wiener theorem affirms that taking a filter ($h_\theta(t)$) that is the most accurate representation of the true signal ($h^{\text{signal}}(t)$) is the best way to extract the signal from the noise data.

The latter equation can be re-written as:

$$\rho^2_{\text{max}} = \int \frac{|f\ \tilde{h}(f)|^2}{f\ S_n(f)}\ \frac{\mathrm{d}f}{f} = \int \frac{|h_\text{s}(f)|^2}{h^2_\text{n}(f)}\ \mathrm{d}(\ln f), \tag{1.64}$$

in order to see the signal-to-noise ratio as the area over a curve on a log-axis (generally a $\log_{10}$ plot). This formula is computable analytically, using the waveform given by numerical relativity (NR), analytical Effective One Body (EOB)[1] (+ numerical) or even using the quadratic formula, eq. (1.44) [22] (in that case, the computed SNR is not very accurate but the main idea is the good one: see appendix B and particularly its eq. (B.7)).

By doing so, we see that the SNR is inversely proportional to the distance:

$$\rho \propto \frac{1}{D}, \tag{1.65}$$

and we will use this property, see appendix B.

When the maximum SNR is larger than a threshold $\rho_\text{thr} \gg 1$, the observed signal is (with high probability) a gravitational wave detection. Often, one takes $\rho_\text{thr} = 8$ for two detectors, see appendix B. (With more detectors, one has to take into account correlations between detectors and the mathematics is harder, but here is the main idea.)

[1] See ref. [22] for an introduction to EOB.

1.1.4 Recent observations of GWs

Advanced LIGO is composed by two detectors located in Hanford, Washington and in Livingston Parish, Louisiana (USA) [25] and they made the first detection of a GW on 14 September 2015. This GW is called GW150914 (for Gravitational Wave 2015-09-14) [3], it has a SNR of at least 23.6 and was caused by the merge of a binary black hole with $m_1 = 35.6^{+4.7}_{-3.1}$ M$_\odot$ and $m_2 = 30.6^{+3.0}_{-4.4}$ M$_\odot$ at a luminosity distance $d_\mathrm{L} = 440^{+150}_{-170}$ Mpc [3]. Since this first detection, more than fifty other detections have been made [3, 4] in three different runs of the detectors. From the second run, the European detector Virgo, located in Santo Stefano a Macerata (near Pisa) is also operating [26]. A fourth detector, KAGRA, located in the Gifu Prefecture (Japan) has joined the other detectors from the end of the third run (data not yet publicly available) [27]. A timeline of the past and planned runs is shown in fig. 3.7. Detection of the first, second and first half of the third run are publicly available in the *Gravitational Wave Transient Catalogs* (GWTC) 1 and 2 [3,4]. The detected masses of these events are plotted on fig. 1.10.

Some detections are particularly interesting, such as GW170817 (as we discussed in the Introduction) that was caused by the merge of a binary neutron star with $m_1 = 1.46^{+0.12}_{-0.10}$ M$_\odot$ and $m_2 = 1.27 \pm 0.09$ M$_\odot$ at 40^{+7}_{-15} Mpc [3]. This GW had an electromagnetic counterpart, GRB 170817A and together they allowed a measurement of the Hubble constant H_0 [5].

Event GW190521 was sourced by the merge of a binary black hole of masses $m_1 = 95.3^{+28.7}_{-18.9}$ M$_\odot$ and $m_2 = 69.0^{+22.7}_{-23.1}$ M$_\odot$ at $d_\mathrm{L} = 3.92^{+2.19}_{-1.95}$ Gpc. Its heavier BH has a mass that was unexpected from populations models (see section 1.6). A few hypotheses have been put forward to explain this large mass (we discuss some of them in subsection 3.3.1).

Conversely, event GW190814 was caused by the merge of a black hole of mass $m_1 = 23.2^{+1.1}_{-1.0}$ M$_\odot$ with an not identified object of mass $m_2 = 2.59^{+0.08}_{-0.09}$ M$_\odot$ at $d_\mathrm{L} = 0.24^{+0.04}_{-0.05}$ Gpc, that is either the heaviest detected neutron star or the lightest detected black hole [4].

The events GW200105_162426 and GW200115_042309 (numbers after the underscore represent the second of the detection of the coalescence in format hh:mm:ss UTC) were sourced by a black hole that merged with a neutron star. For GW200105_162426: $m_1 = 8.9^{+1.2}_{-1.5}$ M$_\odot$, $m_2 = 1.9^{+0.3}_{-0.2}$ M$_\odot$ and $d_\mathrm{L} = 280 \pm 110$ Mpc, while for GW200115_042309: $m_1 = 5.7^{+1.8}_{-2.1}$ M$_\odot$, $m_2 = 1.5^{+0.7}_{-0.3}$ M$_\odot$ and $d_\mathrm{L} = 300^{+150}_{-100}$ Mpc [30]. (These two events are not part of GWTC-2, because they were detected during run O3b of LIGO/Virgo: its detections are yet published step by step and are not all publicly available.)

1.2 Basics of cosmology

And our galaxy is only one of millions of billions
In this amazing and expanding universe

Monty Python
("Galaxy song", *Monty Python's The Meaning of Life*, 1983)

In this section we recall some basics notions of cosmology. We mostly use refs [31, 32] in which one can find much more topics about cosmology. Ref. [21] has an entire chapter (chap. 17) about basics of FRW cosmology[2] with a nice bibliography.

Since the late 1920s, we know that the Universe is in expansion: the large majority of galaxies around us are redshifted[3] and the further the galaxy, the redshifter it is, meaning that the further

[2]In the present document we call it FLRW cosmology, see note 4 below.
[3]The few blueshifted galaxies (*e.g.* Andromeda that has a "negative redshift": $z = -0.001$ [33]) are part of our

the galaxy the larger its speed with respect to us. It is the Hubble–Lemaître law (Georges Lemaître, 1927 & Edwin Hubble, 1929), that one can write as:

$$v \propto D \;\Leftrightarrow\; v = H_0\ D, \tag{1.66}$$

where H_0 is called the *Hubble constant*. But what is exactly the distance D?

1.2.1 The FLRW metric

If we average over large scales, and as far as we can see, the Universe is (at first order) *isotropic in space*, *i.e.* the number of galaxies in a solid angle does not depend of the direction we are looking, and statistically *homogeneous in space*. By using these two symmetries of space, we can easily see that the overall metric of the Universe does not depend on the spatial position $\boldsymbol{x}$. It is then possible to describe the Universe as a time-ordered sequence of three-dimensional spatial slices, $(\Sigma_t)_{t\in\mathbb{R}}$, each slice being isotropic and homogeneous in space, with a (spatial) line element $\left(\mathrm{d}\ell^2\right)_t = a^2(t)\gamma_{ij}\mathrm{d}x^i\mathrm{d}x^j$. A four-dimensional spacetime line element can then be written as:

$$\mathrm{d}s^2 = c^2\mathrm{d}t^2 - a^2(t)\gamma_{ij}\mathrm{d}x^i\mathrm{d}x^j, \tag{1.67}$$

where $a(t)$ is the *scale factor* that describes the evolution of the Universe. The spatial metric γ_{ij} depends on the overall geometry. In the following, we use units with $c = 1$.

Since each 3D space hypersurface slice is isotropic and homogeneous, the curvature has to be constant on each of them. Hence only three overall geometry are allowed: zero curvature (Euclidean flat space E^3), constant negative curvature (hyperbolic space H^3) and constant positive curvature (spherical space S^3). In these geometries, the space line elements, $\mathrm{d}\ell^2 = \gamma_{ij}\mathrm{d}x^i\mathrm{d}x^j$, in polar coordinates are (see *e.g.* ref. [32] for a demonstration):

$$\mathrm{d}\ell^2 = \frac{\mathrm{d}r^2}{1-kr^2} + r^2(\mathrm{d}\theta^2 + \sin^2\theta\ \mathrm{d}\phi^2),\ \text{where } k = \begin{cases} -1 & \text{for } \mathsf{H}^3; \\ \ \ 0 & \text{for } \mathsf{E}^3; \\ +1 & \text{for } \mathsf{S}^3. \end{cases} \tag{1.68}$$

Inserting eq. (1.68) into eq. (1.67) gives the line element of the *Friedmann–Lemaître–Robertson–Walker* (FLRW) metric[4]:

$$\mathrm{d}s^2 = \mathrm{d}t^2 - a^2(t)\left[\frac{\mathrm{d}r^2}{1-kr^2} + r^2\mathrm{d}\Omega^2\right], \tag{1.69}$$

where we wrote $\mathrm{d}\Omega^2 = \mathrm{d}\theta^2 + \sin^2\theta\ \mathrm{d}\phi^2$.

No one knows the overall geometry of the Universe, but it is, at least locally, extremely flat. In the following we will then use a *flat* FLRW metric ($k = 0$), thus:

$$g_{\mu\nu}(t) = \begin{pmatrix} -1 & 0 & 0 & 0 \\ 0 & a^2(t) & 0 & 0 \\ 0 & 0 & a^2(t) & 0 \\ 0 & 0 & 0 & a^2(t) \end{pmatrix}. \tag{1.70}$$

closest neighbours for which the gravitational attraction is important: in addition of the Hubble flow, each galaxy has a peculiar velocity, see below.

[4] Very often, this metric is just called "FRW" (see *e.g.* ref. [21]) or even "RW" (see *e.g.* ref. [32]).

In the previous equations, t is called the *cosmic time* and r is the *comoving coordinate*. The *physical coordinate* r_{phys} (on which depends the physical results) is given by:

$$r_{\text{phys}}(t) = a(t)r, \tag{1.71}$$

and it is possible to derive it with respect to the cosmic time t to obtain the physical velocity:

$$\begin{align} v_{\text{phys}}(t) = \frac{\mathrm{d}r_{\text{phys}}}{\mathrm{d}t}(t) &= r\frac{\mathrm{d}a}{\mathrm{d}t}(t) + a(t)\frac{\mathrm{d}r}{\mathrm{d}t} \tag{1.72}\\ &\equiv Hr_{\text{phys}} + v_{\text{pec}}, \tag{1.73} \end{align}$$

where we define the *peculiar velocity* $v_{\text{pec}} = a(t)\dot{r}$, and the Hubble flow Hr_{phys}, with the *Hubble parameter*:

$$H(t) = \frac{\dot{a}}{a}(t), \tag{1.74}$$

the dots indicating a derivative with respect to the cosmic time t. When one takes $t = t_0$ (*i.e.* today), the Hubble parameter becomes the (misnamed) Hubble constant H_0. It has units of inverse time (since the scale factor is dimensionless) and is generally given in the form:

$$H_0 = h_0 \cdot 100 \text{ km s}^{-1} \text{ Mpc}^{-1}, \tag{1.75}$$

where h_0 is close to 0.7. (The unit can seem strange, but it allows to interpret the value of H_0 as a velocity of expansion (in km s^{-1}) at a certain distance (in Mpc).) There is yet a tension between different kinds of measurements of the Hubble constant. It is possible to measure it from the late Universe by using type Ia supernovae, in which case we find $H_0^{\text{SNe}} = 73.24 \pm 1.74$ km s^{-1} Mpc^{-1} [21]. It is also possible to measure H_0 from early Universe, using the Cosmic Microwave Background, for example with data of the *Planck* satellite (and Baryon Acoustic Oscillations, BAO) to find $H_0^{Planck} = 66.93 \pm 0.62$ km s^{-1} Mpc^{-1} [21]. These two measurements are incompatible at the level of ≈ 3.4 standard deviations. This incompatibility is called the *Hubble tension*.

Let us come back to eqs (1.71) – (1.73). The peculiar velocity of an object is the velocity that an observer who follows the Hubble flow would measure: indeed if an object is at rest on a FLRW space, then its comoving coordinate is constant and $v_{\text{pec}} = 0$, *i.e.* an observer who is also at rest in space would only measure the Hubble flow that the object follows. This is why some galaxies are blueshifted instead of redshifted: the Hubble flow gives to all galaxies a positive (*i.e.* they move away from us) physical velocity in a radial direction (this is the Hubble–Lemaître law), but furthermore, each galaxy has a peculiar velocity, that can have any orientation. For some galaxies, if r_{phys} is small enough, v_{pec} can be large enough and in the good direction to bring together two galaxies, *i.e.* one galaxy is blueshifted when observed from the other one. Let us see now how the redshift is defined.

First, we introduce the conformal time η given by:

$$\mathrm{d}\eta = \frac{\mathrm{d}t}{a(t)}. \tag{1.76}$$

We suppose that a wave signal with a conformal period $\Delta\eta$ is emitted at the conformal time η_1 and received at the conformal time $\eta_0 = \eta_1 + d$ (where d is the conformal distance between the source and the observer, if $c = 1$). When one measures the period one uses the cosmic time t. So, we have:

$$(\Delta t)_{\text{detector}} = a(\eta_1)\Delta\eta \quad \text{and} \quad (\Delta t)_{\text{source}} = a(\eta_0)\Delta\eta, \tag{1.77}$$

hence,

$$\frac{\lambda_{\text{source}}}{\lambda_{\text{detector}}} \equiv \frac{(\Delta t)_{\text{source}}}{(\Delta t)_{\text{detector}}} = \frac{a(\eta_0)}{a(\eta_1)}. \tag{1.78}$$

In *analogy* with the Doppler effect, it is usual to define the redshift z as the rate of the shift of wavelength of a photon emitted at the cosmic time t_1 and detected at the time t_0, by its wavelength at the emission:

$$z \equiv \frac{\lambda(t_0) - \lambda(t_1)}{\lambda(t_1)}, \tag{1.79}$$

or equivalently:

$$1 + z = \frac{a(t_0)}{a(t_1)} = \frac{1}{a(t_1)}, \tag{1.80}$$

where the second equality comes from the normalisation $a(t_0) \equiv 1$. This definition of redshift only takes into account the Hubble flow and not the peculiar velocity v_{pec}. Since $a(t_1)$ is always larger or equal than 1, a negative redshift (a blueshift) would be impossible to measure (the Universe is expanding). But as we said in note 3 page 16, some galaxies (*e.g.* Andromeda) have a blueshift. So the measured shift of wavelength is the addition of the cosmological redshift (eq. (1.80)) *and* of a real Doppler effect, due to the peculiar velocity of the object with respect to the observer. For a cosmological source, r_{phys} is large enough so that v_{pec} can be neglected (see eq. (1.73)).

For nearby source (*i.e.* $t_1 \not\gg t_0$), we can expand $a(t_1)$ as a Taylor series around t_0:

$$a(t_1) = a(t_0)\left[1 + (t_1 - t_0)H_0 + \cdots\right], \tag{1.81}$$

with $H_0 = (\dot{a}/a)(t_0)$. We can then write the redshift at first order as (using again a Taylor series):

$$z = H_0(t_0 - t_1) + \cdots, \tag{1.82}$$

since $c = 1$, we have $(t_0 - t_1) = d_{\text{phys}}$, the physical distance between the source and the observer. The latter equation is then equivalent to the Hubble–Lemaître law, eq. (1.66). The definition of the distance is difficult in a expanding Universe with a finite speed of light: between the emission and the reception of a light signal, the source has moved following the Hubble flow. The easiest way to define a distance is to use the comoving coordinates of the line element (eq. (1.69)), and one gets the *comoving distance*:

$$d_{\text{com}}(z) = \int_{t_1}^{t_0} \frac{\mathrm{d}t}{a(t)} = \int_0^z \frac{\mathrm{d}\tilde{z}}{H(\tilde{z})}. \tag{1.83}$$

In a non Euclidean space ($k \neq 0$), one can also define the *metric distance*. But in a flat space, both metric and comoving distances are equal. This distance is not observable.

Another definition of the distance is given by the *luminosity distance*. In a flat non expanding space, the measured flux F at a distance D of a light source with luminosity L is given by:

$$F = \frac{L}{4\pi D^2}, \tag{1.84}$$

(the flux is isotropically distributed on the sphere of radius D). In an expanding space, the distance between the source and the observer at time t_0 when the signal is detected is the comoving distance (non measurable). Because of the expansion of the Universe, the energy of

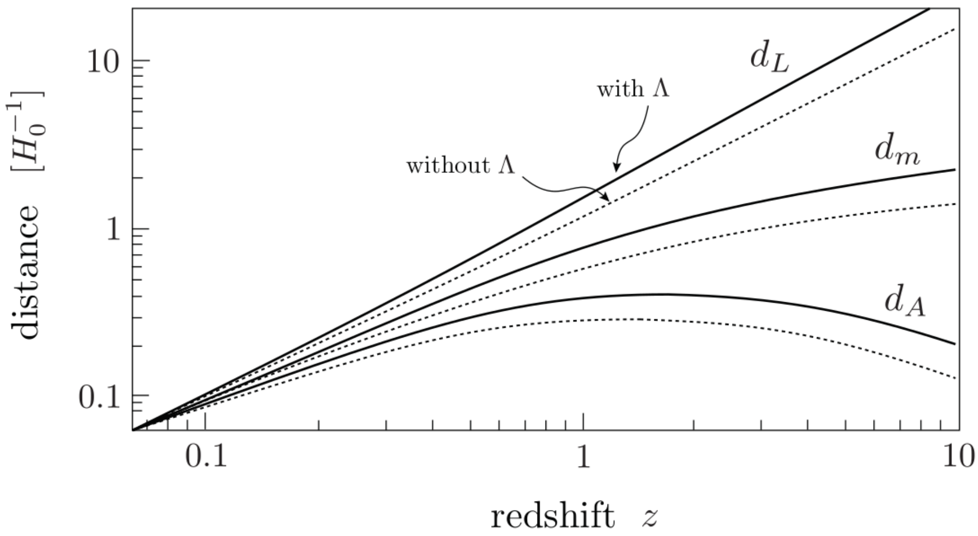

Figure 1.5: *Cosmological distances in a flat FLRW Universe, with only matter content (dotted lines) and with 70% dark energy (solid lines), see subsect. 1.2.2. We see that for $z \ll 1$, the three distances are the same. This figure is fig. 1.6 of Baumann, ref. [32].*

the photons is divided by a factor $(1+z)$, and their rate of arrival is also divided by the same factor. Thus,

$$F = \frac{L}{4\pi\ d_{\mathrm{L}}^2} = \frac{L}{4\pi\ d_{\mathrm{com}}^2 (1+z)^2}, \tag{1.85}$$

and then: $d_{\mathrm{L}} = d_{\mathrm{com}}(1+z) = (1+z)\int_0^z H(\tilde{z})^{-1}\,\mathrm{d}\tilde{z}$. These two definitions of the distance in cosmology are the two we use in this master's project. Another often used distance is the *angular diameter distance*: $d_{\mathrm{A}} = d_{\mathrm{com}}/(1+z)$. These three distances are plotted as functions of the redshift in fig. 1.5. One can see that at small redshift these definitions are equivalent.

We see that with an easy metric of a time function, $a(t)$, one can describe at first order the Universe as we observe it. General Relativity hence allows us to study its dynamics.

1.2.2 Dynamics of the Universe

Il Pendolo mi stava dicendo che, tutto muovendo, il globo, il sistema solare, le nebulose, i buchi neri e i figli tutti della grande emanazione cosmica, [...].

Umberto Eco
(*Il Pendolo di Foucault*, I, 1, 1988)

Here again, we have a metric (the FLRW metric $g_{\mu\nu}$, eq. (1.70)) and General Relativity connects the geometry of the spacetime to its energy content. The Einstein's equations with a cosmological constant Λ are:

$$G_{\mu\nu} = 8\pi G T_{\mu\nu} - \Lambda g_{\mu\nu}, \tag{1.86}$$

let us first compute the Einstein tensor G, then we will study the energy content of the Universe.

For the flat FLRW metric, in Cartesian coordinates, the non-vanishing Christoffel symbols are (the Latin indices indicate the spatial coordinates x, y, z):

$$\Gamma^{0}{}_{ij} = a^2 H \delta_{ij}, \qquad \Gamma^{i}{}_{0j} = H\delta^{i}{}_{j}, \tag{1.87}$$

the Ricci tensor is given by:

$$R_{00} = -3(\dot{H} + H^2), \quad R_{0i} = 0, \quad R_{ij} = a^2(\dot{H} + 3H^2)\delta_{ij}, \tag{1.88}$$

the Ricci scalar is then:

$$R = 6(\dot{H} + 2H^2), \tag{1.89}$$

and the Einstein tensor $G^{\mu}{}_{\nu}$ is given by:

$$G^{0}{}_{0} = -3H^2, \quad G^{0}{}_{i} = 0, \quad G^{i}{}_{j} = -(2\dot{H} + 3H^2)\delta^{i}{}_{j}. \tag{1.90}$$

For the energy content of the Universe, at first order, because of homogeneity and isotropy, we can write the stress-energy tensor as the one of a *perfect fluid*:[5]

$$T^{\mu}{}_{\nu} = (\rho + p)\ u^{\mu} u_{\nu} + p\ \delta^{\mu}{}_{\nu}, \tag{1.91}$$

where ρ is the energy density, p the pressure and u^{μ} is the four-velocity (with respect to the observer: $u^{\mu} \equiv \mathrm{d}x^{\mu}/\mathrm{d}\tau$). In the rest frame of the fluid (hence as seen by a comoving observer), $u^{\mu} = (1, 0, 0, 0)$, thus $u_{\nu} = (-1, 0, 0, 0)$ and then:

$$T^{\mu}{}_{\nu}(t) = \begin{pmatrix} -\rho(t) & 0 & 0 & 0 \\ 0 & p(t) & 0 & 0 \\ 0 & 0 & p(t) & 0 \\ 0 & 0 & 0 & p(t) \end{pmatrix}. \tag{1.92}$$

This stress-energy tensor allows us to write the *Friedmann equations*, using the Einstein's field equations with a cosmological constant, and the Einstein tensor of the flat FLRW metric ($k = 0$), eq. (1.90). The scalar component $(0, 0)$ gives:

$$H^2(t) = \frac{8\pi G}{3}\ \rho(t) + \frac{\Lambda}{3}, \tag{1.93}$$

while the vector components $(0, i)$ and $(i, 0)$ are the trivial $0 = 0$ and the 3-tensor components (i, j) give:

$$2\dot{H}(t) + 3H(t)^2 = -8\pi G\ p(t) + \Lambda. \tag{1.94}$$

The Friedmann equations are then just the Einstein's equations for a FLRW metric and they describe the evolution of the Universe through the scale factor a and its derivative $\dot{a}$, ρ and p the energy density and pressure and Λ, the cosmological constant. From now on, we rescale $\rho \mapsto \rho + \Lambda/(8\pi G)$ and $p \mapsto p - \Lambda/(8\pi G)$ in order to take the cosmological constant into account as an energy component of the Universe.

In General Relativity, the Bianchi identity $\nabla_{\mu} G^{\mu}{}_{\nu} = 0$ imposes the energy-momentum conservation $\nabla_{\mu} T^{\mu}{}_{\nu} = 0$ (it is the equivalent in a Minkowski space of both the continuity equation and the Euler equation). Using

$$\nabla_{\mu} T^{\rho}{}_{\nu} = \partial_{\mu} T^{\rho}{}_{\nu} + \Gamma^{\rho}{}_{\mu\sigma} T^{\sigma}{}_{\nu} - \Gamma^{\sigma}{}_{\mu\nu} T^{\rho}{}_{\sigma} \tag{1.95}$$

[5] As usual, it is possible to prove it by varrying the Einstein–Hilbert action of the FLRW metric, with respect to the FLRW metric.

on the stress-energy tensor eq. (1.92) with the FLRW Christoffel symbols eq. (1.87), we get four equations. The equation with $\nu = 0$ describes the evolution of energy:

$$0 = \partial_\mu T^\rho{}_0 + \Gamma^\rho{}_{\mu\sigma} T^\sigma{}_0 - \Gamma^\sigma{}_{\mu 0} T^\rho{}_\sigma \tag{1.96}$$
$$= \dot{\rho} + 3H(\rho + p). \tag{1.97}$$

Equation (1.97) is the continuity equation.[6] Let us see now what are the components of the Universe. To do so, let us remind the equation of state (EoS) of a perfect fluid:

$$p(t) = w(t)\rho(t), \tag{1.98}$$

where in general $w(t)$ is a function of time. We can solve the continuity equation, eq. (1.97) to write ρ as a function of the scale factor a:

$$\rho(t) \propto a^{-3(1+w(t))}. \tag{1.99}$$

The ΛCDM model

In the ΛCDM model (for the cosmological constant Λ and "Cold Dark Matter") we suppose that a flat Universe is only composed of matter, radiation and with a cosmological constant Λ. With more than one component, ρ and p of the continuity equation (eq. (1.97)) are now the total density and total pressure:

$$\rho_{\mathrm{tot}}(t) = \sum_i \rho_i(t) \tag{1.100}$$
$$p_{\mathrm{tot}}(t) = \sum_i w_i(t)\rho_i(t). \tag{1.101}$$

- **Matter** is composed of all the forms of energy for which the pressure is much smaller than the density: $|P| \ll \rho$. In the Universe, there are two types of matter: *Cold Dark Matter* and "Standard model non-relativistic matter" (that is generally called *baryonic* matter, even it there are also leptons in it). Setting $w = 0$ in the continuity equation (eq. (1.97)), we get:

$$\rho_{\mathrm{m}} \propto a^{-3}, \tag{1.102}$$

  hence the matter is just diluted in the expansion of the volume V of the Universe: $V \propto a^3$;

- **Radiation** is composed of the elements for which $w = 1/3$, it is the case for relativistic particles, as photons, neutrinos and maybe gravitons. Setting $w = 1/3$ in the continuity equation (eq. (1.97)), we get:

$$\rho_{\mathrm{r}} \propto a^{-4}, \tag{1.103}$$

  hence the radiation is diluted by the expansion of the Universe, but its energy is also redshited: $E \propto a^{-1}$;

- **Cosmological constant**: the expansion of the Universe is now in acceleration, *i.e.*: $\ddot{a} > 0$. We can rewrite the Friedmann equation (1.94), as:

$$\frac{\ddot{a}}{a} = -\frac{4\pi G}{3}(\rho + 3p) = -\frac{4\pi G}{3} p\,(1 + 3w)\,, \tag{1.104}$$

[6] For $\nu = i$, the energy-momentum conservation gives $\partial_i p = 0$, which is satisfied.

to ensure $\ddot{a} > 0$ we then need a negative pressure component with $w < -1/3$. Such a component is called *dark energy*. The cosmological constant Λ is a possible explanation of dark energy. It has $w = -1$, and we get:

$$\rho_\Lambda \propto a^0 = \text{const.} \tag{1.105}$$

It means that the cosmological constant density has to be created when the Universe expands.

It is possible to write the Friedmann equation (eq. (1.93)) as the evolution of the Hubble parameter H with respect to the scale factor a. For that, let us define the *critical density* today (an index '0' means 'today'):

$$\begin{aligned}
\rho_{\text{crit},0} &\equiv \frac{3H_0^2}{8\pi G} && (1.106)\\
&= 1.9 \times 10^{-29}\ h_0^2\ \text{g cm}^{-3} && (1.107)\\
&= 2.8 \times 10^{11}\ h_0^2\ \text{M}_\odot\ \text{Mpc}^{-3} && (1.108)\\
&= 1.1 \times 10^{-5}\ h_0^2\ \text{protons cm}^{-3}, && (1.109)
\end{aligned}$$

where we took the numerical values in ref. [32] and where $h_0 \approx 0.7$. The critical density is used to define dimensionless density parameters of the components of the Universe (today):

$$\Omega_{i,0} = \frac{\rho_{i,0}}{\rho_{\text{crit},0}}, \quad \text{for } i = \text{m}, \text{r}, \Lambda, \tag{1.110}$$

and then, we get:

$$H(a) = H_0\ \left(\Omega_{\text{r},0}\ a^{-4} + \Omega_{\text{m},0}\ a^{-3} + \Omega_{\Lambda,0}\right)^{1/2}. \tag{1.111}$$

The wCDM model

The wCDM model is a phenomenological model close to the ΛCDM model: it is composed of Cold Dark Matter, radiation and dark energy. But now the dark energy component and its equation of state w_{DE} are unknown. However, wCDM assumes that w_{DE} is constant in time. Hence, we have:

$$p_{\text{DE}}(t) = w_{\text{DE}}\ p_{\text{DE}}(t), \quad \text{with } w_{\text{DE}} < -1/3, \tag{1.112}$$

(and in fact w_{DE} is observationally constrained to be very close to -1: $w_{\text{DE}}(t_0) = -1.00^{+0.04}_{-0.05}$ [21]). We then have (see eq. (1.99)):

$$\rho_{\text{DE}}(t) \propto a^{-3(1+w_{\text{DE}})}, \tag{1.113}$$

and thus:

$$H(a) = H_0\ \left(\Omega_{\text{r},0}\ a^{-4} + \Omega_{\text{m},0}\ a^{-3} + \Omega_{\text{DE},0}\ a^{-3(1+w_{\text{DE}})}\right)^{1/2}, \tag{1.114}$$

where we defined $\Omega_{\text{DE},0} = \rho_{\text{DE},0}/\rho_{\text{crit},0}$, as in eq. (1.110).

Dynamical Dark Energy

The ΛCDM model supposes a constant dark matter EoS: $w_{\rm DE}(t) = -1$. Small variations to this value are possible for the present value of $w_{\rm DE}$ (as supposed by the wCDM model), but its value can also change with time. In this case, it is usual to expand $w_{\rm DE}(a)$ as a Taylor series:

$$w_{\rm DE}(a) = w_0 + w_a(a-1) \tag{1.115}$$
$$\Leftrightarrow \quad w_{\rm DE}(z) = w_0 + w_a \,\frac{z}{1+z}, \tag{1.116}$$

and the current observational limits are $|w_0 + 1| \sim 0.2$ and $|w_a| \sim 1$ [21]. A dark energy with $w(z) < -1$ is called a *phantom dark energy*:[7] it is a DE whose density increases with the expansion of the Universe, and then predicts a "Big Rip".

1.3 Propagation of gravitational waves in a FLRW Universe

Since the Universe is in expansion, the propagation of GWs is modified with respect to the propagation on a flat Minkowski spacetime: indeed the frequencies are redshited by the expansion of the Universe. In this section, we expose how GWs generated by binary systems propagate in a FLRW Universe, with their main properties. For more information, see ref. [8], subsection 4.1.4 and ref. [21], sect. 19.5.

First we define the *local wave zone*: the observer is far enough from the source so that the gravitational field has a $1/r$ behaviour, but close enough so that the expansion of the Universe between the emission and the reception time is negligible. In the local wave zone, the two polarisations of a GW are given by:

$$h_+(t_s) = h_c(t_s^{\rm ret})\frac{1+\cos^2\iota}{2}\cos\left[2\pi\int_{t_s}^{t_s^{\rm ret}} f_{\rm GW}^{(s)}(t'_s)\,{\rm d}t'_s\right], \tag{1.117}$$
$$h_\times(t_s) = h_c(t_s^{\rm ret})\cos\iota\sin\left[2\pi\int_{t_s}^{t_s^{\rm ret}} f_{\rm GW}^{(s)}(t'_s)\,{\rm d}t'_s\right], \tag{1.118}$$

where

$$h_c(t_s^{\rm ret}) = \frac{4}{a(t_{\rm emis})r}\left(\frac{GM_{\rm c}}{c^2}\right)^{5/3}\left(\frac{\pi f_{\rm GW}^{(s)}(t_s^{\rm ret})}{c}\right)^{2/3}, \tag{1.119}$$

with t_s the time measured in the source-frame, $t_s^{\rm ret}$ the corresponding retarded time (still measured in the source-frame), and ι the inclination angle between the line of sight and the normal to the orbital plane of the source. The scale factor $a(t_{\rm emis})$ is the one of the time of emission, but since we are in a local wave zone, the scale factor is supposed constant, r is the comoving distance between the source and the observer, so that $a(t_{\rm emis})r = r_{\rm phys}$ is the physical distance between them.

If now the wave propagates on a cosmological distance, the factor h_c given by eq. (1.119) must be changed. At first order, by supposing $2\pi f_{\rm GW} \gg t_0^{-1}$, where t_0 is the present age of the Universe, it gives (see ref. [8], subsection 4.1.4):

$$h_c(t_s^{\rm ret}) = \frac{4}{a(t_0)r}\left(\frac{GM_{\rm c}}{c^2}\right)^{5/3}\left(\frac{\pi f_{\rm GW}^{(s)}(t_s^{\rm ret})}{c}\right)^{2/3}. \tag{1.120}$$

[7] It is interesting to note that allowing $w_{\rm DE}$ to be below -1 gives a larger value for H_0 than in the case of the ΛCDM model, thus the Hubble tension is less important (see ref. [21], chap. 19).

We can rewrite eq. (1.120) in terms of quantities that are measurable by the observer. First the frequency of the wave is redshifted:

$$f_{\mathrm{GW}}^{(s)} = (1+z)\ f_{\mathrm{GW}}^{(\mathrm{obs})}, \tag{1.121}$$

and since the measure $\mathrm{d}t$ also changes with the redshift, we get:

$$\int_{t_s}^{t_s^{\mathrm{ret}}} f_{\mathrm{GW}}^{(s)}(t'_s)\ \mathrm{d}t'_s = \int_{t_{\mathrm{obs}}}^{t_{\mathrm{obs}}^{\mathrm{ret}}} f_{\mathrm{GW}}^{(\mathrm{obs})}(t'_{\mathrm{obs}})\ \mathrm{d}t'_{\mathrm{obs}}. \tag{1.122}$$

Equation (1.120) then becomes:

$$h_c(t_{\mathrm{obs}}^{\mathrm{ret}}) = \frac{4}{a(t_0)r}(1+z)^{2/3}\left(\frac{GM_{\mathrm{c}}}{c^2}\right)^{5/3}\left(\frac{\pi f_{\mathrm{GW}}^{(\mathrm{obs})}(t_{\mathrm{obs}}^{\mathrm{ret}})}{c}\right)^{2/3} \tag{1.123}$$

$$= \frac{4}{d_{\mathrm{L}}(z)}(1+z)^{5/3}\left(\frac{GM_{\mathrm{c}}}{c^2}\right)^{5/3}\left(\frac{\pi f_{\mathrm{GW}}^{(\mathrm{obs})}(t_{\mathrm{obs}}^{\mathrm{ret}})}{c}\right)^{2/3}, \tag{1.124}$$

where we used the luminosity distance (see eq. (1.85)). If we furthermore introduce the *redshifted chirp mass*:

$$\mathcal{M}_{\mathrm{c}} = (1+z)M_{\mathrm{c}} = (1+z)\mu^{3/5}m^{2/5}, \tag{1.125}$$

we can rewrite eq. (1.124) as

$$h_c(t_{\mathrm{obs}}^{\mathrm{ret}}) = \frac{4}{d_{\mathrm{L}}}\left(\frac{G\mathcal{M}_{\mathrm{c}}}{c^2}\right)^{5/3}\left(\frac{\pi f_{\mathrm{GW}}^{(\mathrm{obs})}(t_{\mathrm{obs}}^{\mathrm{ret}})}{c}\right)^{2/3}. \tag{1.126}$$

The frequency of the GW, eq. (1.49), in the observer frame can be rewritten (see ref. [8]):

$$f_{\mathrm{GW}}^{(\mathrm{obs})}(t_{\mathrm{obs}}^{\mathrm{ret}}) = \frac{1}{\pi}\left(\frac{5}{256}\frac{1}{\tau_{\mathrm{obs}}}\right)^{3/8}\left(\frac{G\mathcal{M}_{\mathrm{c}}}{c^3}\right)^{-5/8}, \tag{1.127}$$

where τ_{obs} is the time to coalescence ($= t - t_{\mathrm{coal}}$) measured in the detector frame. This result can also be understood by noticing that GM_{c}/c^3 is the time-scale of the frequency of GWs. In an expanding FLRW Universe, the time scale is redshifted: $GM_{\mathrm{c}}/c^3 \mapsto (1+z)GM_{\mathrm{c}}/c^3 = G\mathcal{M}_{\mathrm{c}}/c^3$.

Hence we see that a GW amplitude is inversely proportional to the luminosity distance and proportional to (a power 5/3 of) the redshifted mass. And if an observer measures h_c and $f_{\mathrm{GW}}^{(\mathrm{obs})}$, he has access to the values of d_{L} *and* $\mathcal{M}_{\mathrm{c}}$ *together*: there is a degeneracy between these parameters. The redshifted chirp mass is also measurable from the time derivative of the observed frequency of the GW (eq. (1.127)):

$$\dot{f}_{\mathrm{GW}}^{(\mathrm{obs})} = \frac{96}{5}\pi^{8/3}\left(\frac{G\mathcal{M}_{\mathrm{c}}(z)}{c^3}\right)^{5/3}\left[f_{\mathrm{GW}}^{(\mathrm{obs})}\right]^{11/3}, \tag{1.128}$$

and from the measurements of h_c, $f_{\mathrm{GW}}^{(\mathrm{obs})}$ and $\dot{f}_{\mathrm{GW}}^{(\mathrm{obs})}$, the observer knows the value of the chirp mass $\mathcal{M}_{\mathrm{c}}$ *and* the value of the luminosity distance d_{L}. We will use that property to obtain our results (see section 1.4 and chapter 2).

However, it is not h_c that is detected, but a linear combination of the two polarisations:

$$F_+h_+ + F_\times h_\times \tag{1.129}$$

where $F_{+,\times}$ are the pattern functions of the interferometer and where:

$$h_+(t_{\rm obs}) = h_c(t_{\rm obs}) \frac{1+\cos^2\iota}{2} \cos\left[\Phi(\tau_{\rm obs})\right], \tag{1.130}$$

$$h_\times(t_{\rm obs}) = h_c(t_{\rm obs}) \cos\iota \sin\left[\Phi(\tau_{\rm obs})\right], \tag{1.131}$$

with

$$\Phi(\tau_{\rm obs}) = -2\left(\frac{5G\mathcal{M}_{\rm c}(z)}{c^3}\right)^{-5/8} \tau_{\rm obs}^{5/8} + \Phi_0, \tag{1.132}$$

and with $h_c(t_{\rm obs})$ given in eq. (1.126). Thus, the amplitude of h_+ is $h_c\left(1+\cos^2\iota\right)/2$ and the amplitude of $h_\times$ is $h_c\cos\iota$. The inclination angle ι between the line of sight and the normal to the orbital plane of the source is unknown. If the two polarisations and the chirp mass are known separately, the value of $\cos\iota$ is simply given from the ratio $h_+/h_\times$, then the luminosity distance $d_{\rm L}$ is measured. However since the detection is a linear combination of the two polarisations, these parameters are estimated simultaneously, this is why the errors on the measurements of distances with GWs are large.

Another useful result about the propagation of GWs in a FLRW Universe is derived in chapter 19 of ref. [21]. Let us quickly summarise it here. A GW can be seen as a *tensor perturbation* over the FLRW Universe. We can perturbe the Einstein's equations for a FLRW metric (or equivalently perturbe the Friedmann equations), we get:

$$\delta G^\mu{}_\nu = \frac{8\pi G}{c^4}\,\delta T^\mu{}_\nu = 0 \text{ (in vacuum)}, \tag{1.133}$$

and the perturbed FLRW metric (eq. (1.69)) is given in conformal time η by (taking $c=1$ again):

$$\mathrm{d}s^2 = a^2\left[-\mathrm{d}\eta^2 + \left(\delta_{ij} + h_{ij}^{\rm TT}\right)\mathrm{d}x^i\mathrm{d}x^j\right], \tag{1.134}$$

one can then compute the Christoffel symbols $\Gamma^\sigma{}_{\mu\nu}$ (see *e.g.* eqs (18.99)–(18.104) of ref. [21]), and one gets:

$$\delta G^0{}_0 = 0 = \delta G^i{}_0, \quad \delta G^i{}_0 = \frac{1}{2a^2}\left[\left(h_{ij}^{\rm TT}\right)'' + 2\mathcal{H}\left(h_{ij}^{\rm TT}\right)' - \nabla^2 h_{ij}^{\rm TT}\right], \tag{1.135}$$

where $\mathcal{H} = a'/a$, with the prime denoting a derivative with respect to the conformal time η (instead of the cosmic time t for the "normal" Hubble parameter H, eq. (1.74)). In vacuum, we then get:

$$\left(h_{ij}^{\rm TT}\right)'' + 2\mathcal{H}\left(h_{ij}^{\rm TT}\right)' - \nabla^2 h_{ij}^{\rm TT} = 0, \tag{1.136}$$

or equivalently by going into the momentum (Fourier) space:

$$\tilde{h}_A'' + 2\mathcal{H}\tilde{h}_A' + k^2\tilde{h}_A = 0, \tag{1.137}$$

for $A = +, \times$. Equation (1.137) governs the free propagation of tensor perturbations in a FLRW Universe.

1.4 Standard sirens and tests of cosmology

On the upper surface of each circle is a Siren, who goes round with them, hymning a single tone or note.

Plato
("Myth of Er", *The Republic*, Book X, trad. Benjamin Jowett)

In cosmological observations, one needs measurements of distance and of redshift to be able to measure parameters of cosmological models. In "classical" cosmology (*i.e.* cosmology with electromagnetic waves) distances can be measured from type Ia supernovae (SNe) (together with an intermediate "distance ladder" to calibrate the SN, generally Cepheids variables). Type Ia SNe always[8] explode at the same (known) mass, producing the same (known) absolute magnitude and the further the SN, the larger its apparent magnitude.[9] Since we use their light, type Ia SNe are called *standard candles*. Other techniques exist, *e.g.* using the CMB or BAO. However, GWs give another way to measure cosmological distances. Let us see in this section how, and how it can be used to test cosmological models.

As any spherical wave, a GW amplitude varies as the inverse of the distance (this is normal: the energy E goes as the amplitude a squared, and the energy is isotropically distributed on a sphere centered on the source: $E \propto d^{-2} \Rightarrow a \propto d^{-1}$). This behaviour in the case of the GW can be seen in the wave general equation far away from the source (eq. (1.33)):

$$h_{ij}^{\mathrm{TT}} \propto \frac{1}{r}. \tag{1.138}$$

As we saw in section 1.3, in the case of GWs produced by a binary system at a cosmological distance, we have (see eqs (1.130) and (1.131)):

$$h_+ = h_c\,\frac{1+\cos^2\iota}{2} \tag{1.139}$$

$$h_\times = h_c \cos\iota \tag{1.140}$$

where (see eq. (1.126)):

$$h_c \propto \frac{\mathcal{M}_{\mathrm{c}}^{5/3}\,(f_{\mathrm{GW}}^{(\mathrm{obs})})^{2/3}}{d_{\mathrm{L}}}. \tag{1.141}$$

The redshifted chirp mass $\mathcal{M}_{\mathrm{c}}(z)$ is measurable from the evolution of the observed frequency of the wave (see eq. (1.128)), hence, independent measurements of both GW polarisations' amplitudes and measurements of the frequency of the GW and of its time derivative give a direct measurement of the luminosity distance $d_{\mathrm{L}}(z)$ between the source and the observer. By analogy between GWs and sound wave (both types of waves' detectors have almost a 4π sr sensitivity), coalescing binaries at cosmological distances are called *standard sirens*.

Given a choice of cosmological model, the luminosity distance is expressed as a function of the redshift (we see it by inserting eq. (1.111) or eq. (1.114) into eq. (1.83)):

$$d_{\mathrm{L}}(z) = \frac{1+z}{H_0}\int_0^z \frac{\mathrm{d}\tilde{z}}{\sqrt{\Omega_{\mathrm{r},0}(1+\tilde{z})^4 + \Omega_{\mathrm{m},0}(1+\tilde{z})^3 + \rho_{\mathrm{DE}}(\tilde{z})/\rho_{\mathrm{crit},0}}}, \tag{1.142}$$

[8] Of course, this is an approximation and corrections are always needed.
[9] Remember that the larger the magnitude, the less the object is visible.

where the density of dark energy (DE) at a redshift z is given in all generality (*i.e.* the EoS of DE may be not constant in time) by:

$$\rho_{\mathrm{DE}}(z) = \rho_{\mathrm{DE}}(0) \exp\left\{3 \int_0^z \frac{1 + w_{\mathrm{DE}}(\tilde{z})}{1+\tilde{z}}\, \mathrm{d}\tilde{z}\right\}, \tag{1.143}$$

where we supposed that DE does not exchange energy with radiation and matter (the equation of continuity (1.97) normally holds for the total energy density and total pressure).

Equation (1.142) allows us to test a cosmological model given the distance d_{L} and the redshift z of an object. A standard siren alone does not give any indication on the redshift of the source. But a few techniques can be used to skirt this problem. First possibility, proposed in ref. [34] (Bernard F. Schutz, 1986): mergers of neutrons stars can produce a gamma-ray burst, that is an electromagnetic counterpart of the gravitational wave. The electromagnetic wave is redshifted and this redshift can be measured from known spectral lines. This ideal scenario already happened on 17 August 2017: the γ-ray burst GRB 170817A is the electromagnetic counterpart of GW170817 (the probability that these two events are independent, given the temporal and spatial observations, was estimated to 5.0×10^{-8} at the detection time [6]), allowing (after correction of the peculiar velocity of the host galaxy) a measurement of the Hubble constant:

$$H_0 = 70.0^{+12.0}_{-8.0}\ \mathrm{km\ s^{-1}\ Mpc^{-1}} \quad [5], \tag{1.144}$$

this value is yet not accurate enough to solve the Hubble tension,[10] but the error bars decrease by a factor $\sim 1/\sqrt{N_{\mathrm{obs}}}$, where N_{obs} is the number of observed GWs with an EM counterpart. Hence, with $\mathcal{O}(10^2)$ GWs observations with electromagnetic counterpart, we should be able to distinguish between the different values of H_0 (see note 10).

When we do not have any EM counterpart to the GW (and that is the case for the large majority of the events), the standard siren is called a *dark siren*. In the case of dark sirens, statistical methods can be used to estimate the redshift of the source. This statistical approach was also proposed by Schutz in ref. [34]. Ref. [35] reviews the statistical formalisms. In particular, it is explained in refs [13, 36] and similar techniques have been used to constrain the value of H_0, on mock data (representing five years of observation by advLIGO at design sensitivity) [11]; for GW170717 (without using its EM counterpart) [37]; for GW170814 [38] and for GW190815 [39]. Statistical methods have also been used to constrain modified GW propagation, in ref. [12] on the parametrisation c_{M}, see section 1.5, and in ref. [10], whose authors have constrain the same parameters as those that we are interested in: $\{H_0, \Xi_0, \cdots\}$, see section 1.5.

A first possibility consists in using a galaxy catalog that gives the position and the redshift of galaxies, then to statistically estimate the probability that the source is in a given galaxy of the catalog. That is what was done in ref. [10] in order to constrain modified GW propagation with the same parametrisation as us.

Another possibility consists in using the fact that the detector-frame mass is the source-frame mass times the redshift (plus one): $m^z = (1+z)m^0$ (see eq. (1.125)). Thus if one knows the source-frame mass of the source and the associated detector-frame mass, one has a measurement of the redshift of the source. Of course there is no way to know exactly the source-frame mass of a single cosmological source. But black holes and neutron stars follow a mass population distribution. For (stellar origin) black holes, we discuss some models of mass population in sect. 1.6, while for neutrons stars it is even simpler: they have a known mass distribution, peaked near 1.35 $\mathrm{M}_\odot$. This "redshifted masses" technique is the technique we use for this master's project.

[10] Let us recall that measurements of the Hubble constant using type Ia SNe and using the Cosmic Microwave Background of the *Planck* satellite (and BAO) are incompatible at the level of ≈ 3.4 standard deviations: $H_0^{Planck} = 66.93 \pm 0.62$ km s^{-1} Mpc^{-1} and $H_0^{\mathrm{SNe}} = 73.24 \pm 1.74$ km s^{-1} Mpc^{-1} [21]. This incompatibility is called the "Hubble tension".

It was also used in refs [11, 40] (on simulated observations without modified GW propagation) and in ref. [12], on the LIGO and Virgo observations (refs [3, 4]) with modified gravity, but with a different parametrisation and without testing on mock data the efficiency of the method to constrain modified gravity.

The statistical method we use is described in details in chapter 2.

What cosmological parameters can be measured from standard sirens? By expanding eq. (1.142) around $z = 0$, we get:

$$d_{\mathrm{L}}(z) = \frac{z}{H_0} + \mathcal{O}(z^2), \tag{1.145}$$

which is the Hubble–Lemaître law, eq. (1.82). We then see that for small redshifts only H_0 has a large enough effect on measurements. We then need events at a large redshift (so that the z^2 corrections in eq. (1.145) are not negligible) to constrain the values of other parameters of a cosmological model, such as $w_{\mathrm{DE}}(t_0)$. However, impacts of a modified GW propagation (see next section) would be easier to test at large redshift [9].[11]

1.5 An introduction to modified gravity

The interest in modifications of gravity at cosmological scales is important since the end of the 1990s, after the discovery of the accelerated expansion of the Universe (in the sense that the rate of expansion is increasing: $\ddot{a} > 0$). Indeed the Friedmann equations without cosmological constant ($\Lambda = 0$ in eq. (1.94)), implies a decreasing rate of expansion ($\ddot{a} < 0$). This is known as the *dark energy problem*. By introducing a scalar field Λ with a positive value, one can explain the acceleration of the expansion. This is the ΛCDM model (also called the standard model of cosmology), see subsection 1.2.2. However another way to explain the accelerated expansion it to suppose that the Einstein's equations are not the true equations to describe gravity at a cosmological scale: they must be modified.

A few different ways of modifying the GR equations are possible. A lot of modified gravity theories start from a generalisation of the GR action:

$$\begin{aligned} S_{\mathrm{GR}} &= \frac{1}{16\pi G} \int \sqrt{-g}\; R\left[g_{\mu\nu}\right]\; \mathrm{d}^4x + S_{\mathrm{m}}\left[g_{\mu\nu}, \cdots\right] \qquad (1.146) \\ &= S_{\mathrm{EH}}\left[g_{\mu\nu}\right] + S_{\mathrm{m}}\left[g_{\mu\nu}, \cdots\right], \qquad (1.147) \end{aligned}$$

where $S_{\mathrm{EH}}\left[g_{\mu\nu}\right]$ is the Einstein–Hilbert action and $S_{\mathrm{m}}\left[g_{\mu\nu}, \cdots\right]$ is the action of the matter, universally and minimally coupled to the metric $g_{\mu\nu}$. It can be shown, in particular using Weinberg's theorems (*General Relativity (with a cosmological constant) is the unique local and Lorentz invariant theory describing an interacting single massless spin two particle that couples to matter*) that the Einstein–Hilbert action (see eq. (1.147)) is unique in 4D.

To write this section, we used refs [10, 42–48], in which many more information about modified gravity can be found.

[11] Since the waveform also depends on the number π (through the frequency, eq. (1.127)), it is even possible to measure it from GWs! And it was done in ref. [41]: $\pi = 3.115^{+0.048}_{-0.088}$. OK, it is not very accurate, but still!

1.5.1 Some models of modified gravity

To modify the GR action, eq. (1.147), various possibilities exist [42, 43]: adding new scalar, vector or tensor fields, see § **Additional fields**, page 29; introducing a massive graviton (giving a massive gravity theory), see § **Massive gravity**, page 31, breaking a fundamental assumption of GR, see § **Breaking fundamental assumptions**, page 32 or taking into account quantum corrections to the Einstein–Hilbert action, eq. (1.147), see § **Quantum corrections to the Einstein–Hilbert action**, page 32. The RR and RT models are theories of that latter type. We will introduce them in subsection 1.5.4. Some modified gravity theories lie in different categories, as bigravity that has a tensor field and is a massive gravity, but this categorisation is nice for a first look on modified gravity theories.

A sketch of the main modified gravity theories is given in fig. 1.6, but the theories that are called "non-local" in this figure break the locality principle, while the theories we call "nonlocal" in this document (the RR and RT models) *do not* break the locality of GR. We do not discuss here the modified gravity theories that break locality.

In the following we only consider the theories for which the velocity of GWs is c (the velocity of light): GW170817 along with its EM counterpart gave a bound to the velocity of GWs: $|c_{\rm GW} - c|/c < \mathcal{O}(10^{-15})$ [6], then we can say with high precision that $c_{\rm GW} = c$ (as GR predicts).

Additional fields

A first way to change the gravity equations consists in introducing fields that interact with the metric. These fields can be scalar, vector or tensor fields. As usual, scalar fields being the easiest case, let us start by them. Many scalar modified gravity theories are part of the class of *Horndeski theories of gravity* that have 2nd order derivatives in the action and 2nd order derivatives in the equations of movement (EoM). The general form of a Horndeski theory follows from the Horndeski action:

$$S_{\rm H} = \int \sqrt{-g}\left[\frac{1}{8\pi G}\sum_{i=2}^{5}\mathcal{L}_i\left[g_{\mu\nu},\phi\right] + \mathcal{L}_{\rm m}\left[g_{\mu\nu},\psi_{\rm m}\right]\right]\, {\rm d}^4x, \tag{1.148}$$

where G is the Newton's constant, $\mathcal{L}_{\rm m}$ is the Lagrangian density of the matter and we introduce the Lagrangian densities [45, 46]:

$$\mathcal{L}_2 = G_2(\phi, X) \tag{1.149}$$
$$\mathcal{L}_3 = G_3(\phi, X)\,\Box\phi \tag{1.150}$$
$$\mathcal{L}_4 = G_4(\phi, X)R - 2G_{4,X}(\phi, X)\left[(\Box\phi)^2 - \phi_{;\mu\nu}\phi^{;\mu\nu}\right] \tag{1.151}$$
$$\mathcal{L}_5 = G_5(\phi, X)G_{\mu\nu}\phi^{;\mu\nu} + \frac{1}{3}G_{5,X}(\phi, X)\left[(\Box\phi)^3 - 3\phi_{;\mu\nu}\phi^{;\mu\nu}\Box\phi + 2\phi_{;\mu}{}^{;\nu}\phi_{;\nu}{}^{;\alpha}\phi_{;\alpha}{}^{;\mu}\right], \tag{1.152}$$

R and $G_{\mu\nu}$ being the Ricci scalar and Einstein tensor of the Jordan frame[12] metric $g_{\mu\nu}$ and where as usual, comma indicate a partial derivative ∂ and semicolons indicate a covariant derivative ∇. We furthermore introduce:

$$X = g^{\mu\nu}\phi_{;\mu}\phi_{;\nu} \quad \text{and} \quad \Box\phi = g^{\mu\nu}\phi_{;\mu\nu}. \tag{1.153}$$

[12] In the Jordan frame, matter fields follow the geodesics obtained from the modified gravity equations while in the Einstein frame, the geodesics come from the Einstein's equations, but the matter fields do not follow these geodesics [49].

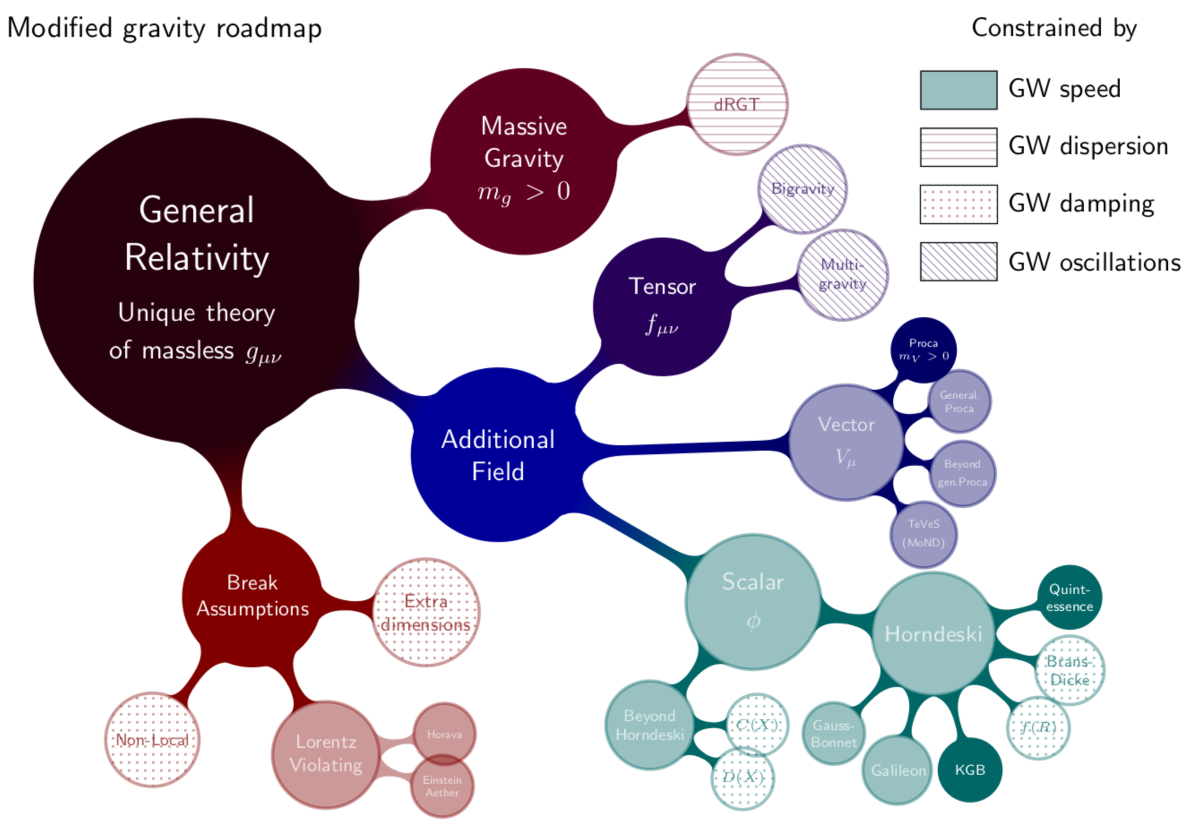

Figure 1.6: *A sketch of the main modified gravity theories. We introduce additional fields modified gravity theories in § **Additional fields**; massive gravity in § **Massive gravity** and breaking fundamental assumptions theories in § **Breaking fundamental assumptions**, but the non-local theories presented here* do not *correspond to the nonlocal theories we will discuss in § **Quantum corrections to the Einstein–Hilbert action**. All the theories in a light color (not only light green) are constrained by the GW speed: $|c_{GW} - 1| < \mathcal{O}(10^{-15})$. This figure is fig. 3 of Ezquiaga & Zumalacárregui, 2018, ref. [42].*

The functions G_i $(i = 2, \cdots, 5)$ are generic functions of X. Different Horndeski theories use different choices of functions G_i and of field ϕ. In a general Horndeski theory, tensor fluctuations (as the GWs) propagate at a velocity $v \neq c$. To guarantee $v = c$, we have to constrain:

$$G_{4,X} \approx 0 \quad \text{and} \quad G_5 \approx \text{const.} \tag{1.154}$$

As example of Horndeski theories, if only G_2 is non zero, we obtain a *k-essence theory*. On the other hand, the *Galileon theories* are based on the fact that for the Minkowski space, the only dynamical field is the scalar field. Furthermore they suppose that ϕ has the symmetry:

$$\phi_\mu \longmapsto \phi_\mu + c_\mu, \quad \text{with } c_\mu = \text{const.}, \tag{1.155}$$

and the Lagrangian densities $\mathcal{L}_i^{\text{Gal}}$ are given by [46]:

$$\mathcal{L}_2^{\mathrm{Gal}} = -\frac{1}{2}(\partial\phi)^2 \tag{1.156}$$
$$\mathcal{L}_3^{\mathrm{Gal}} = -\frac{1}{2}(\partial\phi)^2 \Box\phi \tag{1.157}$$
$$\mathcal{L}_4^{\mathrm{Gal}} = -\frac{1}{2}(\partial\phi)^2 \left[(\Box\phi)^2 - (\partial_\mu\partial_\nu\phi)^2\right] \tag{1.158}$$
$$\mathcal{L}_5^{\mathrm{Gal}} = -\frac{1}{4}(\partial\phi)^2 \left[(\Box\phi)^3 - 3\,\Box\phi\,(\partial_\mu\partial_\nu\phi)^2 + 2\,(\partial_\mu\partial_\nu\phi)^3\right], \tag{1.159}$$

since a flat Minkowski metric is used, the covariant derivative ∇ is the standard partial derivative ∂, in particular: $\Box\phi = \eta^{\mu\nu}\partial_\mu\partial_\nu\phi$. These Lagrangian densities give a second order derivatives EoM.

Other scalar fields theories have 2nd order derivatives in the action and higher orders derivatives in the EoM. These theories are called *beyond Horndeski theories* and an example of such theories is given by the Gleyzes–Langlois–Piazza–Vernizzi (GLPV) action [42]:

$$S_{\mathrm{BH}} = S_{\mathrm{H}} + \int \sqrt{-g}\,(\mathcal{B}_4 + \mathcal{B}_5)\ \mathrm{d}^4x, \tag{1.160}$$

where S_{H} is the Horndeski action, eq. (1.148), and where

$$\mathcal{B}_4 = F_4(\phi, X)\varepsilon^{\mu\nu\rho}{}_{\sigma}\varepsilon^{\mu'\nu'\rho'\sigma}\phi_{;\mu}\phi_{;\mu'}\phi_{;\nu\nu'}\phi_{;\rho\rho'} \tag{1.161}$$
$$\mathcal{B}_5 = F_5(\phi, X)\varepsilon^{\mu\nu\rho\sigma}\varepsilon^{\mu'\nu'\rho'\sigma'}\phi_{;\mu}\phi_{;\mu'}\phi_{;\nu\nu'}\phi_{;\rho\rho'}\phi_{;\sigma\sigma'} \tag{1.162}$$

with ε the Levi-Civita symbol, and with F_4 and F_5 two additional functions of ϕ and of X. In this latter action, the EoM contain 3rd order derivatives.

The added field can also be a vector field. In that case, one should be careful at the conservation of the isotropy of space. It is possible to conserve isotropy by using only vectors that point in the time direction (and that only depend of time):

$$A_\mu = (A_0(t), 0, 0, 0)\,, \tag{1.163}$$

or by considering that isotropy is only true in average: the background is isotropic in average, but tensor perturbations (as GWs) can have a remnant anisotropy. A Proca theory is obtained by adding a $m^2 A_\mu^2$ term to the Lagrangian (they need a massive tensor field with mass m). Another theory with vector field is the Tensor-Vector-Scalar (TeVeS) theory (a theory able to describe a Modified Newtonian Dynamics – MOND – and thus also an alternative to dark matter).

Massive gravity

Adding a mass to the graviton could explain the accelerated expansion of the Universe: the force mediated by a massive graviton has a finite range (as any force mediated by a massive boson): $V \sim (1/r)\exp(-r/\lambda_{\mathrm{g}})$, where λ_{g} is the Compton wavelength of the graviton. Hence for distances larger than $\lambda_{\mathrm{g}} = \hbar/\left(m_{\mathrm{g}}c^2\right)$, the gravitational force is weaker. For $m_{\mathrm{g}} \sim H_0$, then massive gravity causes acceleration of the expansion of the Universe at late time.

The *Ghost Free Massive Gravity* (also called de Rham–Gabadadze–Tolley, dRGT) model or *bigravity* models introduce a massive graviton. Bigravity models use a tensor additional field, they are then also often categorised as being *tensor additional fields* theories. See references of ref. [42] for more information.

However, from different experiments, the graviton's mass is constrained to:

$$m_{\mathrm{g}} \lesssim 10^{-30}\ \mathrm{eV} \quad [48]. \tag{1.164}$$

Breaking fundamental assumptions

It is also possible to reject part of the fundamental assumptions of GR: for example breaking the Lorentz invariance or introducing extra dimensions.

By introducing *extra dimensions*, one can include new operators constructed from the metric. Examples of these operators are given by the Lovelock invariants (see *e.g.* [14] for more information on the Lovelock's theorem in higher dimensions), such as the Gauss–Bonnet term, that do not contribute to the EoM. Of course higher dimensions never were observed yet, hence such modified gravity theories must include some mechanism to hide the higher dimensions to an observer. The higher dimensions can be compactified and then small enough to being not accessible to experimental tests. Another possibility is a Braneworld construction: our $3+1$ dimensions are embedded in a higher dimensional space. The Dvali–Gabadadze–Porrati (DGP) model is such a theory: it assumes a $4+1$ Minkowski space in which the $3+1$ Minkowski space is embedded. The 4D term in the action dominates at small scale, while the 5D term dominates at large scale. This model can give a self-accelerating term, thus explaining the accelerated expansion of the Universe.

Another assumption that can be broken is the *Lorentz invariance* (*i.e.* invariance under a Lorentz transformation). In these theories, the invariance is generally broken by the emergence of a preferred time direction. For example in the Hořava(–Lifshitz) gravity, the spacetime is foliated and space is separated from time at high energy, but the Lorentz symmetry holds for low energies.

Quantum corrections to the Einstein–Hilbert action

It is also possible to assume that the Einstein–Hilbert action of GR is the true classical action of gravity and to compute its quantum corrections in infrared (IR). If we want to compute a quantum gravity theory, the action we are interested in is the quantum effective action (*i.e.* the action whose variation determines the equations of motion of the vacuum expectations values of the quantum fields): for a scalar field $\varphi(x)$ in flat space with an action $S[\varphi]$, we can define the quantum effective (QE) action through a path integral formalism, by introducing the source $J(x)$ and the Green's function $G[J]$ [47] (in natural units with $c = \hbar = 1$):

$$\mathrm{e}^{\mathrm{i}G[J]} = \int \mathrm{e}^{\mathrm{i}S[\varphi]+\mathrm{i}\int J(x)\varphi(x)\ \mathrm{d}^D x}\ \mathcal{D}\varphi(x), \tag{1.165}$$

and the quantum effective action $\mathit{\Gamma}$ is a functional of the expectation value of the field: $\delta G[J]/\delta J(x) = \langle 0|\varphi(x)|0\rangle_J \equiv \phi[J]$ given in the functional form by:

$$\mathrm{e}^{\mathrm{i}\mathit{\Gamma}[\phi]} = \int \mathrm{e}^{\mathrm{i}S[\varphi+\phi]-\mathrm{i}\int (\delta\mathit{\Gamma}[\phi]/\delta\phi)\varphi(x)\ \mathrm{d}^D x}\ \mathcal{D}\varphi(x). \tag{1.166}$$

A property of such actions is that if the fundamental theory has massless particles, then the quantum effective action *must have* nonlocal terms. Gravity has a massless graviton, then it should also have nonlocal terms in its QE action. Typically, these models have nonlocal general functions: $Rf\left(\Box^{-1}R\right)$, and in particular linear terms: $R\left(m^2/\Box^2\right)R$. These nonlocal terms could in principle affect the infrared (IR) behaviour of the theory (*i.e.* the effects at low energy). A phenomenological approach can be used to understand these IR effects. One of the main effect of nonlocal terms is that they can describe a dynamical mass generation from quantum fluctuations (by quantum loops of massless particles): it is the m factor in the linear term $R\left(m^2/\Box^2\right)R$. We will see in more details two models of nonlocal modified gravity in subsection 1.5.4.

1.5.2 Propagation of GWs in modified gravities

We saw that the GWs free propagation is given in GR by equation (1.137):

$$\tilde{h}''_A + 2\mathcal{H}\tilde{h}'_A + c^2k^2\tilde{h}_A = 0. \tag{1.167}$$

Some theories of modified gravity predict variations from this propagation equation. There exists two ways to modify eq. (1.167): by changing the coefficient of the $\tilde{h}_A$ term or by changing the "friction term" (proportional to $\tilde{h}'_A$):

$$\tilde{h}''_A + 2\mathcal{H}\left[1-\delta(\eta)\right]\tilde{h}'_A + \left[c_{\mathrm{GW}}^2k^2 + a^2m_{\mathrm{g}}^2\right]\tilde{h}_A = 0, \tag{1.168}$$

where $\delta(\eta)$ (also sometimes denoted by $2\delta(\eta) = -\nu(\eta)$) is a function of the friction that depends on the modified gravity model, c_{GW} is the velocity of GWs and m_{g} is the mass of the graviton. As already said, we are considering here only modified gravity theories with $c_{\mathrm{GW}} = c$. We also consider massless graviton theories ($m_{\mathrm{g}} = 0$). Hence, we have the modified GWs propagation given in natural units ($c = 1$) by:

$$\tilde{h}''_A + 2\mathcal{H}\left[1-\delta(\eta)\right]\tilde{h}'_A + k^2\tilde{h}_A = 0. \tag{1.169}$$

By introducing $\tilde{\chi}_A(\eta, \boldsymbol{k})$ as (see *e.g.* ref. [21]):

$$\tilde{\chi}_A(\eta, \boldsymbol{k}) = \tilde{a}(\eta)\ \tilde{h}_A(\eta, \boldsymbol{k}), \tag{1.170}$$

where

$$\frac{\tilde{a}'}{\tilde{a}} = \mathcal{H}\left[1-\delta(\eta)\right] \equiv \tilde{\mathcal{H}}, \tag{1.171}$$

we can rewrite the free propagation of GWs as:

$$\tilde{\chi}''_A + \left(k^2 - \frac{\tilde{a}''}{\tilde{a}}\right)\ \tilde{\chi}_A = 0. \tag{1.172}$$

Inside the cosmological horizon, the term $\tilde{a}''/\tilde{a}$ is very small, hence we neglect it and thus GWs travel at the speed of light. But $\tilde{h}_A$ now decreases as $1/\tilde{a}$ instead of $1/a$. In GR, the polarisation modes follow (see eqs (1.130) and (1.131)):

$$h_A(t, z) = \frac{1}{d_{\mathrm{L}}(z)}\ g_A(t, z), \tag{1.173}$$

and in such modified gravity theories, we rather have:

$$h_A(t, z) = \frac{\tilde{a}(z)}{\tilde{a}(0)}\ \frac{a(0)}{a(z)}\ \frac{1}{d_{\mathrm{L}}(z)}\ g_A(t, z), \tag{1.174}$$

where as in eq. (1.80) we can normalise $\tilde{a}(0) = 1 = a(0)$:

$$h_A(t, z) = \frac{\tilde{a}(z)}{a(z)}\ \frac{1}{d_{\mathrm{L}}(z)}\ g_A(t, z), \tag{1.175}$$

(we see that if $\tilde{a} = a$, then we recover the GR formula). Gravitational waves in modified gravity theories hence measure a *gravitational wave luminosity distance*, defined by:

$$d_{\rm L}^{\rm GW}(z) \equiv \frac{a(z)}{\tilde{a}(z)}\, d_{\rm L}^{\rm EM}(z) \tag{1.176}$$

$$= \frac{1}{(1+z)\tilde{a}(z)}\, d_{\rm L}^{\rm EM}(z), \tag{1.177}$$

where $d_{\rm L}^{\rm EM}(z)$ is the "standard" luminosity distance, defined in eq. (1.85). We can rewrite eq. (1.171) as:

$$\frac{\mathrm{d}}{\mathrm{d}\eta}\log\left(\frac{a}{\tilde{a}}\right) = \delta(\eta)\mathcal{H}(\eta), \tag{1.178}$$

and then, by integrating over dz (see *e.g.* ref. [21], subsection 19.6.4):

$$d_{\rm L}^{\rm GW}(z) = d_{\rm L}^{\rm EM}(z)\ \exp\left\{-\int_0^z \frac{\delta(z')}{1+z'}\mathrm{d}z'\right\}. \tag{1.179}$$

Modified gravity theories give us another function that is testable with standard sirens: $\delta(z)$. So, in addition to the Hubble parameter H_0 and to the DE EoS $w_{\rm DE}(t)$, an important function can be constrained by standard sirens: $\delta(z)$, the two first describing the evolution of the background and the latter describing the evolution of GWs on the background. Various modified gravity models predict that $|\delta(z)| \sim |w(z)+1|$ [21], but the effects of $\delta(z)$ can give a dominant contribution with respect to $w_{\rm DE}(t)$ [9]. This deviation $\delta(z)$ between GR and modified gravity cannot be measured from "electromagnetic" cosmology, since it only affects gravity and not light.

The gravitational luminosity distance does not correspond to the distance between the source and the observer: it is still given by the EM luminosity distance $d_{\rm L}^{\rm EM}$ (or by the EM angular diameter distance, according to the definition of distance we are interested in).

1.5.3 The (Ξ_0, n) parametrisation

The function $\delta(z)$ can be hard to measure. It is easier to approximate it by a parametrisation, and to measure the values of its parameters.

Two main parametrisations are used. For the first one (ref. [12] uses the same kind of methodology as us (see chapter 2) applied to this parametrisation), the function $\delta(z)$ is parametrised by a single parameter, $c_{\rm M}$ and is supposed to be a friction term with dark energy:

$$[-2\delta(z)]_{\mathrm{param}(c_{\rm M})} \equiv [\nu(z)]_{\mathrm{param}(c_{\rm M})} = c_{\rm M}\frac{\Omega_{\rm DE}(z)}{\Omega_{\rm DE}(0)}, \tag{1.180}$$

where $\Omega_{\rm DE}(z) = \rho_{\rm DE}(z)/\rho_{\rm crit,0}$ (as in the eq. (1.114) following the definition given by eq. (1.110)). This one parameter parametrisation supposes that the $\delta(z)$ function is a constant friction with the dark energy. We do not use this parametrisation in this work.

Another parametrisation, introduced in ref. [9], is interested in parametrising the ratio $d_{\rm L}^{\rm GW}/d_{\rm L}^{\rm EM}$ (that is observable with standard sirens) instead of directly parametrise $\delta(z)$. It is a two parameters parametrisation:

$$\left[\frac{d_{\rm L}^{\rm GW}}{d_{\rm L}^{\rm EM}}\right]_{\mathrm{param}(\Xi_0,n)} \equiv \Xi_0 + \frac{1-\Xi_0}{(1+z)^n} = \Xi(z;\Xi_0,n). \tag{1.181}$$

Since eq. (1.179) can be inverted as:

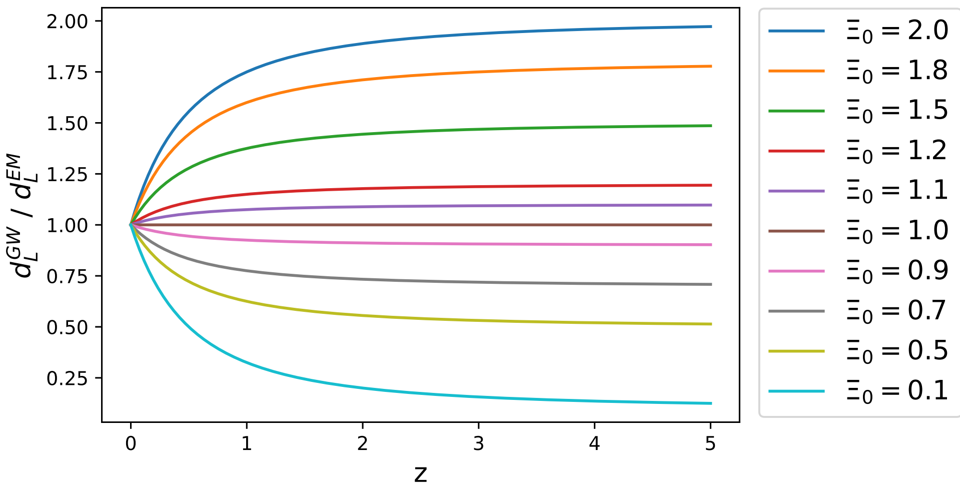

Figure 1.7: *Plot of the ratio d_L^{GW}/d_L^{EM} as a function of the redshift z for different values of Ξ_0 (with $n = 2$).*

$$\delta(z) = -(1+z)\,\frac{\mathrm{d}}{\mathrm{d}z}\log\left(\frac{d_{\mathrm{L}}^{\mathrm{GW}}}{d_{\mathrm{L}}^{\mathrm{EM}}}\right), \tag{1.182}$$

we get:

$$[\delta(z)]_{\mathrm{param}(\Xi_0,n)} = \frac{n(1-\Xi_0)}{1-\Xi_0+\Xi_0(1+z)^n}. \tag{1.183}$$

The GR prediction is a special case of this (Ξ_0, n) parametrisation: indeed taking $\Xi_0 = 1$ (and n finite), one gets $d_{\mathrm{L}}^{\mathrm{GW}}/d_{\mathrm{L}}^{\mathrm{EM}} = 1$ and $\delta(z) = 0$. This parametrisation reproduces the fact that when z is small, the ratio $d_{\mathrm{L}}^{\mathrm{GW}}/d_{\mathrm{L}}^{\mathrm{EM}}$ goes to 1, since modified gravity propagation does not act enough to be measurable. On the other hand, when z becomes infinite, the luminosity distances ratio goes to the constant Ξ_0, and that is consistent with most modified gravity scenarios (they generally predict that deviations from GR only appears in a recent cosmological epoch, see discussion of ref. [10]). The parameter Ξ_0 is then the most important parameter of this parametrisation, it gives the magnitude of the effects of modified gravity, while the parameter n gives the power-law shape between the two extremes: $d_{\mathrm{L}}^{\mathrm{GW}}/d_{\mathrm{L}}^{\mathrm{EM}} = 1$ and $d_{\mathrm{L}}^{\mathrm{GW}}/d_{\mathrm{L}}^{\mathrm{EM}} = \Xi_0$. The parameter n is generally ~ 2 [10, 45]. The ratio $d_{\mathrm{L}}^{\mathrm{GW}}/d_{\mathrm{L}}^{\mathrm{EM}}$ as a function of the redshift z is plotted in fig. 1.7 for different values of Ξ_0 (taking $n = 2$). The limit behaviours $z \to 0$ and $z \to \infty$ of the ratio $\Xi(z)$ are clearly visible on fig. 1.7.

This two parameters parametrisation works very well for most modified gravity models (as shown in ref. [45]), and particularly for the RR and RT models (for which this parametrisation was introduced in ref. [9]), see subsection 1.5.4.

In ref. [45], one can find a few examples of modified gravity models with their respective analytical expressions for Ξ_0 and for n.

1.5.4 The RR & RT nonlocal models

In this subsection, we present two nonlocal modified gravity models that have been proposed and studied in the past years by the Michele Maggiore's group at the University of Geneva. The review ref. [43] presents many more details about these models, their implications and their tests.

These two models come from the same idea: we start from linearized GR with introduction of nonlocal mass terms. In this case, the quadratic quantum effective action has the form [43]:

$$\Gamma^{(2)} = \frac{1}{64\pi G} \int \left[h_{\mu\nu} \mathcal{E}^{\mu\nu,\rho\sigma} h_{\rho\sigma} - \frac{2}{3} m^2 \left(P^{\mu\nu} h_{\mu\nu}\right)^2 \right] \, \mathrm{d}^4 x, \tag{1.184}$$

where $\mathcal{E}^{\mu\nu,\rho\sigma}$ is the Lichnerowicz operator and where we introduce the projector $P^{\mu\nu} = \eta^{\mu\nu} - (\partial^\mu \partial^\nu \Box)$. The Einstein's equations take the form:

$$\mathcal{E}^{\mu\nu,\rho\sigma} h_{\rho\sigma} - \frac{2}{3} m^2 P^{\mu\nu} P^{\rho\sigma} h_{\rho\sigma} = -16\pi G T^{\mu\nu}. \tag{1.185}$$

To obtain a nonlocal gravity model, one then needs to covariantize either eq. (1.184) or eq. (1.185) in order to obtain a covariant theory of gravity.

The RR model

The RR model (also called Maggiore–Mancarella model), proposed in refs [50, 51] starts from the covariantization of the quantum effective action (1.184).

To covariantize eq. (1.184), we match:

$$\frac{1}{4} h_{\mu\nu} \mathcal{E}^{\mu\nu,\rho\sigma} h_{\rho\sigma} \, \mathrm{d}^4 x \longleftrightarrow \sqrt{-g} R \, \mathrm{d}^4 x \tag{1.186}$$

while $(P^{\mu\nu} h_{\mu\nu})^2 = \left(\Box_\eta^{-1} R^{(1)}\right)^2 \longleftrightarrow \left(\Box^{-1} R\right)^2$ (with $R^{(1)}$ being the Ricci scalar at linear level) and we obtain:

$$\Gamma_{\mathrm{RR}} = \frac{m_{\mathrm{Pl}}^2}{2} \int \sqrt{-g} \left[R - \frac{m^2}{6} \left(\Box^{-1} R\right)^2 \right] \, \mathrm{d}^4 x \tag{1.187}$$

$$= \frac{m_{\mathrm{Pl}}^2}{2} \int \sqrt{-g} \left[R - \frac{m^2}{6} R \frac{1}{\Box^2} R \right] \, \mathrm{d}^4 x, \tag{1.188}$$

where m_{Pl} is the reduced Planck mass ($= (\hbar c/8\pi G)^{1/2} \approx 2.4 \times 10^{18}$ GeV/$c^2 \approx 4.3$ µg) and m is the mass parameter created by the quantum fluctuations. This mass parameter replaces the cosmological constant Λ of the ΛCDM model. This model is not really a "modified gravity" theory because it does not change the Einstein–Hilbert action as being the fundamental theory of gravity, but just takes into account its leading quantum effects in the IR domain. The "RR" of the name comes from the fact that the Ricci scalar is present twice in the quantum correction of the classical action.

To check the predictions of this QE action, it is useful to introduce two auxiliary fields:

$$U = -\Box^{-1} R \quad \text{and} \quad S = -\Box^{-1} U, \tag{1.189}$$

so that

$$\Gamma_{\mathrm{RR}} = \frac{m_{\mathrm{Pl}}^2}{2} \int \sqrt{-g} \left[R - \frac{m^2}{6} R S \right] \, \mathrm{d}^4 x. \tag{1.190}$$

The EoM can then be numerically integrated and one finds that the Friedmann equation takes the form:

$$H(a) = H_0 \left[\Omega_{\mathrm{r},0} a^{-4} + \Omega_{\mathrm{m},0} a^{-3} + \Omega_{\mathrm{DE},0} \right]^{1/2}, \tag{1.191}$$

with $\Omega_{\mathrm{DE},0}$ being governed by the cosmological evolutions of the auxiliary fields U and S. The nonlocal term gives a dynamical DE, which generates an accelerated expansion of the Universe

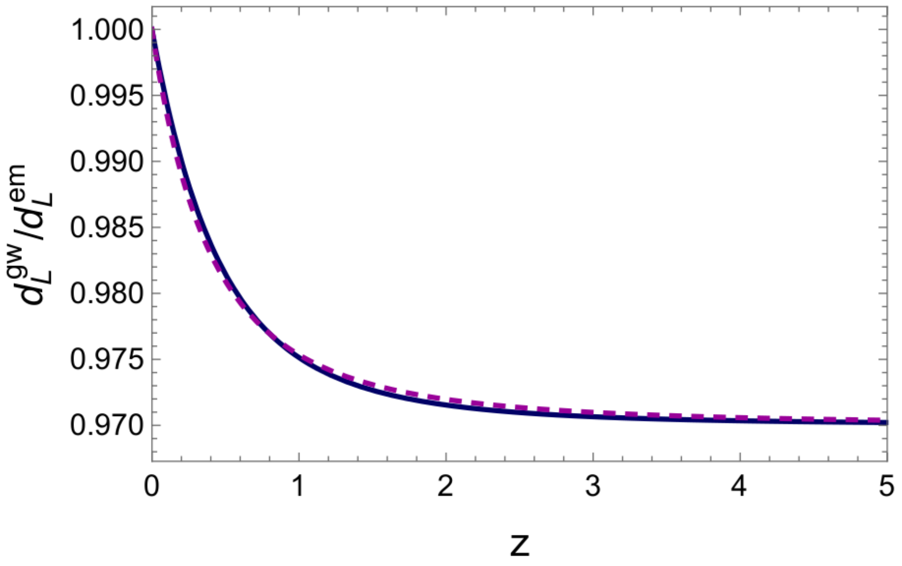

Figure 1.8: *Plot of the ratio d_L^{GW}/d_L^{EM} (solid line) and of its (Ξ_0, n) parametrisation (dotted line) for the RR (Maggiore–Mancarella) model. This figure is fig. 3 of Belgacem* et al.*, 2018, ref. [9].*

in the recent cosmological epoch. Its EoS gives $w(z) < -1$ (this is a phantom dark energy). In § **Tests of the RR & RT models**, we will see how the RR model's predictions fit cosmological data.

Another interesting aspect of the RR model is that it gives a non-trivial propagation equation for GWs. Indeed for the function $\delta(\eta)$ (see eq. (1.169)), the RR model gives:

$$\delta(\eta) = \frac{3\gamma \left[\mathrm{d}\bar{V} / \mathrm{d}(\log a)\right]}{2\left(1 - 3\gamma\bar{V}\right)}, \tag{1.192}$$

where $\bar{V}$ is the background evolution of the auxiliary dimensionless field $V = H_0^2 S$ and where $\gamma = m^2 / \left(9H_0^2\right)$.

When applying a (Ξ_0, n) parametrisation (see eq. (1.181)), one finds that the parametrisation is very good (this parametrisation was indeed introduced to fit the RR model), with $n \approx 5/2$ and $\Xi_0 \approx 0.970$ [9], see fig. 1.8 (in that case, since $\Xi_0 < 1$, the GW luminosity distance is smaller than the EM luminosity distance (the "classic" one)).

The RT model

Unlike the RR model, the RT model starts from the covariantization of the Einstein's equation eq. (1.185). In order to do so, we use again the match $(P^{\mu\nu}h_{\mu\nu})^2 = \left(\Box_\eta^{-1}R^{(1)}\right)^2 \longleftrightarrow \left(\Box^{-1}R\right)^2$ and also the linear order of the Einstein tensor: $G_{\mu\nu}^{(1)} = -\left(1/2\right)\mathcal{E}_{\mu\nu,\rho\sigma}h^{\rho\sigma}$. Therefore, eq. (1.185) is equivalent to:

$$-2G_{\mu\nu}^{(1)} + \frac{2}{3}m^2 P_{\mu\nu}\Box_\eta^{-1}R^{(1)} = -16\pi G T_{\mu\nu}. \tag{1.193}$$

At linear order over the flat Minkowski space, $P_{\mu\nu}\Box_\eta^{-1}R^{(1)}$ is the same as the transverse part of the tensor $\left(\eta_{\mu\nu}\Box_\eta^{-1}R^{(1)}\right)$, thus, eq. (1.193) can be written as:

$$G^{(1)}_{\mu\nu} - \frac{1}{3}m^2 \left(\eta_{\mu\nu}\Box^{-1}_\eta R^{(1)}\right)^{\mathrm{T}} = 8\pi G T_{\mu\nu}, \tag{1.194}$$

and that is easily covariantized as:

$$G_{\mu\nu} - \frac{m^2}{3}\left(g_{\mu\nu}\Box^{-1}R\right)^{\mathrm{T}} = 8\pi G T_{\mu\nu}, \tag{1.195}$$

where again, m is a mass term created by quantum perturbations. This model is the "RT model" (the 'R' signifying "one Ricci scalar", the 'T' because it takes the transverse part of $(g_{\mu\nu}\Box^{-1}R)$).

The RT model was also proposed from ref. [51] and is very well discussed in ref. [43].

Like the RR model, RT shows a viable cosmological evolution. In a FLRW metric, eq. (1.70), the Friedmann equations become [43]:

$$H^2 - \frac{m^2}{9}\left(U - \dot{S}_0\right) = \frac{8\pi G}{3}\rho \tag{1.196}$$

$$\ddot{U} + 3H\dot{U} = 6\dot{H} + 12H^2 \tag{1.197}$$

$$\ddot{S}_0 + 3H\dot{S}_0 - 3H^2 S_0 = \dot{U}, \tag{1.198}$$

where the auxiliary fields S and U are defined as for the RR model (see eq. (1.189)) and we get:

$$H(x) = H_0\left[\Omega_{\mathrm{r},0}\ \mathrm{e}^{-4x} + \Omega_{\mathrm{m},0}\ \mathrm{e}^{-3x} + \gamma Y(x)\right]^{1/2}, \tag{1.199}$$

where we wrote $x = \ln a(t)$, $\gamma = m^2/(9H_0^2)$ and $Y = U - \dot{S}_0$. Like the RR model, the RT model has a dynamical phantom dark energy: $w_{\mathrm{DE}}(t) < -1$.

The RT nonlocal model also predicts a non-trivial propagation of GWs, with:

$$\delta(\eta) = \frac{m^2\bar{S}_0(\eta)}{6H(\eta)}, \tag{1.200}$$

where $\bar{S}_0$ is the background cosmological solution for the field S_0. Equation (1.200) depends on the number ΔN of e-folds before the end of the inflation, and for a large number of e-folds, Ξ_0 saturates to $\Xi_0 \approx 1.8$. (In that case, since $\Xi_0 > 1$, the GW luminosity distance is larger than the EM luminosity distance.)

Tests of the RR & RT models

We saw in the previous paragraphs that the RR and RT nonlocal models predict an accelerating expansion of the Universe along with a non trivial GWs propagation ($\delta(\eta) \neq 0$). These models have been compared with data in a few articles, in particular ref. [52], that we quickly summarise here. For more information see directly ref. [52].

To test the values of parameters in a theory given some data, one needs to perform Bayesian inferences (see chapter 2), generally together with a Markov chain Monte Carlo technique (MCMC) to compute the values (see appendix A for an introduction to MCMC). This is exactly what was done in ref. [52] to test the RR and RT models, using different datasets:

- **CMB:** the *Planck* satellite measured the Cosmic Microwave Background with high precision [53]. From the angular power spectrum of the CMB one can infer the values of cosmological parameters. In ref. [52], the authors use the 2015 values of *Planck* (see ref. [53]);

- **Type Ia SNae:** type Ia supernovae are used as standard candles. In ref. [52], the authors use the SDSS-II/SNLS3 Joint Light-curve Analysis (JLA);
- **BAO:** the Baryon Acoustic Oscillations from different datasets are used in ref. [52] (see references [91-93] of ref. [52]);
- H_0 **prior:** two different prior ranges for H_0 (see chapter 2) are used in ref. [52]: $H_0 = 70.6 \pm 3.3$ km s^{-1} Mpc^{-1} and $H_0 = 73.8 \pm 2.4$ km s^{-1} Mpc^{-1}.

Bayesian inference is done over the six independent parameters of the flat ΛCDM model:

$$\theta = \{H_0, \omega_{\rm b}, \omega_{\rm c}, A_s, n_s, \tau_{\rm re}\}\,, \tag{1.201}$$

where $H_0 = 100h_0$ km s^{-1} Mpc^{-1} is the Hubble constant, $\omega_{\rm b} = h_0^2\Omega_{\rm b}$ and $\omega_{\rm c} = h_0^2\Omega_{\rm c}$ being the physical baryon (b) and cold dark matter (c) density fractions today, A_s the amplitude of the primordial scalar perturbation, n_s the spectral tilt and $\tau_{\rm re}$ the reionization optical depth.

By choosing a flat prior on each parameter (except for $\tau_{\rm re}$ that is bounded from below at the value of 0.01), ref. [52] obtains the values presented in fig. 1.9.

In fig. 1.9, in addition to the six independent parameters of the flat ΛCDM model, eq. (1.201), are also indicated σ_8, the present root-mean-square matter fluctuation averaged over a sphere of radius 8 h_0^{-1} Mpc and $z_{\rm re}$, the redshift of reionization, and more important, the results of a χ^2 test. This test allows comparisons between two models $\mathcal{M}_i$ and $\mathcal{M}_j$ for their respective goodness to fit data. To do this, one defines $|\Delta\chi^2_{ij}| = |\chi^2_{{\rm min},i} - \chi^2_{{\rm min},j}|$, and the larger the value of $|\Delta\chi^2_{ij}|$, the higher the evidence for the model ($\mathcal{M}_i$ or $\mathcal{M}_j$) with the smallest goodness-to-fit $\chi^2_{\rm min}$. In ref. [52], the following thresholds are quoted: $|\Delta\chi^2_{ij}| \leq 2$ implies a statistical equivalence between the models $\mathcal{M}_i$ and $\mathcal{M}_j$, while $2 \lesssim |\Delta\chi^2_{ij}| \lesssim 6$ is a "weak" evidence and $|\Delta\chi^2_{ij}| \gtrsim 6$ is a "strong" evidence for one model over the other.

When RR and RT models are compared with ΛCDM, one finds that each model fit data of the cosmic microwave background (CMB), baryon acoustic oscillations (BAO) and type Ia SNe at the same accuracy (within the statistical interval) for the same number of parameters. It is also interesting to note that the RR and RT nonlocal models give a higher value for H_0 than ΛCDM, this reducing the Hubble tension between local measurements (with type Ia SNe) and global measurements (with CMB and BAO) (see note 10 page 27).

However, another test must be taken into account against the RR model: the Lunar Laser Ranging (LLR). For sub-horizon modes, the RR model implies a time variation of the Newton's constant (see ref. [43]):

$$\frac{G_{\rm eff}(t)}{G} = \left[1 - \frac{1}{3}m^2\bar{S}(t)\right]^{-1}\left[1 + \mathcal{O}\left(\frac{1}{\hat{k}^2}\right)\right], \tag{1.202}$$

where $\bar{S}(t)$ is the background cosmological solution for the auxiliary field S, see eq. (1.189). By setting the value of $\bar{S}(t)$ that corresponds to a FLRW background, one finds that $G_{\rm eff}(t)/G \sim H_0$. But the LLR (the measurement of the Earth–Moon distance using lasers and the retroreflectors installed on the Moon by Apollo 11, 14 and 15 and by Lunokhod 1 and 2) is so precise that even at the Earth–Moon scale over five decades, it gives a bound on the evolution of the Newton's constant [43]:

$$\frac{\dot{G}}{G} = (0.99 \pm 1.06) \times 10^{-3}\left(\frac{0.7}{h_0}\right) H_0. \tag{1.203}$$

	Planck			BAO+Planck+JLA		
Param	ΛCDM	RT	RR	ΛCDM	RT	RR
$100\ \omega_b$	$2.225^{+0.016}_{-0.016}$	$2.224^{+0.016}_{-0.016}$	$2.227^{+0.016}_{-0.016}$	$2.228^{+0.014}_{-0.015}$	$2.223^{+0.014}_{-0.014}$	$2.213^{+0.014}_{-0.014}$
ω_c	$0.1194^{+0.0014}_{-0.0015}$	$0.1195^{+0.0014}_{-0.0015}$	$0.1191^{+0.0014}_{-0.0015}$	$0.119^{+0.0011}_{-0.0011}$	$0.1197^{+0.0011}_{-0.00096}$	$0.121^{+0.001}_{-0.001}$
H_0	$67.5^{+0.65}_{-0.66}$	$68.86^{+0.69}_{-0.7}$	$71.51^{+0.81}_{-0.84}$	$67.67^{+0.47}_{-0.5}$	$68.76^{+0.46}_{-0.51}$	$70.44^{+0.56}_{-0.56}$
$\ln(10^{10}A_s)$	$3.064^{+0.025}_{-0.025}$	$3.057^{+0.026}_{-0.026}$	$3.047^{+0.026}_{-0.025}$	$3.066^{+0.019}_{-0.026}$	$3.056^{+0.021}_{-0.023}$	$3.027^{+0.027}_{-0.023}$
n_s	$0.9647^{+0.0048}_{-0.0049}$	$0.9643^{+0.0049}_{-0.005}$	$0.9649^{+0.0049}_{-0.0049}$	$0.9656^{+0.0041}_{-0.0043}$	$0.9637^{+0.0039}_{-0.0041}$	$0.9601^{+0.004}_{-0.0039}$
$\tau_{\rm re}$	$0.0653^{+0.014}_{-0.014}$	$0.06221^{+0.014}_{-0.014}$	$0.05733^{+0.014}_{-0.014}$	$0.06678^{+0.011}_{-0.013}$	$0.0611^{+0.011}_{-0.013}$	$0.04516^{+0.014}_{-0.012}$
$z_{\rm re}$	$8.752^{+1.4}_{-1.2}$	$8.442^{+1.5}_{-1.2}$	$7.932^{+1.5}_{-1.2}$	$8.893^{+1.1}_{-1.2}$	$8.359^{+1.2}_{-1.2}$	$6.707^{+1.7}_{-1.2}$
σ_8	$0.8171^{+0.0089}_{-0.0089}$	$0.8283^{+0.0092}_{-0.0096}$	$0.8487^{+0.0097}_{-0.0096}$	$0.817^{+0.0076}_{-0.0095}$	$0.8283^{+0.0085}_{-0.0093}$	$0.8443^{+0.01}_{-0.0099}$
$\chi^2_{\rm min}$	12943.3	12943.1	12941.7	13631.0	13631.6	13637.0
$\Delta\chi^2_{\rm min}$	1.6	1.4	0	0	0.6	6.0

	BAO+Planck+JLA+($\mathrm{H}_0 = 70.6$)			BAO+Planck+JLA+($\mathrm{H}_0 = 73.8$)		
Param	ΛCDM	RT	RR	ΛCDM	RT	RR
$100\ \omega_b$	$2.229^{+0.014}_{-0.015}$	$2.223^{+0.014}_{-0.014}$	$2.215^{+0.014}_{-0.014}$	$2.233^{+0.014}_{-0.014}$	$2.226^{+0.014}_{-0.014}$	$2.217^{+0.014}_{-0.014}$
ω_c	$0.1188^{+0.001}_{-0.0011}$	$0.1197^{+0.001}_{-0.0011}$	$0.1208^{+0.00099}_{-0.001}$	$0.1185^{+0.00097}_{-0.0011}$	$0.1194^{+0.001}_{-0.001}$	$0.1207^{+0.00096}_{-0.00097}$
H_0	$67.75^{+0.48}_{-0.47}$	$68.75^{+0.49}_{-0.48}$	$70.57^{+0.54}_{-0.56}$	$67.93^{+0.48}_{-0.43}$	$68.91^{+0.49}_{-0.5}$	$70.65^{+0.52}_{-0.54}$
$\log(10^{10}A_s)$	$3.069^{+0.024}_{-0.024}$	$3.056^{+0.026}_{-0.022}$	$3.03^{+0.021}_{-0.021}$	$3.077^{+0.026}_{-0.019}$	$3.061^{+0.026}_{-0.022}$	$3.031^{+0.018}_{-0.022}$
n_s	$0.9662^{+0.0042}_{-0.0042}$	$0.9637^{+0.0041}_{-0.0042}$	$0.9607^{+0.0039}_{-0.0041}$	$0.9671^{+0.0041}_{-0.0041}$	$0.9645^{+0.004}_{-0.0041}$	$0.9611^{+0.0038}_{-0.004}$
$\tau_{\rm re}$	$0.06883^{+0.012}_{-0.013}$	$0.06099^{+0.014}_{-0.011}$	$0.04701^{+0.011}_{-0.011}$	$0.07275^{+0.014}_{-0.01}$	$0.0641^{+0.013}_{-0.012}$	$0.04791^{+0.01}_{-0.011}$
$z_{\rm re}$	$9.081^{+1.2}_{-1.1}$	$8.341^{+1.4}_{-1}$	$6.922^{+1.3}_{-1.1}$	$9.435^{+1.3}_{-0.85}$	$8.636^{+1.3}_{-1.1}$	$7.02^{+1.1}_{-1.2}$
σ_8	$0.8179^{+0.0089}_{-0.0089}$	$0.8283^{+0.0095}_{-0.0089}$	$0.8452^{+0.0085}_{-0.0086}$	$0.8197^{+0.0096}_{-0.0075}$	$0.8298^{+0.0095}_{-0.0086}$	$0.8456^{+0.0081}_{-0.0088}$
$\chi^2_{\rm min}$	13631.9	13631.9	13637.0	13637.5	13636.1	13638.9
$\Delta\chi^2_{\rm min}$	0	0	5.1	1.4	0	2.8

Figure 1.9: *Parameter tables for ΛCDM and for the RR and RT non-local models. This figure is table 1 of Dirian* et al.*, 2016, ref. [52].*

The RR model does not have any screening mechanism that could explain that the time variation of the Newton's constant cannot appear at a small scale. Then it does not pass this test. On the other hand, the RT model does not give a time dependence to G_{eff}, hence it trivially satisfies the LLR limit. In more recent works, *e.g.* ref. [10], only the RT model is considered.

1.6 Binary Black Holes populations

In this last section of the chapter, we quickly introduce some Binary Black Holes (BBHs) populations. As we saw in sections 1.3 and 1.4, one can use the cosmological redshift of the masses along with the standard siren property of the GW to constrain cosmological parameters (it is then a *dark siren*). However, in order to be able to measure the redshift from the detected mass, one has to know the corresponding source-frame mass. Of course it is not possible event by event, but if one has enough events, the detected mass population can be compared with the modeled mass population in source-frame. Let us see some mass population models (see *e.g.* ref. [54] that gives a little review and ref. [55] that is a recent proposed model).

Gravitational waves have already give us many new information about population of black holes. The main result is that stellar-mass black holes are in average heavier that we previously thought, with an average mass of $\mathcal{O}(40)$ $\mathrm{M}_\odot$ (instead of $\mathcal{O}(10)$ $\mathrm{M}_\odot$ as previously believed; see fig. 1.10, where the violet dots show the previously known BHs and the blue dots the new discovered BHs). We now have enough samples to sketch the BBHs mass population (see *e.g.* ref. [54]).

There are three main types of BHs: astrophysical (formed by the collapse of a star), primordial (formed by a density fluctuation during the radiation domination area of the Universe) and intermediate-mass/supermassive. Only the first two types of black holes' coalescences are accessible to ground-based GW detectors: the frequencies of the gravitational waves that supermassive BHs emit when they merge are from far not high enough to be detected with current detectors, but will be detectable with LISA (see fig. 1.4). Like the LIGO/Virgo collaborations (LVC) (see *e.g.* ref. [54]), we only consider astrophysical black holes (*i.e.* we assume that all the GWs that are yet detected come either from a Neutron star–Neutron star (NS–NS) merger, or from a Neutron star–astrophysical BH (NS–BH) merger, or from an astrophysical BH–astrophysical BH (BH–BH) merger. We only consider the latter case).

This choice can be justified: astrophysical BHs are pretty common and lies in the good range of masses. Furthermore the theoretical understanding of the astrophysical Schwarzschild BHs is really strong so that we are certain that BHs can be formed from a collapsed dying star. For primordial black holes (PBHs), it is harder: some PBHs could have the good mass to be detected by the LVC surveys (some detected GWs are indeed consistent with a PBHs origin, see ref. [57]) but this hypothesis is not needed to explain the detections. Furthermore the mass populations are adjustable enough to take into account a few PBHs in the detections. In a first work we can then simply neglect the PBHs scenario.

In the following, we use the convention where m_1 is the mass of the heavier black hole and m_2 the mass of the lighter black hole of the binary.

There are two behaviours for extremes masses BHs. The easiest is the low-mass limit. When a low-mass star collapses, it can form a white dwarf (that is what will happen to our Sun) or a neutron star. The Tolman–Oppenheimer–Volkoff limit says that only remnant stars with a mass higher than ~ 3 $\mathrm{M}_\odot$ will form a black hole. The second behaviour is for the large-mass limit. Very massive stars (with initial mass $M_{\mathrm{i}} \sim 130-250$ $\mathrm{M}_\odot$) ends their star life by a pair-instability supernova (PISN): some γ-rays produced in the star core have enough energy (> 1.022 MeV)

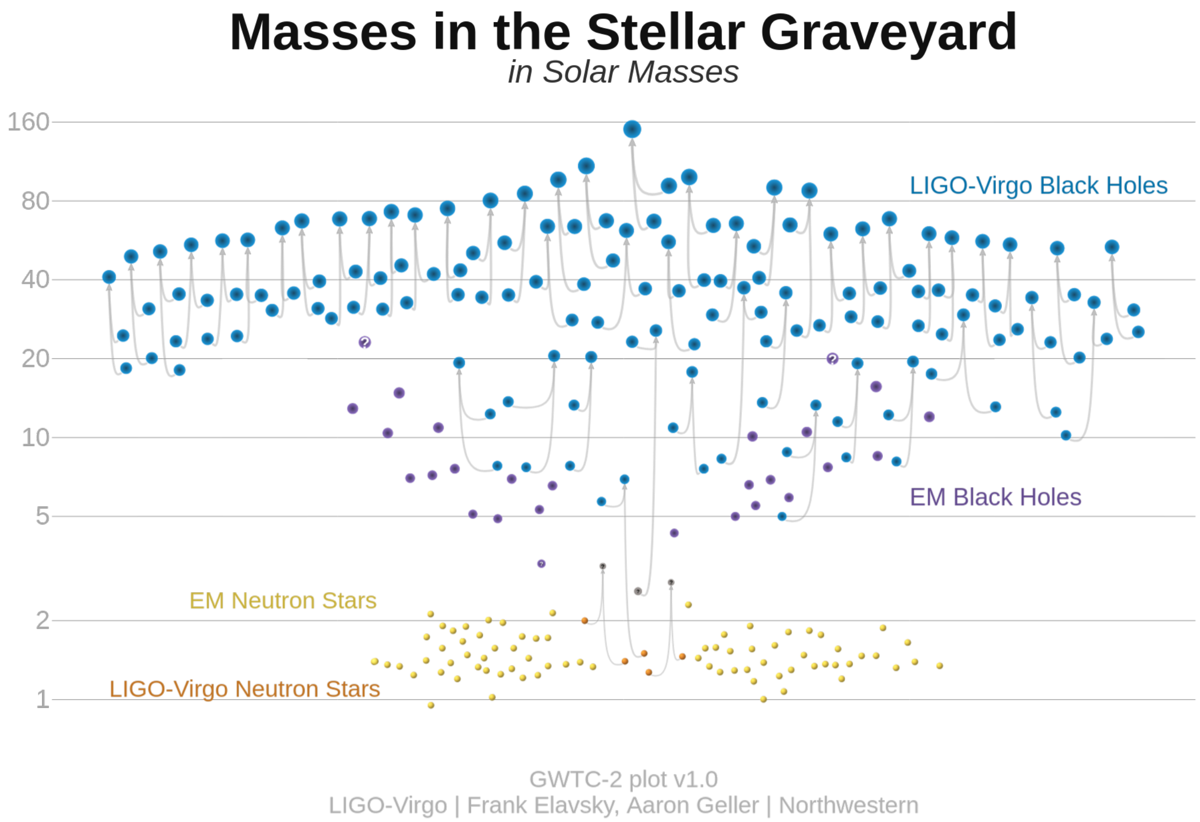

Figure 1.10: *"Masses in the Stellar Graveyard"* (i.e. *we indeed assume that these BHs are from stellar origin). The blue dots show the BHs discovered by GWs: two BHs merge into a third BH, this process is shown by the gray arrows. Violet dots indicate the BHs that are known from EM waves (generally BHs in a binary system with a star, thus emitting X-rays). As for the BHs, the neutron stars are known from GWs: they merge into another body (orange dots), and from EM observations (yellow dots). Figure of LIGO-Virgo, Northwestern, Frank Elavsky, Aaron Geller (Originally designed and developed by Frank Elavsky at Northwestern IT Data collection by Frank Elavsky, Aaron Geller and CIERA Layout and maintenance by Aaron Geller) [56].*

to produce an electron-positron pair. Hence the radiation energy decreases, the core collapses, the temperature increases, more γ-rays have enough energy to produce electron-positron pair, etc. This process is unstable and ends by a thermonuclear-type explosion of the star, that leaves no black hole. The PISN predicts that astrophysical black holes with a mass higher than $m_{\max} \sim 50 - 150\ \mathrm{M}_\odot$ cannot exist. For even larger masses, non astrophysical BHs are expected to be found. It is this gap between mass of stellar BHs and intermediate mass BHs that is called the *black hole mass gap*. However some BHs have already been found in the gap (in particular GW190521 that we will discuss in more details in subsection 3.3.1). A few hypotheses exist to explain these BHs: it could be second generation BHs (*i.e.* a black hole that is formed by the previous merge of two stellar BHs) or a primordial BH (as suggested for GW190521 in ref. [57]).

Let us see now some examples of mass population functions for astrophysical BBHs that are used (taken from refs [11, 54]), theses functions for m_1 are plotted in fig. 1.11. There also exists spin population functions, but as we said in the subsection 1.1.2, the spin only affects the 2PN expansion of the amplitude, so we neglect them in the present work.

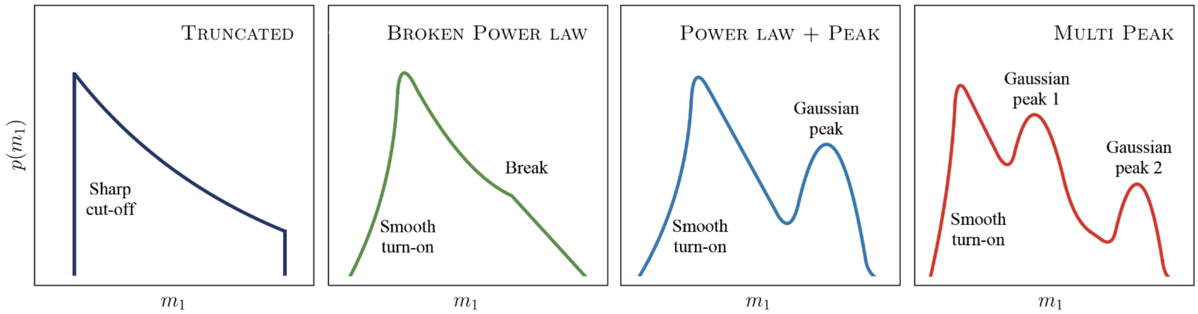

Figure 1.11: *Sketches of some BBH mass populations for the heavier mass m_1 of the binary. We do not discuss the "multi peak mass model" here, for more information see [54]. This figure is fig. 1 of Abbott* et al. *(LVC), 2021, ref. [54].*

- **Truncated mass model** [54] has four independent parameters and:

$$p_{\rm pop}(m_1|\alpha, m_{\rm min}, m_{\rm max}) \propto m_1^{-\alpha}\ \Theta(m_{\rm max} - m_1)\ \Theta(m_1 - m_{\rm min}), \tag{1.204}$$

while the mass-ratio $q \equiv m_2/m_1$ follows

$$p_{\rm pop}(q|\beta_q, m_{\rm min}, m_1) \propto q^{\beta_q}\ \Theta(m_2 - m_{\rm min})\ \Theta(m_1 - m_2). \tag{1.205}$$

- **"Smoothed truncated mass model"** (proposed in ref. [11], similar to the "Broken Power Law mass model" [54], see below) has six independent parameters (it is the truncated mass model but with a smoothing on the mass gaps):

$$\begin{aligned} p_{\rm pop}(m_1, m_2|\alpha, \beta, m_l, m_h, \sigma_l, \sigma_h) \propto\ & m_1^{-\alpha}\ m_2^{\beta}\ \Theta(m_1 - m_2) \\ & \times f_{\rm smooth}(m_1|m_l, \sigma_l, m_h, \sigma_h)\ f_{\rm smooth}(m_2|m_l, \sigma_l, m_h, \sigma_h), \end{aligned} \tag{1.206}$$

with

$$f_{\rm smooth}(m_i|m_l, \sigma_l, m_h, \sigma_h) = \Phi\left(\frac{\ln(m/m_l)}{\sigma_l}\right)\left[1 - \Phi\left(\frac{\ln(m/m_h)}{\sigma_h}\right)\right], \tag{1.207}$$

where $\Phi(x)$ is the standard normal cumulative distribution function (see subsection 2.4.1);

- **Power Law + Peak mass model** [54] (also discussed in ref. [55]) has eight independent parameters. It is a power law model (as the last two) but it also has a Gaussian peak. The model is given by

$$\begin{aligned} p_{\rm pop}(m_1|\lambda_{\rm peak}, \alpha, m_{\rm min}, \delta_m, m_{\rm max}, \mu_m, \sigma_m) = & \left[(1 - \lambda_{\rm peak})\,\mathcal{P}(m_1|(-\alpha), m_{\rm max})\right. \\ & \left.+\lambda_{\rm peak}\mathcal{G}(m_1|\mu_m, \sigma_m)\right] \times \mathcal{S}(m_1|m_{\rm min}, \delta_m), \end{aligned} \tag{1.208}$$

where $\mathcal{P}(m_1|(-\alpha), m_{\rm max})$ is a normalised power-law distribution with exponent $-\alpha$ and maximum mass $m_{\rm max}$, $\mathcal{G}(m_1|\mu_m, \sigma_m)$ is the probability distribution function of a Gaussian with mean μ_m and width σ_m and $\mathcal{S}(m_1|m_{\rm min}, \delta_m)$ is a function to smooth the turn-on at law masses (to have its exact expression, see subsection 3.2.2, eqs (3.10) and (3.11)). This model is then an easy power law model with a Gaussian peak in it. This peak has mean μ_m and standard deviation σ_m and a proportion $\lambda_{\rm peak}$ of the population is part of the Gaussian. (We see that if we take $\lambda_{\rm peak} = 0$, we recover a power law model);

- **Broken Power Law mass model** [54] (used *e.g.* in refs [10, 12]) is an extension of the truncated model and has seven independent parameters:

$$p_{\rm pop}(m_1|\alpha_1,\alpha_2,m_{\rm min},\delta_m,m_{\rm max},b) \propto \begin{cases} m_1^{-\alpha_1}\ \mathcal{S}(m_1|m_{\rm min},\delta_m) & \text{if } m_{\rm min}<m_1<m_{\rm break};\\ m_1^{-\alpha_2}\ \mathcal{S}(m_1|m_{\rm min},\delta_m) & \text{if } m_{\rm break}<m_1<m_{\rm max};\\ 0 & \text{otherwise,}\end{cases} \tag{1.209}$$

  where

$$m_{\rm break} = m_{\rm min} + b(m_{\rm max} - m_{\rm min}). \tag{1.210}$$

  $p_{\rm pop}(q|\beta_q, m_{\rm min}, m_1)$ is the same as in the truncated mass model (eq. (1.205)) and $\mathcal{S}(m_1|m_{\rm min},\delta_m)$ as in the power law + peak mass model. The broken power law mass model is explained in more details in subsection 3.2.2.

These mass population functions are independent of the redshift: indeed they are the probability distributions of the intrinsic parameters θ (here $\theta = \{m_1, m_2\}$) of the BBHs population, $p(\theta|\lambda_{\rm BBH})$. But with GWs, also an extrinsic function is measured: the overall merger rate density $\mathcal{R}$. In general $\mathcal{R}$ depends on the redshift z. The evolving merger rate density $\mathcal{R}(z)$ can be parametrised as (see ref. [58]):

$$\mathcal{R}(z|\gamma, R_0) = R_0\ (1+z)^{\gamma}, \tag{1.211}$$

where γ (also often called λ or κ) describes the shape of the evolving merger rate density as a function of the redshift, see *e.g.* refs [10–12, 54], while $R_0 = \mathcal{R}(0)$ ensures normalisation. Another parametrisation we use is (see ref. [12]):

$$\mathcal{R}(z|\alpha_z,\beta_z,z_p,R_0) = R_0 C_0 \frac{(1+z)^{\alpha_z}}{1+\left(\frac{1+z}{1+z_p}\right)^{\alpha_z+\beta_z}}, \tag{1.212}$$

where $C_0(z_p,\alpha_z,\beta_z) = 1+(1+z_p)^{-\alpha_z-\beta_z}$ sets $\mathcal{R}(0) = R_0$ and where the parameter z_p corresponds to the redshift of the peak of star formation.

The general equation that gives the total number $\mathcal{N}$ of GW events that occur within the horizon of detection (*i.e.* the redshift for which the SNR of an event with given parameters θ is $\rho_{\rm thr}$, see subsection 1.1.3.) over an observation time $T_{\rm obs}$, is given by (see ref. [58]):

$$\frac{{\rm d}^2\mathcal{N}}{{\rm d}\theta{\rm d}z}(\mathit{\Lambda}) = \mathcal{R}(z|\gamma)\left[\frac{{\rm d}V_{\rm c}}{{\rm d}z}(z)\right]\frac{T_{\rm obs}}{1+z}\ p(\theta|\lambda_{\rm BBH}), \tag{1.213}$$

where $({\rm d}V_{\rm c}/{\rm d}z)$ is the differential comoving volume (see chapter 2, eq. (2.64)); and where $\mathit{\Lambda}$ is the vector containing all the hyperparameters $\lambda_{\rm BBH}$ and γ (see chapter 2).

1.7 Summary

In the following section we summarise the notions we introduced in this first chapter.

- By linearizing the Einstein's field equations, *i.e.* writing

$$G_{\mu\nu} = \kappa T_{\mu\nu}, \tag{1.214}$$

with a metric g given by a perturbation h on a Minkowski background $\boldsymbol{\eta}$:

$$g_{\mu\nu} = \eta_{\mu\nu} + h_{\mu\nu}, \quad \text{with } h_{\mu\nu} = h_{\nu\mu} \text{ and } |h_{\mu\nu}| \ll 1, \tag{1.215}$$

we get in vacuum ($T_{\mu\nu} = 0$) a wave equation:

$$\Box\bar{h} = -16\pi G T_{\mu\nu} = 0, \tag{1.216}$$

where $\bar{h}$ is defined in eq. (1.8) and where the d'Alembertian is $\Box = \partial_\mu\partial^\mu$. This wave is the gravitational wave. In the good gauges, it has two polarisations: h_+ and $h_\times$.

- The Universe is described at first order by a flat FLRW metric (see eq. (1.70)). And the Einstein's equations applied to this metric become the Friedmann equation:

$$H^2(t) = \frac{8\pi G}{3}\rho(t) + \frac{\Lambda}{3}, \tag{1.217}$$

with $\rho(t) = T_{00}$ the total density of energy in the Universe. This energy content of the Universe can be modeled in various cosmological models, especially ΛCDM model (the Universe has matter, radiation and a cosmological constant Λ, each one having a different equation of state $p(t) = w(t)\rho(t)$, for $p(t) = T_{ii}$ the pressure. For example Λ has $w = -1$) and the wCDM model (matter and radiation as in the ΛCDM model, but with dark energy being described by an EoS with $w \neq 1$).

- A GW that is produced by a binary system of chirp mass M_c ($= (m_1 m_2)^{3/5} \cdot (m_1+m_2)^{-1/5}$ with $m_1 \geq m_2$ the masses of the heavier and the lighter bodies of the binary) in circular orbit, that propagates into a FLRW Universe, has polarisations h_+ and $h_\times$ that follow at first order:

$$h_+(t) = h_\mathrm{c}\ \frac{1+\cos^2\iota}{2}\ \cos\Phi(t) \tag{1.218}$$

$$h_\times(t) = h_\mathrm{c}\ \cos\iota\ \sin\Phi(t), \tag{1.219}$$

with

$$h_\mathrm{c} \propto \frac{[(1+z)M_\mathrm{c}]^{5/3} f_\mathrm{GW}^{2/3}}{d_\mathrm{L}}, \tag{1.220}$$

where d_L is the luminosity distance, defined by eq. (1.85), while $(1+z)M_\mathrm{c}$ is measurable from the time derivative of the observed frequency of the GW, $\dot{f}_\mathrm{GW}$ (see eq. (1.128)). A linear combination of h_+ and $h_\times$ is detected, if furthermore f_GW and $\dot{f}_\mathrm{GW}$ are observed, then the luminosity distance is measurable.

- A binary black hole (or neutron star) that merge gives us a direct measurement of the luminosity distance between the source and the observer. They are called *standard sirens*. Furthermore the measured chirp mass is $(1+z)M_\mathrm{c}$ instead of M_c, so if one knows the value of M_c, then one knows the redshift z of the source. If a standard siren is used alone (without EM counterpart), it is called a *dark siren*.

- The evolution of a GW amplitude h in a FLRW Universe follows the free propagation equation for tensors modes:

$$\tilde{h}''_A + 2\mathcal{H}\left[1-\delta(\eta)\right]\tilde{h}'_A + c^2k^2\tilde{h}_A = 0, \tag{1.221}$$

where $\mathcal{H}$ is defined in sect. 1.3. In GR, $\delta(\eta)=0$ but in modified gravity models, we can have $\delta(\eta)\neq 0$. In such cases, GWs do not give a direct measurement of the luminosity distance d_L but rather of the *GW luminosity distance*, d_L^GW, defined by:

$$d_\mathrm{L}^\mathrm{GW}(z) = d_\mathrm{L}(z)\ \exp\left\{-\int_0^z \frac{\delta(z')}{1+z'}\,\mathrm{d}z'\right\}, \tag{1.222}$$

and we can parametrise the ratio $d_\mathrm{L}^\mathrm{GW}/d_\mathrm{L}$ by:

$$\left[\frac{d_\mathrm{L}^\mathrm{GW}}{d_\mathrm{L}}\right]_{\mathrm{param}(\Xi_0,n)} \equiv \Xi_0 + \frac{1-\Xi_0}{(1+z)^n}. \tag{1.223}$$

We discuss some examples of modified gravity models in section 1.5. In particular, the RT nonlocal model passes all the cosmological tests at the same accuracy at ΛCDM. However, the RT nonlocal model predicts $\delta(\eta)\neq 0$ (contrary to ΛCDM). Our goal is to use dark sirens to constrain the values of the parameters (Ξ_0, n).

- To use dark sirens with the mass redshift, we need to have enough detections of GWs to statistically compare them with astrophysical models of sources population. Some models of mass population of binary black holes are given in sect. 1.6. They all have in common a mass gap (*i.e.* a maximum mass of stellar-mass BHs in source-frame, before the intermediate mass BHs). For example, the simplest mass population model is given by:

$$p_\mathrm{pop}(m_1, m_2|\alpha, \beta, m_\mathrm{max}, m_\mathrm{min}) \propto m_1^{-\alpha} m_2^{\beta}\ \Theta(m_1-m_2)\Theta(m_\mathrm{max}-m_1)\Theta(m_2-m_\mathrm{min}). \tag{1.224}$$

Our statistical approach is explained in details in chapter 2.

Chapter 2

Methodology

Contents

In this chapter we first present a small review of Bayesian inference and of hierarchical Bayesian inference. As an illustration, we apply a Bayesian inference on Gaussian samples. We then present the hierarchical Bayesian inference we use for this master's project to constrain the values of cosmological parameters by using the mass gap of the black hole population (see chapter 1).

2.1 Generalities about Bayesian inference

Bayesian inference is a technique based on the Bayesian interpretation of probability. It allows the computation of the *probability of a theory* (or the probability that a parameter takes a particular value) *given data* on the predictions of the theory. Introductions to this method are given in refs [8, 13, 35, 59].

This method can be used in a large range of topics, when one has to find the value of a parameter given observed data, from characterisation of an exoplanet's radius and mass, to the efficiency of a vaccine.

In the case of gravitational-wave astronomy, Bayesian inference is used to determine the masses, spins, distance, etc. of the black holes (or neutrons stars) that produced a detected GW (see *e.g.* ref. [54]).

2.1.1 Bayes' formula and Bayesian interpretation of probability

Let us first formally define *probability* (see *e.g.* [60]). Let S be a set with subsets S_i ($i = 1, 2, \cdots, n$), and $\mathcal{A}$ be a σ-algebra on S (*i.e.* it is a collection of the subsets S_i's of S and that includes $\varnothing$ and S itself). Let A_j be an element of the σ-algebra $\mathcal{A}$.

An abstract definition of a probability is given by the function P satisfying:

$$\begin{aligned} \mathsf{P}:\ \mathcal{A} &\longrightarrow [0,1] \\ A_j &\longmapsto \mathsf{P}(A_j), \end{aligned} \tag{2.1}$$

with $\mathsf{P}(A_j)$ being the probability of the event 'A_j' and satisfying the *Kolmogorov axioms* (Andrei Kolmogorov, 1933):

1. $\forall A_j \in \mathcal{A}, \mathsf{P}(A_j) \geq 0$;
2. $\mathsf{P}(S) = 1$ (this is the *unitarity* of the probability);
3. For any countable sequence of disjoint subsets of $\mathcal{A}$, A_1, A_2, $\cdots$, A_m (*i.e.* mutually exclusive subsets: $A_i \cap\ A_j\ =\ \delta_{ij} A_i$), we have: $\mathsf{P}(\bigcup_{i=1}^{m} A_i) = \sum_{i=1}^{m} \mathsf{P}(A_i)$. (This is called the "σ-additivity".)

$(S, \mathcal{A}, \mathsf{P})$ is a *probability space*, where the set S is the *sample space*, the σ-algebra $\mathcal{A}$ is the *event space* and P is the *probability function*.

It also necessary to define the conditional probability: let A and B be two events (*i.e.* two elements of the event space $\mathcal{A}$). If $\mathsf{P}(A) \neq 0$, then the *conditional probability* of the event B given the event A (denoted: $\mathsf{P}(B|A)$), is:

$$\mathsf{P}(B|A) = \frac{\mathsf{P}(A \cap B)}{\mathsf{P}(A)}. \tag{2.2}$$

This equation means that after a first try, the event A comes. Then for a second try, the sample space is now A instead of S. (By putting $A = S$ in eq. (2.2), we trivially find $\mathsf{P}(B|S) = \mathsf{P}(B)$.) And eq. (2.2) is the probability that the second try gives B. So, in general, $P(B|A) \neq P(A|B)$ and unitarity now holds on the new sample space A: $\mathsf{P}(A|A) = 1$.

Equation (2.2) is symmetric under the transformation $A \leftrightarrow B$ (assuming $\mathsf{P}(B) \neq 0$), hence we get:

$$\mathsf{P}(A|B) = \frac{\mathsf{P}(B \cap A)}{\mathsf{P}(B)}, \tag{2.3}$$

and since $B \cap A = A \cap B$, we can link both conditional probabilities in:

$$\mathsf{P}(A|B) = \frac{\mathsf{P}(B|A)\ \mathsf{P}(A)}{\mathsf{P}(B)}. \tag{2.4}$$

Equation (2.4) is the well-known *Bayes' formula* (or *theorem*) (Thomas Bayes, 1763).

For A_i $(i = 1, \cdots, m)$, disjoint subsets such that $\bigcup_{i=1}^m A_i = S$, we can write:

$$\mathsf{P}(B) = \sum_{i=1}^{m} \mathsf{P}(B|A_i)\mathsf{P}(A_i). \tag{2.5}$$

(The probability of B is the sum of the probabilities of B given A_i weighted by the probability of A_i, for each non-overlapping subset A_i of S.) We can then write the Bayes' formula (eq. (2.4)) as:

$$\mathsf{P}(A|B) = \frac{\mathsf{P}(B|A)\ \mathsf{P}(A)}{\sum_{i=1}^{m} \mathsf{P}(B|A_i)\mathsf{P}(A_i)}. \tag{2.6}$$

It is possible to give different interpretations to the concept of probability (a discussion on that aspect can be found in ref. [8], sect. 7.4). Two main approaches exist. First, the *frequentist view* (the "classical" view) of probability, a probability corresponds to the limit of the ratio of the number of successes by the number of tries, when the number of tries goes to infinity:

$$\mathsf{P}(\text{“success”}) = \lim_{\#\text{ of tries}\to\infty} \frac{\#\text{ of successes}}{\#\text{ of tries}}, \tag{2.7}$$

of course this equation only holds for countable events.[1] The basic example is a cubic non-biased dice: the probability to obtain 5, is $\mathsf{P}(5) = 1/6$: indeed within a large set of rolls, we can expect that one sixth of the rolls would give a 5. It is the law of large numbers that allows us to interpret probability in such a way.

In this frequentist interpretation of probability, one can speak about the probability that data appears given a theory (or hypothesis)[2] or given a parameter in a theory. But it is meaningless to speak *e.g.* about the probability that I will obtain a good grade for the present thesis: this cannot be the outcome of a repeatable experiment. More generally one cannot speak about the probability that a parameter takes a given value, nor about the probability that a theory is true.

To allow us to consider such kind of probability, we must use the Bayesian interpretation of probability.

In this interpretation, we start from the Bayes' formula (eq. (2.4)) to write:

$$\mathsf{P}(\text{hypothesis} \mid \text{data}) = \frac{\mathsf{P}(\text{data} \mid \text{hypothesis}) \cdot \mathsf{P}(\text{hypothesis})}{\mathsf{P}(\text{data})}, \tag{2.8}$$

or even:

$$\mathsf{P}(\text{parameter} = x \mid \text{data}) = \frac{\mathsf{P}(\text{data} \mid \text{parameter} = x) \cdot \mathsf{P}(\text{parameter} = x)}{\mathsf{P}(\text{data})}. \tag{2.9}$$

The latter equation can be interpreted by saying that each physical parameter has a certain probability to take a value, given the data we have, instead of having one defined value without changing it with the data we have. Philosophically, it is still a question to understand if Bayesian interpretation of probability is really fundamental (see *e.g.* [61]). But in the present work, we use Bayesian interpretation because it works, not necessarily because its philosophical interpretation is better than the frequentist's.

[1] For example if one picks an instant in a period $[0, t]$, the probability to obtain precisely t_0 is zero for all $t_0 \in [0, t]$: hence, we can say that events with zero probability happen every day.

[2] Here and in this chapter, we use *theory* and *hypothesis* as synonyms.

2.1.2 Bayesian inference

To perform Bayesian inference in order to obtain the value of a parameter in a theory, given some data we start from eq. (2.9).

If we are interested in the value of some parameter θ (or in the values of a vector of parameters $\vec{\theta}$) from the data $\mathcal{D}$ we have, the Bayes' formula gives:

$$\mathsf{P}(\theta|\mathcal{D}) = \frac{\mathsf{P}(\mathcal{D}|\theta)\ \mathsf{P}(\theta)}{\mathsf{P}(\mathcal{D})}. \tag{2.10}$$

To be fully rigorous, the parameter θ lies in the framework of a theory T, then eq. (2.10) should be written as

$$\mathsf{P}(\theta|\mathcal{D},T) = \frac{\mathsf{P}(\mathcal{D}|\theta,T)\ \mathsf{P}(\theta|T)}{\mathsf{P}(\mathcal{D}|T)}. \tag{2.11}$$

In the latter equations, we introduced the shorthand notation $\mathsf{P}(A,B)$ for $\mathsf{P}(A \cup B)$ and we will often use it in the following. From now on, we will not specify in the equations the theory 'T' in which we work, but one has to remember that the parameters always take place in the framework of a given theory.

In our case, we use four different notations for the probability functions, to distinguish between the different kinds of probabilities:

$$p(\theta|\mathcal{D}) = \frac{\mathcal{L}(\mathcal{D}|\theta)\ \pi(\theta)}{\mathcal{Z}(\mathcal{D})}. \tag{2.12}$$

$\mathcal{Z}(\mathcal{D})$ is called the *evidence* and is defined as the integral of the numerator of the r.h.s. of eq. (2.12) over θ (then it does not depend on the parameter θ):

$$\mathcal{Z}(\mathcal{D}) = \int \mathcal{L}(\mathcal{D}|\theta)\ \pi(\theta)\ \mathrm{d}\theta. \tag{2.13}$$

(It is the continuous case of the discrete eq. (2.5).)

In eq. (2.12) we use different notations for the different probability distribution functions:

- $p(\theta|\mathcal{D})$ is called the *posterior* probability distribution function (pdf) of the parameter θ given the data $\mathcal{D}$. This pdf is the result we are interested in by performing Bayesian inference, it gives the probability that a certain parameter takes a certain value in the framework of a theory;[3]

- $\mathcal{L}(\mathcal{D}|\theta)$ is called the *likelihood* probability distribution function of the data $\mathcal{D}$ given the parameter θ. It gives the probability of having the data $\mathcal{D}$ given the theory T with the parameter θ. A classical physical theory (T) generally predicts one single output ($\mathcal{D}$) for one input (θ), however the measurement of $\mathcal{D}$ is never perfect, it always has systematical uncertainty. This uncertainty must be taken into account into the likelihood;

- $\pi(\theta)$ is called the *prior* probability distribution function for the parameter θ. This pdf is chosen in agreement with the prior knowledge we have on the value of the parameter θ. For example if an approximate value of the parameter is already known from a previous inference, one can choose to take the posterior of the previous inference as prior for the

[3] If we suppose that the parameter has one unique "true" value, its posterior must be given by a Dirac delta on this value. Practically, we have uncertainties. With enough data, the central limit theorem ensures us to obtain a Gaussian distribution, and the more data, the smaller the standard deviation, hence with an infinite number of measurements we obtain the Dirac distribution on the "true" value.

next inference. When one does not know the value of the parameter θ (except its order of magnitude) a common choice is a flat prior. When even the order of magnitude of θ is unknown (or supposed to be) another common choice is a logarithmic prior. As we can see from the Bayes' formula, eq. (2.4), the choice of prior is important: if the prior gives a zero probability to a particular value of θ, then this value will always have a zero probability in the posterior, even if it is the "true" value of the parameter (in other words, if the prior is wrong, the inference cannot work);

- $\mathcal{Z}(\mathcal{D})$ is the *evidence* and it corresponds to "the probability of having data $\mathcal{D}$". This interpretation holds only if we consider the probability of having $\mathcal{D}$ given the theory T (and the systematical uncertainty). In an easier way of seeing it, $\mathcal{Z}(\mathcal{D})$ can just be seen as a normalisation factor depending on the data $\mathcal{D}$, in order that the posterior follows unitarity (Kolmogorov's 2nd axiom): $\int p(\theta|\mathcal{D})\, \mathrm{d}\theta = 1$.

Bayesian inference is a technique that highly depends on the data: adding new data to the inference can change the shape of the posterior pdf. However, Bayesian inference does not give one value for the parameter but a pdf: it gives credible intervals around the maximum posterior value. We can then write expressions such: $\theta = x^{+\Delta_{(+)}x}_{-\Delta_{(-)}x}$. In the ideal case of all observations having the same precision, the credible intervals, $\Delta_{(\pm)}x$, evolve as $1/\sqrt{N_{\mathrm{obs}}}$, where N_{obs} is the number of observations.

In the context of GW astronomy, the theory T is composed of GR + ΛCDM, or modified gravity, plus a model of the detector. The surveys (*e.g.* advLIGO [25], advVirgo [26] or KAGRA [27]) detect the data $\mathcal{D}$ and one is interested in the values of the parameters $\vec{\theta}$ of the GW source. $\vec{\theta}$ is a 15 dimensional vector containing all the parameters of gravitational waves' sources (intrinsic parameters: masses of the merging objects, their spins, etc. and extrinsic parameters: their (GW) luminosity distance, their position in the sky, etc.). By performing Bayesian inference (see eq. (2.12)), one is able to estimate the values of these parameters with uncertainties. It is then important to note that the uncertainties on the values of the parameters in GW astronomy are not only systematical uncertainty (*i.e.* uncertainty on the measurement of $\mathcal{D}$), but also statistical uncertainty due to Bayesian inference.

There are several different ways to quote a value and its associated uncertainty: maximum, median or mean value of the posterior, for the central value, and quantiles, symmetric intervals around the maximum, etc. of the posterior, for the uncertainty. In this work, we use the median of the posterior for the central value and other quantiles of the posterior for the uncertainty (for example the 16th and 84th percentiles for a credible level of 68%).

2.2 Hierarchical Bayesian inference

The probability of having the parameter θ can be given itself by a parent-distribution. This distribution might be conditioned on a *hyperparameter* Λ (or on a vector of hyperparameters $\vec{\Lambda}$), *i.e.* θ follows a distribution $p_{\mathrm{pop}}(\theta|\Lambda)$. Our goal is to perform an inference on the value of the hyperparameter Λ.

Example 2.1: The mass m of an astrophysical black hole follows the mass population of black holes. At a first approximation the mass population is (for $m < m_{\mathrm{gap}} \sim 50 - 150\ \mathrm{M}_\odot$) [54]:

$$p_{\mathrm{pop}}(m|\alpha) \propto m^{-\alpha}, \tag{2.14}$$

m corresponds to the parameter θ while α corresponds to the hyperparameter Λ.
An example of $p_{\mathrm{pop}}(m|\alpha)$ (for $\alpha = 0.75$) is shown in fig. 2.1. ◊

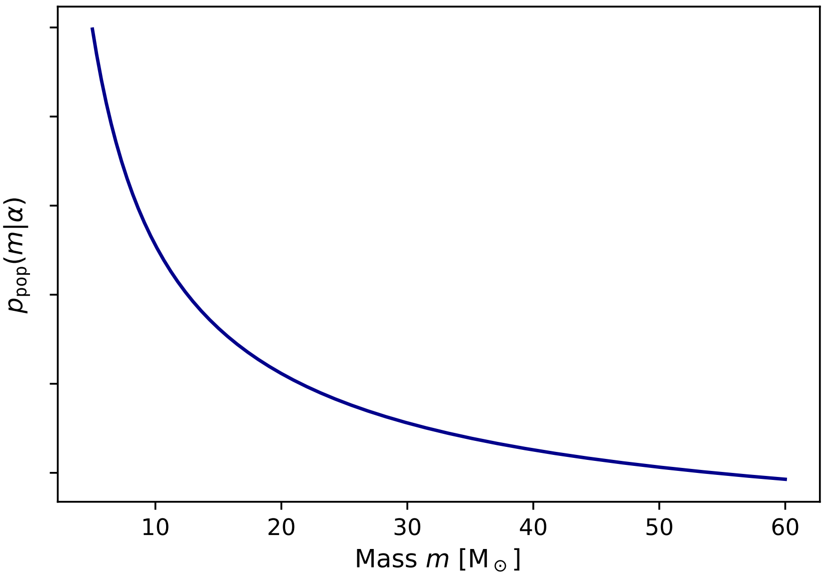

Figure 2.1: *Example of mass population of black holes* $p_{\text{pop}}(m|\alpha)$ *(see example 1), where we take* $\alpha = 0.75$*.*

To perform an inference on the hyperparameter Λ, when the data give direct information on θ, we use *hierarchical Bayesian inference*. To distinguish between hierarchical Bayesian inference and Bayesian inference, it is customary to talk about *hyper-posterior*, *hyper-likelihood*, etc. for the posterior, likelihood, etc. of the hierarchical inference [35, 59]. We follow this convention in the following.

2.2.1 Hierarchy

Since we are interested in the hyper-posterior of Λ given $\mathcal{D}$, we need to introduce the hyper-likelihood ($\mathcal{D}$ given Λ). The key is to *marginalise* over the whole θ space, with $\theta \sim p_{\text{pop}}(\theta|\Lambda)$.[4] We thus get the marginalised hyper-likelihood:

$$\mathcal{L}(\mathcal{D}|\Lambda) = \int \mathcal{L}(\mathcal{D}|\theta)\ p_{\text{pop}}(\theta|\Lambda)\ \mathrm{d}\theta. \tag{2.15}$$

The hyper-posterior then follows directly from the Bayes' formula (eq. (2.4)):

$$p(\Lambda|\mathcal{D}) = \frac{\mathcal{L}(\mathcal{D}|\Lambda)\ \pi(\Lambda)}{\mathcal{Z}(\mathcal{D})}, \tag{2.16}$$

where, as usual, the hyper-evidence $\mathcal{Z}(\mathcal{D})$ is given by the integral of the numerator of the r.h.s. of eq. (2.16) over the hyperparameter Λ:

$$\mathcal{Z}(\mathcal{D}) = \int \left\{ \int \mathcal{L}(\mathcal{D}|\theta)\ p_{\text{pop}}(\theta|\Lambda)\ \mathrm{d}\theta \right\}\ \pi(\Lambda)\ \mathrm{d}\Lambda. \tag{2.17}$$

If we have N_{obs} independent measurements, we can write the total hyper-likelihood as the product of each independent hyper-likelihood (they are independent probabilities):

[4] Here notation "$\sim$" is used in its probabilistic meaning: $\theta \sim p_{\text{pop}}(\theta|\Lambda)$ signifies that the distribution of the random variable θ is the pdf $p_{\text{pop}}(\theta|\Lambda)$.

$$\mathcal{L}_{\text{tot}}(\mathcal{D}|\Lambda) = \prod_{i=1}^{N_{\text{obs}}} \int \mathcal{L}(\mathcal{D}_i|\theta_i)\ p_{\text{pop}}(\theta_i|\Lambda)\ \mathrm{d}\theta_i, \tag{2.18}$$

In the latter equation, θ_i is the parameter (or the ensemble of all parameters) of the i-th measurement, while $\mathcal{D}_i$ is the data of the i-th measurement ($i \in [\![1, N_{\text{obs}}]\!]$), thus $\mathcal{D} = \{\mathcal{D}_1, \mathcal{D}_2, \cdots, \mathcal{D}_{N_{\text{obs}}}\}$. To obtain eq. (2.18), we furthermore supposed that all the observations were coming from the same population function $p_{\text{pop}}(\theta|\Lambda)$.

To compute the hyper-likelihood, eq. (2.18), it is useful to rewrite the likelihood $\mathcal{L}(\mathcal{D}_i|\theta_i)$ as (by the Bayes' theorem (eq. (2.12)):

$$\mathcal{L}(\mathcal{D}_i|\theta_i) = \mathcal{Z}(\mathcal{D}_i)\ \frac{p(\theta_i|\mathcal{D}_i)}{\pi(\theta_i)}. \tag{2.19}$$

Therefore, plugging eq. (2.19) into eq. (2.18), gives:

$$\mathcal{L}_{\text{tot}}(\mathcal{D}|\Lambda) = \prod_{i=1}^{N_{\text{obs}}} \int \mathcal{Z}(\mathcal{D}_i)\ p(\theta_i|\mathcal{D}_i)\ \frac{p_{\text{pop}}(\theta_i|\Lambda)}{\pi(\theta_i)}\ \mathrm{d}\theta_i. \tag{2.20}$$

It is now straightforward to compute the hyper-posterior probability distribution function for Λ (using again Bayes' theorem):

$$p(\Lambda|\mathcal{D}) = \frac{\mathcal{L}_{\text{tot}}(\mathcal{D}|\Lambda)\ \pi(\Lambda)}{\mathcal{Z}_{\text{tot}}(\mathcal{D})}, \tag{2.21}$$

and it gives:

$$p(\Lambda|\mathcal{D}) = \frac{\pi(\Lambda)}{\mathcal{Z}_{\text{tot}}(\mathcal{D})} \prod_{i=1}^{N_{\text{obs}}} \int \mathcal{Z}(\mathcal{D}_i)\ p(\theta_i|\mathcal{D}_i)\ \frac{p_{\text{pop}}(\theta_i|\Lambda)}{\pi(\theta_i)}\ \mathrm{d}\theta_i. \tag{2.22}$$

Example 2.2: In ref. [10], the authors use eq. (2.18) to obtain the likelihood of the gravitational-wave data given the Hubble constant. In order to obtain this equation, they start by writing the parameter $\vec{\theta}$ as the vector $(d_{\text{L}}, \hat{\Omega}, \boldsymbol{\theta'})$, with the luminosity distance d_{L} and the direction $\hat{\Omega}$ of the source in the sky and the other parameters $\boldsymbol{\theta'}$. By marginalising over these different parameters, they get:

$$\mathcal{L}(\mathcal{D}|H_0) = \int \mathcal{L}(\mathcal{D}|d_{\text{L}}, \hat{\Omega}, \boldsymbol{\theta'})\ p_{\text{pop}}(d_{\text{L}}, \hat{\Omega}, \boldsymbol{\theta'}|H_0)\ \mathrm{d}d_{\text{L}}\ \mathrm{d}\hat{\Omega}\ \mathrm{d}\boldsymbol{\theta'}, \tag{2.23}$$

which is equivalent to their eq. (3.15). One can rewrite $p_{\text{pop}}(d_{\text{L}}, \hat{\Omega}, \boldsymbol{\theta'}|H_0)$, by noticing that d_{L} is given by a redshift z and a choice of cosmology H_0 and that one can measure the (gravitational) luminosity distance with the GW signal ($h \propto 1/d_{\text{L}}^{\text{GW}}$). One can then marginalise over z to get:

$$p_{\text{pop}}(d_{\text{L}}, \hat{\Omega}, \boldsymbol{\theta'}|H_0) = \int \delta\left(d_{\text{L}}^{\text{measured}} - d_{\text{L}}(H_0, z)\right)\ p_0(z, \hat{\Omega}, \boldsymbol{\theta'})\ \mathrm{d}z, \tag{2.24}$$

where $\delta(x)$ is the Dirac delta distribution, $p_0(z, \hat{\Omega}, \boldsymbol{\theta'})$ is the probability to have a galaxy (which can host the GW source) at the given parameters $(z, \hat{\Omega}, \boldsymbol{\theta'})$. In ref. [10], the authors use a galaxy catalog to compute this distribution p_0. The integration over the delta distribution then gives:

$$\mathcal{L}(\mathcal{D}|H_0) = \int \mathcal{L}\left(\mathcal{D}\ \middle|\ d_{\text{L}}(z, H_0), \hat{\Omega}, \boldsymbol{\theta'}\right)\ p_0(z, \hat{\Omega}, \boldsymbol{\theta'})\ \mathrm{d}z\ \mathrm{d}\hat{\Omega}\ \mathrm{d}\boldsymbol{\theta'}, \tag{2.25}$$

which is equation (3.17) of ref. [10] (up to some notation differences and to a normalisation factor, see below, subsection 2.2.2). ♢

2.2.2 Selection bias

Until now, we implicitly considered that our observations $\mathcal{D}$ were a *representative sample of the likelihood* $\mathcal{L}(\mathcal{D}|\Lambda)$. This is not always the case because of an observation bias: only one part of the population can be detected, hence the data $\mathcal{D}$ is a sample of this part only and not of the entire population.

In observational astronomy such a selection bias is known as the “Malmquist bias” (Gunnar Malmquist, 1922) (see ref. [62]): surveys are limited, and stars (or now galaxies) with an apparent magnitude above[5] the detectability threshold of the survey cannot be detected. Then, only objects with a maximum apparent magnitude can appear in catalogs. The catalogs only present partial data. The incompleteness is dependent of the distance, since the apparent magnitude is given by:

$$m = -2.5 \log_{10} \left(\frac{L}{4\pi d^2} \right) + \text{constant}, \tag{2.26}$$

let us say that to be detectable, an object has to have an apparent magnitude below a threshold $m\star$, we see from the latter equation that the further the object (d), the higher its luminosity (L) has to be in order to be detectable (the effect is even quadratic in the distance). So clearly, the further the distance, the less accurate the catalog. In appendix A of ref. [10], the authors discuss the completeness of a galaxy catalog. (They also discuss about other bias, such as non-isotropy of the incompleteness because of the Milky Way, etc.)

In the case of gravitational-wave astronomy, the problem is almost the same. Instead of a maximum apparent magnitude, the gravitational wave signals have to be above a certain signal-to-noise ratio:[6] some signals are too tiny to be detected (this is the effect of the intrinsic parameters of the source) while others can even be in a detector’s blind spot (this is the effect of the extrinsic parameters of the source), etc.

But if we know the detector, and the shape of the overall population of sources, we can estimate in a very accurate way the probability of detection of a signal. Then we can take into account the selection bias into Bayesian inference.

In this section, we explicitly take the example of the gravitational wave selection bias, following the notation and the derivation of ref. [13]. N is the total number of GW events in the Universe.

Bottom-up derivation

Here we present the so-called “bottom-up” derivation of the selection bias. We use ref. [13], in which one can also find another derivation, that is equivalent.

First of all, we need to integrate only on the events that are detectable by our surveys. To do so, we must normalise the total hyper-likelihood, eq. (2.18), in order to ensure unitarity of the hyper-posterior $p(\Lambda|\mathcal{D})$ over all observable events. We then introduce the normalisation factor $\alpha(\Lambda)$, such that:

$$\mathcal{L}_{\text{tot}}(\mathcal{D}|\Lambda) = \prod_{i=1}^{N_{\text{obs}}} \frac{1}{\alpha(\Lambda)} \int \mathcal{L}(\mathcal{D}_i|\theta_i)\; p_{\text{pop}}(\theta_i|\Lambda)\; \mathrm{d}\theta_i, \tag{2.27}$$

[5] Remember that because of the minus sign in eq. (2.26), the larger the magnitude, the less one sees the object... (see also note 9 page 26).

[6] Or equivalently: below a certain false-alarm rate (FAR).

where $\alpha(\Lambda)$ is the integral of the total hyper-likelihood over the observable events:

$$\begin{aligned}\alpha(\Lambda) &= \int_{\mathcal{D}\,>\,\text{threshold}} \left[\int \mathcal{L}(\mathcal{D}|\theta)\; p_{\text{pop}}(\theta|\Lambda)\; \mathrm{d}\theta\right]\; \mathrm{d}\mathcal{D} \\ &= \int p_{\text{pop}}(\theta|\Lambda) \left[\int_{\mathcal{D}\,>\,\text{threshold}} \mathcal{L}(\mathcal{D}|\theta)\; \mathrm{d}\mathcal{D}\right]\; \mathrm{d}\theta \\ &= \int p_{\text{det}}(\theta)\; p_{\text{pop}}(\theta|\Lambda)\; \mathrm{d}\theta. \end{aligned} \tag{2.28}$$

In eq. (2.28), we introduce the probability of detection of a gravitational wave whose source has parameters θ. This is mathematically:

$$p_{\text{det}}(\theta) = \int_{\mathcal{D}\,>\,\text{threshold}} \mathcal{L}(\mathcal{D}|\theta)\; \mathrm{d}\mathcal{D}. \tag{2.29}$$

A typical criterion of detection in GW astronomy is given by a certain false-alarm-rate, FAR (for example below 2.0 yr^{-1} for GWTC-1 [4]) that can be empirically converted into a signal-to-noise ratio (SNR), see subsection 1.1.3. We generally say that a GW event is detected by a two detectors surveys when its SNR is larger than 8 (in both detectors). Then $p_{\text{det}}(\theta)$ is given by:

$$p_{\text{det}}(\theta) \equiv p_{\text{det}}^{\text{exp}}(\theta) = \Theta\left(\text{SNR}(\theta) - 8\right), \tag{2.30}$$

where

$$\forall x \in \mathbb{R}, \quad \Theta(x) = \begin{cases} 0 & \text{if} \quad x < 0; \\ 1 & \text{if} \quad x \geq 0, \end{cases} \tag{2.31}$$

is the Heaviside step function.

We can check that for a hyperparameter Λ that allows all events to be detected, $\alpha(\Lambda) = 1$, and the total hyper-likelihood *with* a selection bias, eq. (2.27), becomes the total hyper-likelihood *without* selection bias, eq. (2.18).

Another effect to take into account is that if we expect to observe N_{exp} events (for example, N_{exp} can be computed from the population of events' sources – for GWs, now, stellar-mass black holes and neutrons stars – and using a model of detection), the probability to observe N_{obs} events follows a Poisson distribution:

$$\mathsf{P}(N_{\text{obs}}|N_{\text{exp}}) = \mathrm{e}^{-N_{\text{exp}}} (N_{\text{exp}})^{N_{\text{obs}}}, \tag{2.32}$$

where we did not write the normalisation factor $1/N_{\text{obs}}!$ because the events are distinguishable. For a precise derivation, see *e.g.* ref. [13]: we assumed a constant source rate and no background. If N is the total number of GW events, then it is connected to N_{exp} by: $N\alpha(\Lambda) = N_{\text{exp}}$. Indeed, $\alpha(\Lambda)$ is the proportion of events that is detectable given the hyperparameters Λ, so $\alpha(\Lambda)$ times the total number of events N, gives the number of events one *expects* to detect: N_{exp}.

It is then possible to write the hyper-posterior of Λ *and* N given $\mathcal{D}$:

$$p(\Lambda, N|\mathcal{D}) \propto \pi(\Lambda)\pi(N) \prod_{i=1}^{N_{\text{obs}}} \left[\int \frac{p(\theta_i|\mathcal{D}_i)}{\alpha(\Lambda)}\; \frac{p_{\text{pop}}(\theta_i|\Lambda)}{\pi(\theta_i)}\; \mathrm{d}\theta_i\right] \cdot \mathrm{e}^{-N_{\text{exp}}} (N_{\text{exp}})^{N_{\text{obs}}}, \tag{2.33}$$

that we can (numerically) marginalise over N to obtain the hyper-prior of Λ given data $\mathcal{D}$:

$$p(\Lambda|\mathcal{D}) \propto \int \pi(N)\pi(\Lambda) \prod_{i=1}^{N_{\text{obs}}} \left[\int \frac{p(\theta_i|\mathcal{D}_i)}{\alpha(\Lambda)} \frac{p_{\text{pop}}(\theta_i|\Lambda)}{\pi(\theta_i)} \, \mathrm{d}\theta_i \right] \cdot \mathrm{e}^{-N\alpha(\Lambda)}(N\alpha(\Lambda))^{N_{\text{obs}}} \, \mathrm{d}N. \tag{2.34}$$

The proportionalities in eqs (2.33) and (2.34) come from the fact that we did not write the hyper-evidence factors $\mathcal{Z}(\mathcal{D}_i)$ in the denominators, since they act just as a global normalisation factor that does not depend on the hyperparameter Λ nor on N.

Example 2.3: As in ref. [13] we can use a Jeffreys prior for a Poisson distribution,[7] $\pi(N) \propto 1/N$, and since $\mathrm{d}N = \mathrm{d}N_{\text{exp}}/\alpha(\Lambda)$, we obtain:

$$\int \frac{\mathrm{e}^{-N\alpha(\Lambda)}}{N} (N\alpha(\Lambda))^{N_{\text{obs}}} \, \mathrm{d}N = \int \mathrm{e}^{-N_{\text{exp}}} (N_{\text{exp}})^{N_{\text{obs}}-1} \, \mathrm{d}N_{\text{exp}} = \Gamma(N_{\text{obs}}) = (N_{\text{obs}}-1)! \tag{2.35}$$

thus

$$p(\Lambda|\mathcal{D}) \propto \pi(\Lambda) \prod_{i=1}^{N_{\text{obs}}} \int \frac{p(\theta_i|\mathcal{D}_i)}{\alpha(\Lambda)} \frac{p_{\text{pop}}(\theta_i|\Lambda)}{\pi(\theta_i)} \, \mathrm{d}\theta_i. \tag{2.36}$$

$\diamondsuit$

The function of the bias effect $\alpha(\Lambda)$ is sometimes called $\beta(\Lambda)$, *e.g.* in refs [10, 63] (often because α has another significance in these papers) but in the present document we use the standard notation "α".

2.2.3 Discretisation of the integrals

La découverte des logarithmes [...] en réduisant à quelques jours le travail de plusieurs mois, double, si l'on peut dire, la vie des astronomes [...].
Pierre-Simon de Laplace
(*Exposition du système du monde*, Livre V, chapitre IV, 1796)

Equation (2.33) has a number of integrals which is linear on the number of measurements: in the GW case, there are $15N_{\text{obs}}$ integrals ($\theta \in \mathscr{D} \subset \mathbb{R}^{15}$). (In our work we will use only a few parameters (see section 2.4).) It is then useful to discretise the factor between the square brackets of eq. (2.33), using a Monte Carlo integration (cf. eq. (22) of ref. [35] and appendix A, eq. (A.9)):

$$\langle f(x) \rangle_{p(x)} = \int_{\mathbb{R}} p(x) f(x) \, \mathrm{d}x \approx \frac{1}{n_s} \sum_{k=1}^{n_s} f(x_k) \mid_{x_k \sim p(x)}, \tag{2.37}$$

where we simply divide $\mathbb{R}$ in n_s bins with a repartition following $p(x)$, we evaluate f on every bin and we average. This integration come from the strong law of large numbers (see appendix A, page 91 for a demonstration of eq. (2.37) and for a short introduction to Monte Carlo methods).

In the case of the square brackets of eq. (2.33), we can match:

[7] The Jeffreys prior is given by the square root of the determinant of the Fisher information matrix.

$$p(x) \longleftrightarrow \quad p(\theta_i|\mathcal{D}_i); \tag{2.38}$$

$$f(x) \longleftrightarrow \quad \frac{p_{\rm pop}(\theta_i|\Lambda)}{\pi(\theta_i)} = \widetilde{f}(\theta_i); \tag{2.39}$$

$$\mathrm{d}x \longleftrightarrow \quad \mathrm{d}\theta_i; \tag{2.40}$$

$$\mathbb{R} \longleftrightarrow \quad \mathscr{D} \subset \mathbb{R}^d; \tag{2.41}$$

(where d is the number of parameters we are considering). We obtain (also assuming that n_s is very large so that the approximation becomes an equality):

$$\mathcal{L}_{\rm tot}(\mathcal{D}|\Lambda) = \prod_{i=1}^{N_{\rm obs}} \left[\frac{1}{n_s} \sum_{k=1}^{n_s} \frac{p_{\rm pop}(\theta_i^k|\Lambda)}{\pi(\theta_i^k)} \, |_{\theta_i^k \, \sim \, p(\theta_i|\mathcal{D}_i)} \right]. \tag{2.42}$$

and this is eq. (32) of ref. [35].

Inserting eq. (2.42) into eq. (2.33), we get:

$$p(\Lambda, N|\mathcal{D}) \propto \pi(\Lambda)\pi(N) \prod_{i=1}^{N_{\rm obs}} \left[\frac{1}{n_s} \sum_{k=1}^{n_s} \frac{p_{\rm pop}(\theta_i^k|\Lambda)}{\pi(\theta_i^k)} \, |_{\theta_i^k \, \sim \, p(\theta_i|\mathcal{D}_i)} \right] \mathrm{e}^{-N\alpha(\Lambda)} N^{N_{\rm obs}}. \tag{2.43}$$

This equation can be itself very long to estimate: with current (2021) 2nd generation GW detectors (such that advLIGO, advVirgo or KAGRA), we have $\mathcal{O}(50)$ detections. But with 3rd generation GW detectors (such as the *Einstein Telescope* (ET), in the mid-2030s), we will have $\mathcal{O}(10^5 - 10^6)$ detections per year [7], so the product of likelihoods (numbers between 0 and 1) will quickly become a very small number. It is then easier to work with the logarithms:[8]

$$\log\{p(\Lambda, N|\mathcal{D})\} = \log\{\pi(\Lambda)\} + \log\{\pi(N)\} + \sum_{i=1}^{N_{\rm obs}} \log \left\{ \frac{1}{n_s} \sum_{k=1}^{n_s} \frac{p_{\rm pop}(\theta_i^k|\Lambda)}{\pi(\theta_i^k)} \, |_{\theta_i^k \, \sim \, p(\theta_i|\mathcal{D}_i)} \right\} - N \, \alpha(\Lambda) + \text{const.} \tag{2.44}$$

Equivalently we can insert eq. (2.42) into eq. (2.36) (so using the Jeffrey prior for a Poisson distribution to marginalise on N), we finally obtain eq. (14) of ref. [13]:

$$p(\Lambda|\mathcal{D}) = \pi(\Lambda) \prod_{i=1}^{N_{\rm obs}} \left[\frac{1}{n_s} \sum_{k=1}^{n_s} \frac{p_{\rm pop}(\theta_i^k|\Lambda)}{\pi(\theta_i^k)} \, |_{\theta_i^k \, \sim \, p(\theta_i|\mathcal{D}_i)} \right] \alpha^{-N_{\rm obs}}(\Lambda). \tag{2.45}$$

and by taking the logarithm:

$$\log\{p(\Lambda|\mathcal{D})\} = \log\{\pi(\Lambda)\} + \sum_{i=1}^{N_{\rm obs}} \log \left\{ \frac{1}{n_s} \sum_{k=1}^{n_s} \frac{p_{\rm pop}(\theta_i^k|\Lambda)}{\pi(\theta_i^k)} \, |_{\theta_i^k \, \sim \, p(\theta_i|\mathcal{D}_i)} \right\} - N_{\rm obs} \log(\alpha(\Lambda)). \tag{2.46}$$

In the present work, we use the natural logarithm (but the logarithm's basis does not change the results) and we use the Python package `emcee` [64] to compute the integrals with a Markov chain Monte Carlo algorithm (see appendix A.5, page 96 for the explanation of the algorithm).

[8] That is exactly the reason why the logarithms were invented!

2.3 An easy example of Bayesian inference: the Gaussian

We saw that Bayesian inference directly follows from the Bayes' formula, eq. (2.4). But how do we use this technique in a real situation?

In this section, we illustrate Bayesian inference with an easy example: we have samples from a Gaussian (normal) distribution function with unknown mean $\hat{\mu}$ and standard deviation $\hat{\sigma}$. In other words we have numbers that are (representative) samples of a distribution $\mathcal{N}(\hat{\mu}, \hat{\sigma}^2)$ and our goal is to find the values of $\hat{\mu}$ and of $\hat{\sigma}$ from the samples.

Here there is, we think, a first subtlety to understand. $\hat{\mu}$ and $\hat{\sigma}$ are the *true* values of the parameters "mean" and "standard deviation" (*i.e.* the samples come from a distribution with these values for the parameters). During the inference, we work with the variables μ and σ. The goal of the inference is to constrain each variable to an interval: $\mu = I_\mu$ and $\sigma = I_\sigma$, such that: $\hat{\mu} \in I_\mu$ and $\hat{\sigma} \in I_\sigma$ with a given probability (generally 68% or 95%). In the literature, the parameters, their true value and the corresponding variables often have the same name. In this section however, we take care to always make the distinction between the parameter, its true value and its variable. But in the other sections of the present document, we use the usual notation.

This Gaussian example is easy for at least three reasons:

- we suppose that we already have a representative sampling of the Gaussian pdf: we do not have any selection bias to take into account and we do not have to estimate the values of the samples by a first inference;
- we already know the shape of the source population: it is a normal distribution;
- a Gaussian is characterised by only two parameters.

This Bayesian inference follows from eq. (2.12):

$$p(\theta|\mathcal{D}) = \frac{\mathcal{L}(\mathcal{D}|\theta)\ \pi(\theta)}{\mathcal{Z}(\mathcal{D})}, \tag{2.47}$$

with $\theta = \{\mu, \sigma\}$ the vector containing the variables of the parameters that we want to constrain, and where $\mathcal{D}$ is the vector containing our N_{samples} of the unknown Gaussian probability distribution function: $\mathcal{D} = \{\mathcal{D}_1, \cdots, \mathcal{D}_{N_{\text{samples}}}\}$.

First, let us suppose that we do not have any indication on the true value of the parameter $\hat{\theta} = \{\hat{\mu}, \hat{\sigma}\}$, then we can take a constant prior: $\pi(\theta) = \text{const}$. By writing this equality, we say that we do not know the value of $\hat{\theta}$ and that we suppose that any value of a certain range has the same chance to be the true one. This "agnostic" point-of-view has the advantage to allow any value of θ to be the true one, whatever we can think before the inference. If the true value $\hat{\theta}$ has a zero prior, then the inference will never give the true result. The choice of prior is then important, and except mathematical (*e.g.* we do not want a negative value for the mass nor for a distance) or physical good reason (*e.g.* an extreme value for a parameter could be inconsistent with observation), we must avoid any zero probability for a prior.

Since $\mathcal{Z}(\mathcal{D})$ can be viewed as a simple overall normalisation factor, we can write a proportionality instead of an equality, and eq. (2.47) becomes:

$$p(\theta|\mathcal{D}) \propto \prod_{i=1}^{N_{\text{samples}}} \mathcal{L}(\mathcal{D}_i|\theta). \tag{2.48}$$

The r.h.s. is the likelihood function: it gives the probability to have the sample $\mathcal{D}_i$ from a Gaussian with parameters $\theta = \{\mu, \sigma\}$. This is exactly the meaning of the probability distribution function, thus:

$$\mathcal{L}(\mathcal{D}_i|\theta = (\mu,\sigma)\,) = \frac{1}{\sigma\sqrt{2\pi}} \exp\left\{-\frac{1}{2}\left(\frac{\mathcal{D}_i - \mu}{\sigma}\right)^2\right\}. \tag{2.49}$$

Equation (2.48) then says that the probability that the true value of the parameter $(\hat{\theta})$ is θ is just the product (or equivalently the sum of the logarithms) of the probability to obtain the sample $\mathcal{D}_i$ with a Gaussian pdf characterised by a mean and a standard deviation with the value θ. Now the goal is to test many different values for θ and to compute each time the probability of having the sample $\mathcal{D}_i$ for a Gaussian with this value of θ.

This collection of probabilities for many values of θ samples the posterior $p(\theta|\mathcal{D})$. And we can say that the true parameter, $\hat{\theta}$, lies in between the 16th and the 84th percentiles of the posterior $p(\theta|\mathcal{D})$ with a 68% credible interval (or in between the 2nd and the 98th percentiles with a 96% credible interval).

What the inference is doing is in fact easy to understand: it tests a lot of distributions (*i.e.* a lot of different values for the parameters of the distribution) and the tested distribution which maximises the probability to obtain data $\mathcal{D}$ is probably (close to) the true distribution. Of course, the more data $\mathcal{D}$, the more accurate the inference (the credible intervals go as $1/\sqrt{N_{\text{obs}}}$ where N_{obs} is the number of observations).

For example, we created a vector $\mathcal{D}$ of 100 samples (our "observations") coming from a Gaussian with $\hat{\mu} = 5$ and with $\hat{\sigma} = 1$ (the so-called *fiducial values*). We want to find the value of these (supposed unknown) parameters. Let us first suppose that we know $\hat{\sigma} = 1$, and that we want to constrain the value of $\hat{\mu}$. To do this, we evaluate the value of the product of the likelihoods (2.49) in 100 different choices of μ, between $\mu = 3$ and $\mu = 7$. Figure 2.2 shows the plot of (the non normalised) $p(\mu|\mathcal{D}, \hat{\sigma})$ as a function of μ,[9] along with the true value $\hat{\mu} = 5$ of the parameter.

We can see that the posterior distribution function $p(\mu|\mathcal{D}, \hat{\sigma})$ (fig. 2.2) looks very much like a Gaussian with a maximum at approximately $M \approx 4.9$ and with a standard deviation $\Sigma \approx 0.15$. This then means that the true parameter $\hat{\mu}$ is in the interval $[4.75, 5.05]$ with 68% of probability. We generally write: $\mu = 4.9 \pm 0.15$ at 68% C.L. (credible level), or alternatively $\mu = 4.9 \pm 0.3$ at 95% C.L., etc. In this example, the true value is indeed in the 68% credible interval, but this is not necessarily the case.

Note that the Gaussianity of the posterior distribution is *not* connected to the Gaussian source of our samples: with enough samples, the posterior of a Bayesian inference is always a Gaussian, by the central limit theorem (see *e.g.* [65]).

Now if both values of $\hat{\mu}$ and of $\hat{\sigma}$ are unknown, we must test many combinations of values for $\theta = (\mu, \sigma)$. To do this, we can use a Markov chain Monte Carlo (MCMC) algorithm (see appendix A, page 91). For this example (as for the other times we perform a MCMC in the present work), we use the Python package `emcee` [64, 66]. The result is shown in fig. 2.3, for which we use the Python software `corner` [67].

[9] In the general case, to follow the Bayes' formula, we must multiply the likelihood by the prior $\pi(\mu)$ and divide the total by the evidence $\mathcal{Z}(\mathcal{D})$. But here, the prior is flat and we could numerically normalise the pdf to unity at the end.

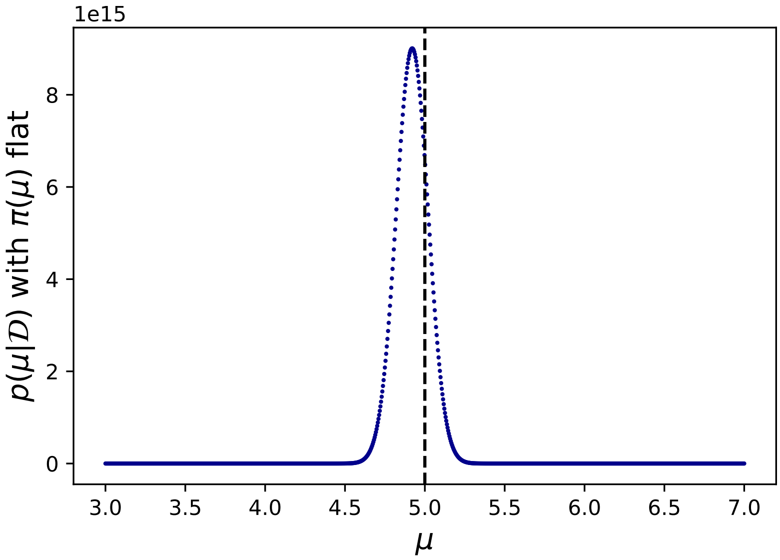

Figure 2.2: *(Non normalised) posterior distribution function of* $p(\mu|\mathcal{D}, \hat{\sigma})$ *as a function of* μ*. The black dashed line corresponds to the fiducial value* $\hat{\mu}$ *of the parameter.*

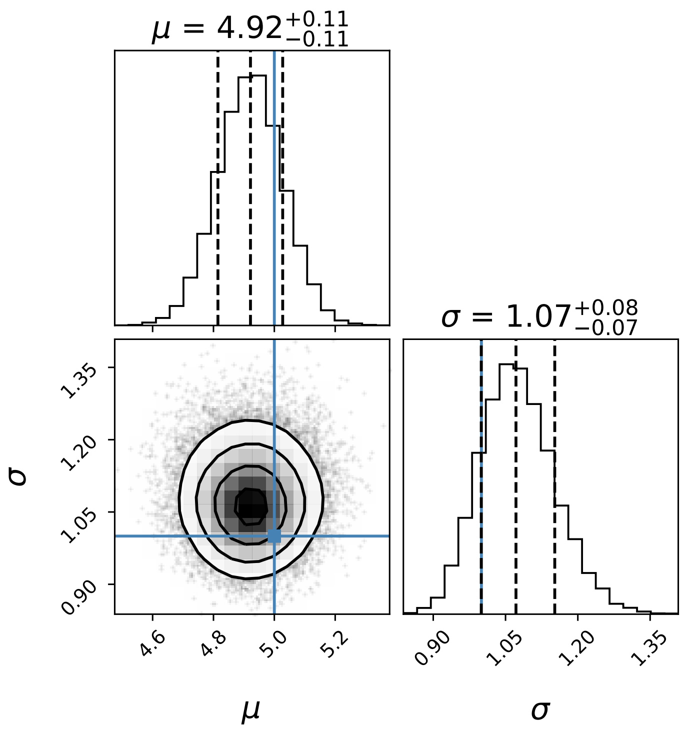

Figure 2.3: *Corner plots of* $p(\mu, \sigma|\mathcal{D})$ *as a function of* μ *and of* σ*. The blue lines correspond to the fiducial values* $\hat{\mu}$ *and* $\hat{\sigma}$ *of the parameters, and the black dotted lines correspond to the 16th, 50th and 84th percentiles of the posteriors.*

Figure 2.3 is called a *corner plot* and is the usual way to represent such posterior pdf's: when we have p parameters to constrain, the posterior is a p-dimensional function. In a corner plot, on the diagonal, we plot the histograms (or sometimes the smoothed pdf's) of a variable (*i.e.* the posterior *marginalised* over the other variables). Hence there are p histograms of one variable to plot a function of p variables.

Here, on the top of each histogram, the 68% credible interval is written. (This interval is also shown on the histograms by the black dashed lines.) Here, we can conclude that $\hat{\mu} \in [4.81, 5.03]$ with 68% C.L. and $\hat{\sigma} \in [1.00, 1.15]$ with 68% C.L.

Under the diagonal are shown the contour plots of two different variables. The contours highlight different credible levels. For example on fig. 2.3, the four levels show the $\{38\%,\ 68\%,\ 87\%,\ 95\%\}$ C.L. ($= \mathrm{erf}(x/\sqrt{2})$, for $x \in \{0.5, 1.0, 1.5, 2.0\}$.) All the 2-by-2 combinations of variables are plotted. We then have $(p-1)p/2$ contour plots of two variables to plot a function of p variables.

2.4 Hierarchical analysis of GWs from BBHs with a mass gap

This section presents the main theoretical result of this master's thesis.

Our goal is to constrain cosmological parameters, astrophysical parameters about the binary black holes population and, maybe the more interesting part, modified gravity parameters, see chapter 1.

Similar technique have been mentioned to be useful to constrain cosmological parameters in refs [35, 40] and have been performed to constrain the value of the Hubble constant, on mock data (representing five years of observation with the detector advLIGO at design sensitivity) in ref. [11] (see section 1.4 for more references). It has been also used to constrain modified GW propagation, *e.g.* in ref. [10], whose authors have constrain the same parameters as those that we are interested in: $\{H_0, \Xi_0, \cdots\}$, see section 1.5, by using dark sirens and a galaxy catalog, and in ref. [12] that used a similar technique on a different parametrisation of modified GW propagation (c_{M}, see section 1.5) by using the mass redshift, but without mock test.

To constrain these parameters, we use eq. (2.33) of hierarchical Bayesian inference with a selection effect:

$$p(\Lambda, N|\mathcal{D}) \propto \pi(\Lambda)\pi(N) \prod_{i=1}^{N_{\mathrm{obs}}} \left[\int \frac{p(\theta_i|\mathcal{D}_i)}{\alpha(\Lambda)} \, \frac{p_{\mathrm{pop}}(\theta_i|\Lambda)}{\pi(\theta_i)} \, \mathrm{d}\theta_i \right] \cdot \mathrm{e}^{-N_{\mathrm{exp}}} (N_{\mathrm{exp}})^{N_{\mathrm{obs}}}, \tag{2.50}$$

or in fact the logarithm of the descretisation of this equation (eq. (2.44)):

$$\log\{p(\Lambda, N|\mathcal{D})\} = \log\{\pi(\Lambda)\} + \log\{\pi(N)\} + \sum_{i=1}^{N_{\mathrm{obs}}} \log \left\{ \frac{1}{n_s} \sum_{k=1}^{n_s} \frac{p_{\mathrm{pop}}(\theta_i^k|\Lambda)}{\pi(\theta_i^k)} \Big|_{\theta_i^k \sim p(\theta_i|\mathcal{D}_i)} \right\} - N\alpha(\Lambda) + \mathrm{const.} \tag{2.51}$$

More precisely, in the present case, the variables of eq. (2.51) are:

- $\mathcal{D}$ the GW data, which corresponds to the detections of gravitational waves (now by the LIGO and Virgo collaborations (LVC) but soon with other detectors, such as KAGRA): it is the collection of the detected GWs;
- θ the source parameters: a 15-dimensional vector of extrinsic and intrinsic parameters. In the following we neglect the effects of some parameters (see chapter 1 and below);
- Λ the hyperparameters we are interested in: cosmological, astrophysical and modified gravity parameters (see below);
- N_{obs} the number of used events ($= \dim \mathcal{D}$);

- n_s the number of samples of the posterior $p(\theta_i|\mathcal{D}_i)$.

The selection bias function $\alpha(\Lambda)$ is computed in details in appendix B, page 97. Here we will assume that it is known.

Import note: the aim of this section is to use the mass gap in the population of astrophysical black holes to operate an inference. It is then important to use only the detections of gravitational waves whose source is a (astrophysical) BBH.

As in the articles [10, 11], we are only interested in the parameters:

$$\theta = \{m_1^z, m_2^z, \Theta, d_{\mathrm{L}}^{\mathrm{GW}}\}, \tag{2.52}$$

where m_1^z and m_2^z are respectively the mass of the heavier black hole and the mass of the lighter one *in the detector frame* ($m_i^z = m_i^0(1+z)$);[10] Θ is the angle of the source's orbital plane with respect to our direction of sight, and $d_{\mathrm{L}}^{\mathrm{GW}}$ is the gravitational wave luminosity distance (see subsection 1.5.2).

The values of $p(\theta_i|\mathcal{D}_i)$ (or more precisely directly the samples $\theta_i^k \sim p(\theta_i|\mathcal{D}_i)$) are publicly given by LVC (see *e.g.* [68]) and they are obtained from a first Bayesian inference.

We are looking for the hyperparameters (as in [10]):

$$\Lambda = \{\vec{\lambda}_{\mathrm{cosmo}}, \vec{\lambda}_{\mathrm{BBH}}, R_0, \gamma\}, \tag{2.53}$$

where $\vec{\lambda}_{\mathrm{cosmo}}$ (also written without the arrow) is the vector of the parameters of our cosmological model (for example, in ΛCDM, H_0, $\Omega_{\mathrm{m},0}$, etc.) *and* the parameters of the parametrisation of the modified gravitational waves propagation that we want to constrain (Ξ_0 and n).[11]

$\vec{\lambda}_{\mathrm{BBH}}$ is the vector of the parameters of the binary astrophysical black holes population. According to the model of population, we can have $\vec{\lambda}_{\mathrm{BBH}} = \{\alpha, \beta, m_l, m_h, \cdots\}$ (see section 1.6). R_0 is the rate of BBHs mergers at redshift $z = 0$ and γ describes the evolution of the rate of mergers as a function of the redshift z: $R(z) = R_0\ (1+z)^\gamma$.

We generally take the prior $\pi(\Lambda)$ flat on a large range of values, this allowing any value of the range to be the true value of the parameter. Sometimes however, we also use a Gaussian prior on H_0 and on $\Omega_{\mathrm{m},0}$ around the values found by the satellite *Planck* in 2018 ($H_0 = 67.66 \pm 0.42$ [km s^{-1}Mpc^{-1}][12] and $\Omega_{\mathrm{m},0} = 0.3111 \pm 0.0056$) [69].

In eq. (2.51), the only result we do not know is the fraction:

$$\mathscr{P}(\theta|\Lambda) \equiv \frac{p_{\mathrm{pop}}(\theta|\Lambda)}{\pi(\theta)}, \tag{2.54}$$

let us evaluate it.

2.4.1 The function $\mathscr{P}(\theta|\Lambda)$

In this subsection, we want to evaluate the function $\mathscr{P}(\theta|\Lambda)$, as given by eq. (2.54).

At the denominator, we have the prior function on the parameter θ. Since $\theta = \{m_1^z, m_2^z, \Theta, d_{\mathrm{L}}^{\mathrm{GW}}\}$, we have:

[10] m_i^z is often written m_i^{det} (because it is the *detected* mass), but 'det' can have many meanings so we prefer m_i^z.
[11] We recall that in this parametrisation, one gets: $d_{\mathrm{L}}^{\mathrm{GW}} = \{\Xi_0 + (1-\Xi_0)/(1+z)^n\}\ d_{\mathrm{L}}^{\mathrm{EM}}$, see subsection 1.5.3.
[12] We will not always write the units of H_0. When it is not precised, then the unit is always km s^{-1}Mpc^{-1}.

$$\pi(\theta) = \pi(m_1^z, m_2^z, \Theta, d_L^{GW}) \tag{2.55}$$
$$= \pi(m_1^z, m_2^z)\ \pi(\Theta)\ \pi(d_L^{GW}), \tag{2.56}$$

where eq. (2.56) follows from the fact that the two masses of the black holes are correlated, but the masses, the distance and the orientation angle are taken to be independent (this is true at a first approximation, but at higher approximation the masses could be correlated with the distance, *e.g.* through the metallicity). This prior is given within the GW results publications, *e.g.* ref. [68] (it is the same prior as used by LVC to obtain the function $p(\theta|\mathcal{D})$).

The numerator of $\mathscr{P}$, $p_{\text{pop}}(\theta|\Lambda)$, is immediately obtained from the differential rate of formation of BBHs, $\mathrm{d}\mathcal{N}/\mathrm{d}\theta$, that is normalised such that:

$$\frac{\mathrm{d}\mathcal{N}(\Lambda, N)}{\mathrm{d}\theta} = N\ p_{\text{pop}}(\theta|\Lambda). \tag{2.57}$$

However, in general, the differential rate of formation of BBHs is given as a function of other parameters than the one we use. We then need to use some Jacobian determinants to transform the parameters into other parameters.

We also need a rate which depends on the redshift (we will see why in subsection 2.4.2). Any credible model of population does.

We will write explicitly a function $\mathscr{P}(\theta|\Lambda)$ depending on a simple formation rate in the § **A simple model for the BBH formation rate**, page 64, but first we need to recall a few cosmological notations.

Cosmological notations

Here we recall some notations (for more information, see section 1.2). The comoving distance is defined as:

$$d_{\text{com}}(z) = \int_0^z \frac{c\ \mathrm{d}z'}{H(z')}, \tag{2.58}$$

where c is the speed of light and $H(z)$ is the Hubble parameter that we can normalise as: $H(z) = H(z=0)\ E(z) \equiv H_0\ E(z)$, hence writing

$$u(z) = \int_0^z \frac{\mathrm{d}z'}{E(z')}, \tag{2.59}$$

one gets:

$$d_{\text{com}}(z) = \frac{c}{H_0} u(z). \tag{2.60}$$

The electromagnetic luminosity distance is linked to the comoving distance by:

$$d_L^{EM} = (1+z)\ d_{\text{com}}(z), \tag{2.61}$$

thus the gravitational luminosity distance $d_L^{GW} = \Xi(z)\ d_L^{EM}$ can be rewritten as:

$$d_L^{GW} = (1+z)\ \Xi(z)\ \frac{c}{H_0} u(z) \equiv s(z)\ \frac{c}{H_0} u(z). \tag{2.62}$$

The comoving volume V_{com} is defined through its derivative:

$$\frac{\mathrm{d}^2 V_{\mathrm{com}}}{\mathrm{d}z\ \mathrm{d}\Omega} = c\ \frac{d_{\mathrm{com}}^2(z)}{H(z)} = \left(\frac{c}{H_0}\right)^3\ \frac{u^2(z)}{E(z)} \equiv \left(\frac{c}{H_0}\right)^3 j(z); \tag{2.63}$$

thus,

$$\frac{\mathrm{d}V_{\mathrm{com}}}{\mathrm{d}z} = \int \frac{\mathrm{d}^2 V_{\mathrm{com}}}{\mathrm{d}z\ \mathrm{d}\Omega}\ \mathrm{d}\Omega = 4\pi \left(\frac{c}{H_0}\right)^3 j(z). \tag{2.64}$$

A simple model for the BBH formation rate

In chapter 3, we will test a few different models of BBH mass population. We will always give the specific function $\mathscr{P}$, but let us first show how to obtain it from a simple model.

We consider the following BBHs formation model proposed in [11] (see their eq. (A1)) and already explained in section 1.6:

$$\begin{aligned}\frac{\mathrm{d}^4\mathcal{N}}{\mathrm{d}m_1\ \mathrm{d}m_2\ \mathrm{d}V_{\mathrm{com}}\ \mathrm{d}\tau} &= \frac{R_{30}}{(30\ \mathrm{M}_\odot)^2}\ \left(\frac{m_1}{30\ \mathrm{M}_\odot}\right)^{-\alpha} \left(\frac{m_2}{30\ \mathrm{M}_\odot}\right)^{\beta}\ (1+z)^\gamma\ \Theta(m_1 - m_2) \\ &\times f_{\mathrm{smooth}}(m_1|m_l, \sigma_l, m_h, \sigma_h)\ f_{\mathrm{smooth}}(m_2|m_l, \sigma_l, m_h, \sigma_h) \qquad (2.65) \\ &\equiv p_{\mathrm{pop}}(m_1, m_2|\vec{\lambda}_{\mathrm{BBH}})\ \cdot\ \frac{R_{30}}{(30\ \mathrm{M}_\odot)^2}\ (1+z)^\gamma\ \Theta(m_1 - m_2) \qquad (2.66)\end{aligned}$$

where $\Theta(x)$ is the Heaviside step-function, τ is the time in the source frame, where $\vec{\lambda}_{\mathrm{BBH}} = \{\alpha, \beta, m_l, \sigma_h, m_h, \sigma_h\}$, R_{30} being the overall mass rate density, normalised for BHs of 30 $\mathrm{M}_\odot$, and where one defines the function (for $i = 1, 2$):

$$f_{\mathrm{smooth}}(m_i|m_l, \sigma_l, m_h, \sigma_h) = \Phi\left(\frac{\ln(m/m_l)}{\sigma_l}\right)\left[1 - \Phi\left(\frac{\ln(m/m_h)}{\sigma_h}\right)\right], \tag{2.67}$$

with $\Phi(x)$ the standard normal cumulative distribution function:

$$\Phi(x) = \frac{1}{\sqrt{2\pi}} \int_{-\infty}^{x} \mathrm{e}^{-t^2/2}\ \mathrm{d}t. \tag{2.68}$$

The BHs mass gap of astrophysical BHs (before the intermediate mass BHs) can be seen from $p_{\mathrm{pop}}(m_1, m_2|\vec{\lambda}_{\mathrm{BBH}})$. This function for $m_2 = 5\ \mathrm{M}_\odot$ is plotted on fig. 2.4.

Equation (2.65) is given as a function of the source frame masses m_1, m_2, comoving volume V_{com} and source frame time τ. But the parameters θ in eq. (2.57) are the detector frame masses m_1^z, m_2^z and GW luminosity distance $d_{\mathrm{L}}^{\mathrm{GW}}$. Hence we need to include the appropriate Jacobian determinants, that contain the cosmological model we test (*e.g.* H_0, Ξ_0, n, $\Omega_{\mathrm{m},0}$, $\cdots$). In our case:

$$N\ p_{\mathrm{pop}}(\theta|\Lambda) = \frac{\mathrm{d}^4\mathcal{N}}{\mathrm{d}m_1^z\ \mathrm{d}m_2^z\ \mathrm{d}\Theta\ \mathrm{d}d_{\mathrm{L}}}, \tag{2.69}$$

we ignore the Θ dependence since $\int \mathrm{d}\Theta = 1$, and we can rewrite:

$$\begin{aligned}\mathrm{d}m_i &= \frac{\mathrm{d}m_i}{\mathrm{d}m_i^z}\ \mathrm{d}m_i^z,\ \text{ for } i = 1, 2 \qquad (2.70) \\ &= \frac{1}{(1+z)}\ \mathrm{d}m_i^z, \qquad (2.71)\end{aligned}$$

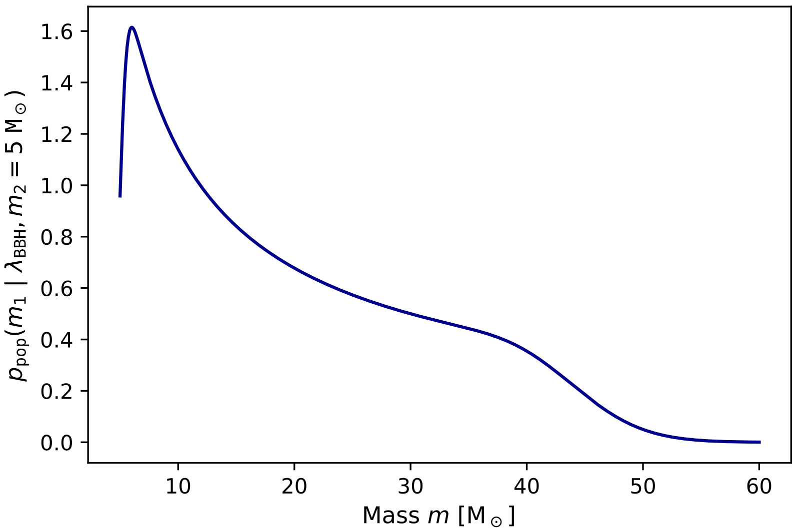

Figure 2.4: *Plot of* $p_{\mathrm{pop}}(m_1 \mid \vec{\lambda}_{\mathrm{BBH}}, m_2 = 5\ \mathrm{M}_\odot)$ *as a function of* m_1 *(see eq. (2.66)).*

and

$$\mathrm{d}V_{\mathrm{com}} = \frac{\mathrm{d}V_{\mathrm{com}}}{\mathrm{d}z}\,\frac{\mathrm{d}z}{\mathrm{d}d_{\mathrm{L}}}\,\mathrm{d}d_{\mathrm{L}} \tag{2.72}$$

so,

$$\begin{aligned} N\ p_{\mathrm{pop}}(\theta|\Lambda) &= \frac{\mathrm{d}^3\mathcal{N}}{\mathrm{d}m_1\ \mathrm{d}m_2\ \mathrm{d}V_{\mathrm{com}}}\ \frac{1}{(1+z^*)^2}\ \frac{\mathrm{d}V_{\mathrm{com}}}{\mathrm{d}z}\ \frac{\mathrm{d}z}{\mathrm{d}d_{\mathrm{L}}}|_{z=z^*} && (2.73)\\ &= \frac{\mathrm{d}^4\mathcal{N}}{\mathrm{d}m_1\ \mathrm{d}m_2\ \mathrm{d}V_{\mathrm{com}}\ \mathrm{d}\tau}\ \frac{1}{(1+z^*)^2}\ \frac{\mathrm{d}V_{\mathrm{com}}}{\mathrm{d}z}\ \frac{\mathrm{d}z}{\mathrm{d}d_{\mathrm{L}}}|_{z=z^*}\cdot\frac{\mathrm{d}\tau}{\mathrm{d}t}\mathrm{d}t && (2.74)\end{aligned}$$

where t is the time in the detector frame and where z^* is the solution of: $d_{\mathrm{L}}^{\mathrm{GW}}(z^*, H_0, \Xi_0, \cdots) = d_{\mathrm{L}}^{\mathrm{measured}}$ (it is the redshift that corresponds to the measured distance, given the cosmological model). Integrating over t, we get:

$$N\ p_{\mathrm{pop}}(\theta|\Lambda) = \frac{\mathrm{d}^4\mathcal{N}}{\mathrm{d}m_1\ \mathrm{d}m_2\ \mathrm{d}V_{\mathrm{com}}\ \mathrm{d}\tau}\ \frac{1}{(1+z^*)^2}\ \frac{\mathrm{d}V_{\mathrm{com}}}{\mathrm{d}z}\ \frac{\mathrm{d}z}{\mathrm{d}d_{\mathrm{L}}}|_{z=z^*}\cdot\frac{T_{\mathrm{obs}}}{(1+z^*)}. \tag{2.75}$$

The Jacobian $\partial z/\partial d_{\mathrm{L}}$ can be expressed as:

$$\begin{aligned} J_z = \frac{\partial d_{\mathrm{L}}^{\mathrm{GW}}}{\partial z} &= \frac{\mathrm{d}}{\mathrm{d}z}\left(\Xi(z)\ d_{\mathrm{L}}^{\mathrm{EM}}(z)\right) && (2.76)\\ &= \frac{\mathrm{d}}{\mathrm{d}z}\left[s(z)\ d_{\mathrm{com}}(z)\right] && (2.77)\\ &= \left(s'(z)\ d_{\mathrm{com}}(z) + s(z)\ d'_{\mathrm{com}}(z)\right) && (2.78)\\ &= \frac{c}{H_0}\left(s'(z)\ u(z) + \frac{s(z)}{E(z)}\right) && (2.79)\end{aligned}$$

where the prime denotes a derivative with respect to z: $f' \equiv \partial_z f$.

And we finally get:

$$\mathscr{P}(\theta|\Lambda) \propto \left(\frac{c}{H_0}\right)^2 \frac{4\pi\ T_{\text{obs}}\ p_{\text{pop}}(m_1, m_2|\vec{\lambda}_{\text{BBH}})\ u^2(z^*)}{\pi(m_1, m_2)\ \pi(d_{\text{L}})\ \pi(\Theta)\ \left[E(z^*)\ s'(z^*)\ u(z^*) + s(z^*)\right]} \cdot \frac{R_{30}}{(30\ \text{M}_\odot)^2}\ (1+z)^{\gamma-3}, \tag{2.80}$$

where $s'(z^*) = \partial_z s(z)_{|z=z^*}$.

$\mathscr{P}(\theta|\Lambda)$ as given by the latter equation is the expression we will use in our codes to infer the hyperparameters $\Lambda = \{\vec{\lambda}_{\text{BBH}}, H_0, \Xi_0, \cdots\}$.

2.4.2 How the hierarchical inference works

One can understand the basic working of this hierarchical Bayesian inference by noticing that we have a relation between the (gravitational) luminosity distance and the redshift that depends on the cosmological model (with the parametrisation of the modified gravitational waves propagation):

$$d_{\text{L}}^{\text{GW}}(z^*, H_0, \Omega_{\text{m},0}, w_{\text{DE}}, \Xi_0, n, \cdots) = d_{\text{L}}^{\text{measured}}. \tag{2.81}$$

The measured distance $d_{\text{L}}^{\text{measured}}$ is a given data from the observations. But the redshift which corresponds to this distance is unknown (without any EM counterpart). Luckily, masses of the sources are redshifted such that:

$$m^z = m^0(1+z), \tag{2.82}$$

so by knowing the source-frame mass of the BBHs and its detector-frame mass one knows the redshift.

In this work we use the shape of the astrophysical BBHs population function, and more particularly its maximum mass cutoff, to evaluate statistically the value of the source masses of the BBHs. We then need a large number of observations of GW coming from BBHs.

The BBHs population function itself depends on the parameters $\vec{\lambda}_{\text{BBH}}$. According to the considered model, one can have at least four parameters in $\vec{\lambda}_{\text{BBH}}$ (see section 1.6).

So, this inference has to constrain the value of the redshift corresponding to an observation, hence the values of $\{\vec{\lambda}_{\text{BBH}}, \vec{\lambda}_{\text{cosmo}}, R_0, \gamma, \cdots\} = \Lambda$ which best fit the observations.

2.4.3 Effects of the selection bias

Let us first remember that:

$$\alpha(\Lambda) = \int p_{\text{det}}(\theta)\ p_{\text{pop}}(\theta|\Lambda)\ \text{d}\theta. \tag{2.83}$$

We explain how to compute it in appendix B.

We can qualitatively predict the effects of the selection bias. This bias reflects the fact that that the further the source, the heavier it has to be, to be detectable. So in a catalog of detected GWs, the further the sources, the heavier their average mass.

But in parallel, the further the source, the more redshifted it is. So even if all sources were detectable, the average *detected* mass must increase with the distance (see eq. (2.82)). So the selection bias accentuates the normal increase of mass with redshift (thus with distance).

Our Bayesian hierarchical inference uses the detected mass (that increases with distance) to estimate the redshift. Since the detected masses are also increased by the selection bias, the redshift corresponding to a certain distance would be overestimated: H_0 is also overestimated.

On the other hand, if the redshift z is overestimated, then the (observed) gravitational luminosity distance has to be smaller than the EM luminosity distance (given by H_0) which fits the estimated redshift. To allow this behaviour, Ξ_0 has to be underestimated.

2.5 Summary

Let us summarise the main points of this chapter.

- In order to constrain the values of the parameters we are interested in, we use Bayesian hierarchical inference. This technique is based on the Bayes' theorem:

$$\mathsf{P}(A|B) = \frac{\mathsf{P}(B|A)\ \mathsf{P}(A)}{\mathsf{P}(B)}. \tag{2.84}$$

- We want to compute the probability that a parameter Λ takes a particular value, given the observed data $\mathcal{D}$. We then re-write the Bayes' formula as:

$$p(\Lambda|\mathcal{D}) = \frac{\pi(\Lambda)}{\mathcal{Z}_{\text{tot}}(\mathcal{D})} \prod_{i=1}^{N} \int \mathcal{Z}(\mathcal{D}_i)\ p(\theta_i|\mathcal{D}_i)\ \frac{p_{\text{pop}}(\theta_i|\Lambda)}{\pi(\theta_i)}\ \mathrm{d}\theta_i. \tag{2.85}$$

- To take into account the fact that all events are not detectable, we have to normalise the latter equation by a factor $\alpha(\Lambda)$, given by:

$$\alpha(\Lambda) = \int p_{\text{det}}(\theta)\ p_{\text{pop}}(\theta|\Lambda)\ \mathrm{d}\theta, \tag{2.86}$$

  and to include a Poisson probability distribution function, to finally get:

$$p(\Lambda, N|\mathcal{D}) \propto \pi(\Lambda)\pi(N) \prod_{i=1}^{N_{\text{obs}}} \left[\int \frac{p(\theta_i|\mathcal{D}_i)}{\alpha(\Lambda)}\ \frac{p_{\text{pop}}(\theta_i|\Lambda)}{\pi(\theta_i)}\ \mathrm{d}\theta_i\right] \cdot \mathrm{e}^{-N_{\text{exp}}}(N_{\text{exp}})^{N_{\text{obs}}}. \tag{2.87}$$

- In order to evaluate such integrals, we use a Monte Carlo integration and we take the logarithms. Equation (2.87) can then be written as:

$$\log\{p(\Lambda, N|\mathcal{D})\} = \log\{\pi(\Lambda)\} + \log\{\pi(N)\} + \sum_{i=1}^{N_{\text{obs}}} \log\left\{\frac{1}{n_s}\sum_{k=1}^{n_s} \frac{p_{\text{pop}}(\theta_i|\Lambda)}{\pi(\theta_i)}\ \Big|_{\theta_i^k \sim p(\theta_i|\mathcal{D}_i)}\right\} \\ - N\alpha(\Lambda) + \text{const.} \tag{2.88}$$

- Figure 2.3 shows the kind of results we are expecting as a result of a Bayesian inference. In section 2.3, we briefly discussed how to read and interpret this kind of plots.

- We note: $\mathscr{P}(\theta_i^k|\Lambda) = p_{\rm pop}(\theta_i|\Lambda)/\pi(\theta_i)$, and we express $p_{\rm pop}$ as a function of the differential formation rate:

$$\frac{\mathrm{d}\mathcal{N}}{\mathrm{d}\theta} = N\ p_{\rm pop}(\theta|\Lambda). \tag{2.89}$$

  $\pi(\Lambda)$ is generally taken flat; $\pi(\theta)$ and $\theta^k \sim p(\theta|\mathcal{D})$ are given in the LVC results publications (*e.g.* [54]) and $\alpha(\Lambda)$ is computed explicitly in appendix B.

- In the simple BBHs formation model given by eq. (2.65), we get:

$$\mathscr{P}(\theta|\Lambda) \propto \left(\frac{c}{H_0}\right)^2 \frac{4\pi\ T_{\rm obs}\ p_{\rm pop}(m_1,m_2|\vec{\lambda}_{\rm BBH})\ u^2(z^*)}{\pi(m_1,m_2)\ \pi(d_{\rm L})\ \pi(\Theta)\ \left[E(z^*)\ s'(z^*)\ u(z^*) + s(z^*)\right]} \times \frac{R_{30}}{(30\ \mathrm{M}_\odot)^2}\ (1+z)^{\gamma-3}, \tag{2.90}$$

  and we evaluate eq. (2.88) together with eq. (2.90) with a Markov chain Monte Carlo technique (see appendix A) to constrain the value of the hyperparameter $\Lambda = \{H_0, \Xi_0, n, \Omega_{\rm m,0}, \vec{\lambda}_{\rm BBH}, \cdots\}$.

The results we obtain by applying this method on mock data and on real data of GWTC-1 and GWTC-2 [3, 4] are presented in chapter 3.

Chapter 3

Results

Contents

This chapter presents and discuss the cosmological and astrophysical results we obtained by applying hierarchical Bayesian inference on GWs emitted by BBHs with a mass gap, as explained in section 2.4.

First we recall some values (obtained by other techniques) for the parameters we are interested in. In a second section we test our Bayesian method (see section 2.4) on mock data. In a third section, we analyse the LIGO–Virgo Collaborations (LVC) *Gravitational Wave Transient Catalogs*: GWTC-1 (LVC runs O1 and O2, ref. [3]) and GWTC-2 (LVC run O3a, ref. [4]).

3.1 Review of known limits on cosmological parameters

In table 3.1 we review some values for the cosmological parameters, obtained by different techniques.

Parameter	Value	Unit	Ref.	Technique
H_0	67.66 ± 0.42	km s^{-1} Mpc^{-1}	[69]	Planck *2018 best fit for ΛCDM*
	$68.86^{+0.69}_{-0.7}$	km s^{-1} Mpc^{-1}	[52]	Planck *2015 best fit for RT model*
	70.8 ± 2.1	km s^{-1} Mpc^{-1}	[70]	*Standard candles (new result uncertainty in the supernova distance ladder)*
	73.24 ± 1.74	km s^{-1} Mpc^{-1}	[21]	*Standard candles ("classical" result)*
	$70^{+12.0}_{-8.0}$	km s^{-1} Mpc^{-1}	[5]	*Standard siren with EM counterpart (GW170817 and GRB 170817A)*
	$67.3^{+27.6}_{-17.9}$	km s^{-1} Mpc^{-1}	[10]	*Dark sirens alone with galaxy catalog*
	$72.2^{+13.9}_{-7.5}$	km s^{-1} Mpc^{-1}	[10]	*Dark sirens with galaxy catalog + Standard siren GW170817*
	74^{+13}_{-7}	km s^{-1} Mpc^{-1}	[63]	*Standard sirens with EM counterpart (GW170817 and GW190521) for ΛCDM*
$w_{\rm DE}$	-1	–	–	*ΛCDM*
	$-1.00^{+0.04}_{-0.05}$	–	[21]	*CMB best fit for wCDM*
$\Omega_{\rm m,0}$	0.3111 ± 0.0056	–	[69]	Planck *2018 best fit for ΛCDM*
	0.58 ± 0.25	–	[63]	*Standard sirens with EM counterpart (GW170817 and GW190521) for ΛCDM*
	0.6 ± 0.4	–	[63]	*Standard sirens with EM counterpart (GW170817 and GW190521) for modified gravity (wide priors)*
Ξ_0	$2.1^{+3.2}_{-1.2}$	–	[10]	*Dark sirens with galaxy catalog*
	$1.8^{+0.9}_{-0.6}$	–	[10]	*Dark sirens with galaxy catalog + using flare ZTF19abanrhr as EM counterpart of GW190521*
	< 10	–	[63]	*Standard sirens with EM counterpart (GW170817 and GW190521) (wide prior)*
	< 4.4	–	[63]	*Standard sirens with EM counterpart (GW170817 and GW190521) (*Planck *prior)*
n	1.91	–	[10]	*Best fit for the RT model*
	6^{+4}_{-5}	–	[63]	*Standard sirens with EM counterpart (GW170817 and GW190521) (wide prior)*
	4^{+5}_{-4}	–	[63]	*Standard sirens with EM counterpart (GW170817 and GW190521) (*Planck *prior)*
$c_{\rm M}$	$-3.2^{+3.4}_{-2.0}$	–	[12]	*Dark sirens with a BH mass gap*
	< 13.4	–	[63]	*Standard sirens with EM counterpart (GW170817 and GW190521) (wide prior)*
	< 7.5	–	[63]	*Standard sirens with EM counterpart (GW170817 and GW190521) (*Planck *prior)*

Table 3.1: *Review of values for the cosmological parameters we are interested in.*

3.2 Mock data

The first step is to test on mock data if our inference works and how much it is efficient. These computations were done on laptops and on the UNIGE Department of Theoretical Physics' workstation.

3.2.1 Publicly available simulated data

To first test hierarchical Bayesian inference, we start from publicly available simulated observations of GWs detections. Ref. [11] simulated five years of observations for advanced LIGO at design sensitivity. The mock samples $\theta_i^k \sim p(\theta_i|\mathcal{D}_i)$ (for $k = 4\,000$) are available on the GitHub [71]. This data was simulated using the simple model for the BBH formation rate we already discussed in subsection 2.4.1. As a reminder, it is (see eqs (2.65) to (2.68)):

$$\begin{aligned}
\frac{\mathrm{d}^4\mathcal{N}}{\mathrm{d}m_1\,\mathrm{d}m_2\,\mathrm{d}V_{\mathrm{com}}\,\mathrm{d}\tau} &= \frac{R_{30}}{(30\ \mathrm{M}_\odot)^2}\left(\frac{m_1}{30\ \mathrm{M}_\odot}\right)^{-\alpha}\left(\frac{m_2}{30\ \mathrm{M}_\odot}\right)^{\beta}(1+z)^{\lambda}\,\Theta(m_1-m_2) \\
&\quad\times f_{\mathrm{smooth}}(m_1|m_l,\sigma_l,m_h,\sigma_h)\,f_{\mathrm{smooth}}(m_2|m_l,\sigma_l,m_h,\sigma_h) \qquad (3.1)\\
&\equiv p_{\mathrm{pop}}(m_1,m_2|\vec{\lambda}_{\mathrm{BBH}})\cdot\frac{R_{30}}{(30\ \mathrm{M}_\odot)^2}(1+z)^{\lambda}\,\Theta(m_1-m_2). \qquad (3.2)
\end{aligned}$$

(Where we write λ instead of γ for the redshift power-law.) $\Theta(x)$ is the Heaviside step-function, τ is the time in the source frame, $\vec{\lambda}_{\mathrm{BBH}} = \{\alpha,\beta,m_l,\sigma_l,m_h,\sigma_h\}$, R_{30} is the overall mass rate density, normalised for BBHs of 30 $\mathrm{M}_\odot$, and we define the function (for $i = 1, 2$):

$$f_{\mathrm{smooth}}(m_i|m_l,\sigma_l,m_h,\sigma_h) = \Phi\left(\frac{\ln(m/m_l)}{\sigma_l}\right)\left[1-\Phi\left(\frac{\ln(m/m_h)}{\sigma_h}\right)\right], \qquad (3.3)$$

with $\Phi(x)$ the standard normal cumulative distribution function:

$$\Phi(x) = \frac{1}{\sqrt{2\pi}}\int_{-\infty}^{x}\mathrm{e}^{-t^2/2}\,\mathrm{d}t. \qquad (3.4)$$

To generate this mock data, the values of table 3.2 were used.

Parameter	R_{30}	α	β	λ	m_l	σ_l	m_h	σ_h
Value	64.4 [$\mathrm{Gpc}^{-3}\ \mathrm{yr}^{-1}$]	0.75	0.00	3.0	5 [$\mathrm{M}_\odot$]	0.1	45 [$\mathrm{M}_\odot$]	0.1

Table 3.2: *Table of the used values for the parameters used in ref. [11] to generate mock data.*

Since mock data comes from a BBHs population following eq. (3.1), we expect our Bayesian inference to find the values of table 3.2.

For the cosmological background, this data was simulated using ΛCDM, with the *Planck* 2015 median values (ref. [53]). As usual, we call these parameters λ_{cosmo}. For five years of observations with advanced LIGO, it gives 5 267 events [71].

We use this mock data to test if our Bayesian hierarchical inference is able to constrain the (known) values of $\{\lambda_{\mathrm{BBH}}, R_{30}, \lambda, \lambda_{\mathrm{cosmo}}\}$. We note that these data assume GR GWs propagation, thus $\Xi_0 = 1$, while n can have any (finite) value.

As already discussed in section 2.4, we must evaluate the posterior:

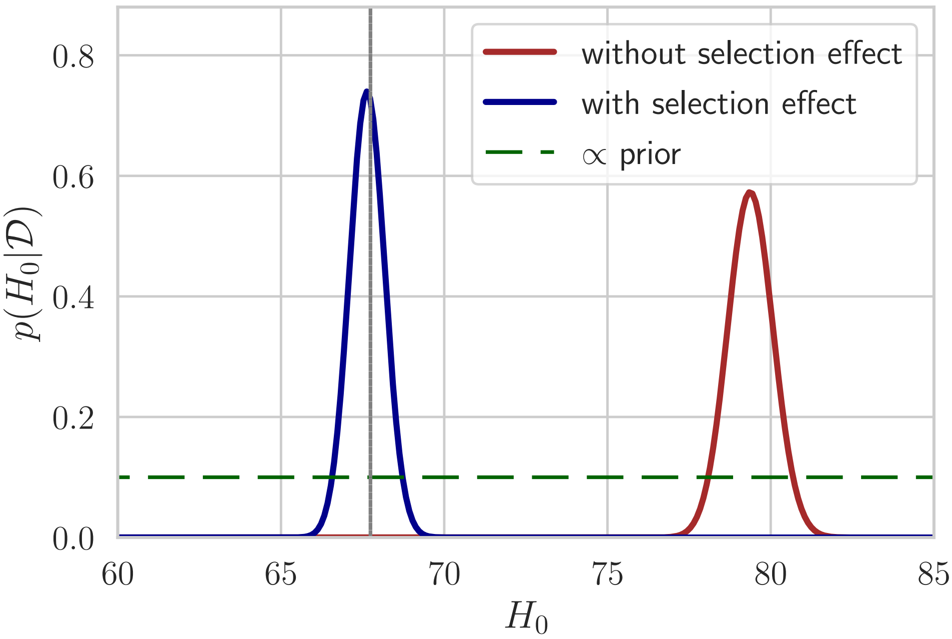

Figure 3.1: *Result of Bayesian inference on mock data for H_0 alone. The solid gray line indicates the fiducial value.*

$$\log\{p(\Lambda, N)\} = \log\{\pi(N)\} + \log\{\pi(\Lambda)\} + \sum_{i=1}^{N_{\rm obs}} \log\left\{\frac{1}{n_s}\sum_{k=1}^{n_s} \mathscr{P}(\theta_i^k|\Lambda)|_{\theta_i^k\sim p(\theta_i|\mathcal{D}_i)}\right\} - N\alpha(\Lambda), \quad (3.5)$$

with:

$$\mathscr{P}(\theta|\Lambda) \propto \frac{4\pi\; T_{\rm obs}\; p_{\rm pop}(m_1, m_2|\vec{\lambda}_{\rm BBH})\; u^2(z^*|\lambda_{\rm cosmo})}{\pi(m_1, m_2)\; \pi(d_{\rm L})\; \pi(\Theta)\;\; [E(z^*|\lambda_{\rm cosmo})\; s'(z^*|\lambda_{\rm cosmo})\; u(z^*|\lambda_{\rm cosmo}) + s(z^*|\lambda_{\rm cosmo})]} \times \left(\frac{c}{H_0}\right)^2 \frac{R_{30}}{(30\;{\rm M}_\odot)^2}\; (1+z)^{\lambda-3}. \quad (3.6)$$

Results with only one free parameter

Since we know the values of all the parameters, a first test consists in setting all the parameters to their fiducial value (*i.e.* the simulation of data was done by using these values), except one, and to evaluate the posterior for this single free parameter.

The first parameter on which we want to test the inference is the Hubble constant, H_0. Fig. 3.1 is the plot of the posterior $p\,(H_0 \mid \mathcal{D}, \lambda_{\rm BBH}, R_{30}, \gamma, \lambda_{\rm cosmo}\backslash\{H_0\})$. (In the following we do not write explicitly that the other parameters are given, *e.g.* here: $p(H_0|\mathcal{D})$.) A flat prior on the interval $(20, 140)$ is used. Both the posterior that takes into account selection effects and the posterior that does not take into account selection effects are plotted.

We can see that hierarchical inference is efficient in order to constrain the value of H_0. The bias effect has a huge impact on the posterior, and, as discussed in subsection 2.4.3, its impact is explicable: the heavier binaries are more likely detected and the further the source the heavier the average detected mass. In parallel the inference uses the redshift of the detected mass, so the bias effect accentuates the increase of the mass of the source with the distance. This corresponds

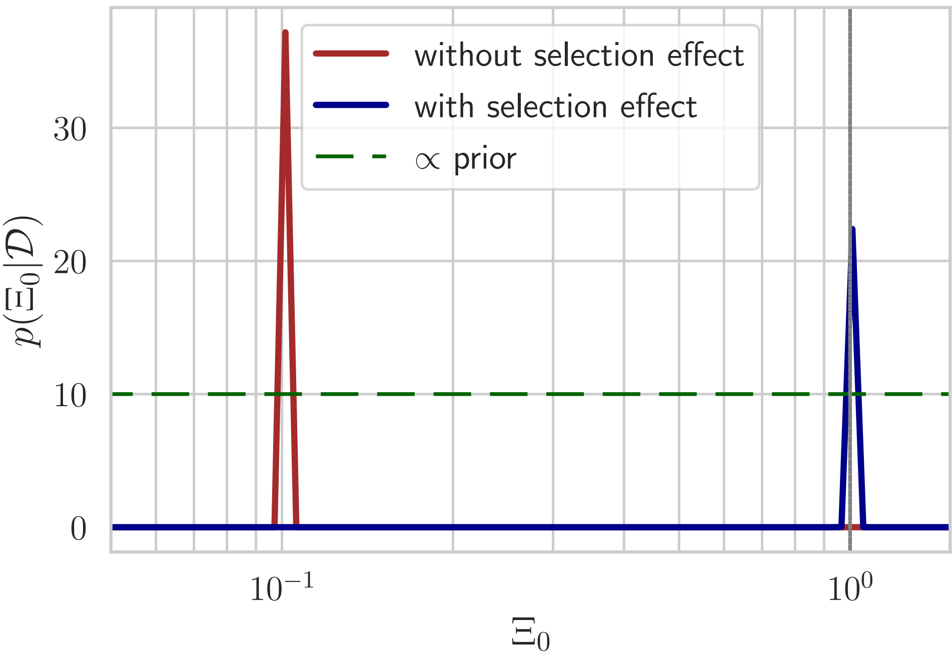

Figure 3.2: *Result of Bayesian inference on mock data for Ξ_0 alone. The posterior that takes into account the bias effects is shown alone on fig. 3.3. The solid gray line indicates the fiducial value (this mock data assumes GR).*

to a higher value of H_0.

Another parameter on which we can test the inference is Ξ_0 that characterises modified gravitational waves propagation. Fig. 3.2 shows the posterior $p(\Xi_0|\mathcal{D})$ with and without taking into account selection effects and fig. 3.3 shows the posterior that takes into account selection effects alone. A flat-in-log prior on $(0, 10)$ is used.

Here too, we can notice that the inference works well for constraining Ξ_0, even if $\Xi_0 = 1$: this inference could decide between GR + ΛCDM or modified gravity. Again, the impact of the selection bias was already explained in subsection 2.4.3: the bias selection accentuates the increase of the detected mass with the distance. This corresponds to an EM luminosity distance larger than the (detected) GW luminosity distance, thus to a Ξ_0 smaller than 1.

The Hubble constant and Ξ_0 are part of λ_{cosmo}. Bayesian hierarchical inference also works on λ_{BBH}, for example, fig. 3.4 shows the posterior with the selection bias for α, the coefficient of the power-law of the mass of the heavier BH. We used a flat prior on $(0, 10)$.

A last result we check is the evolution of the credible intervals. They should go as $1/\sqrt{N_{\text{obs}}}$, where N_{obs} is the number of observations. By performing Bayesian inference on partial mock data, we indeed find this evolution.

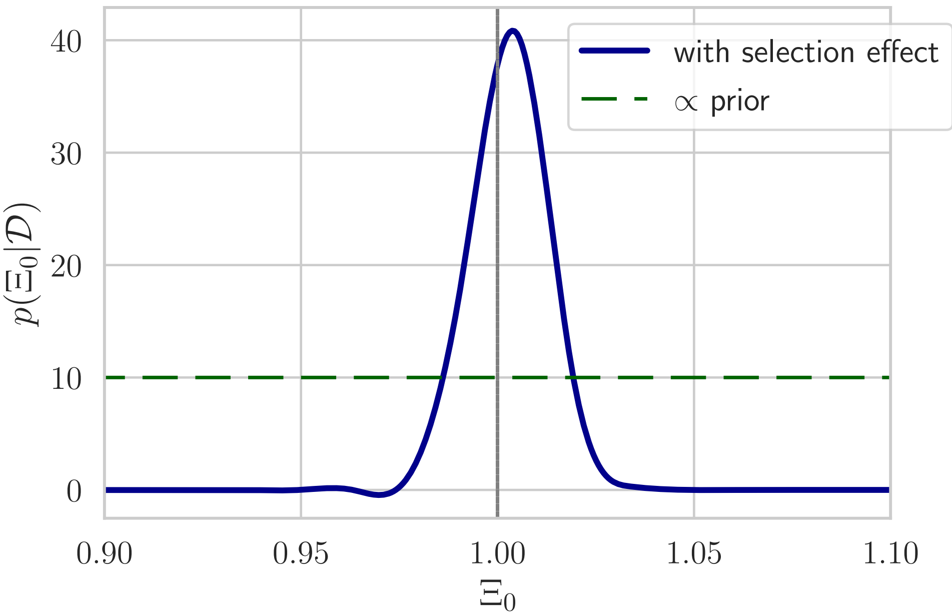

Figure 3.3: *Result of Bayesian inference on mock data for Ξ_0 alone, taking into account the selection effects (it is a zoom on fig. 3.2). The solid gray line indicates the fiducial value (this mock data assumes GR).*

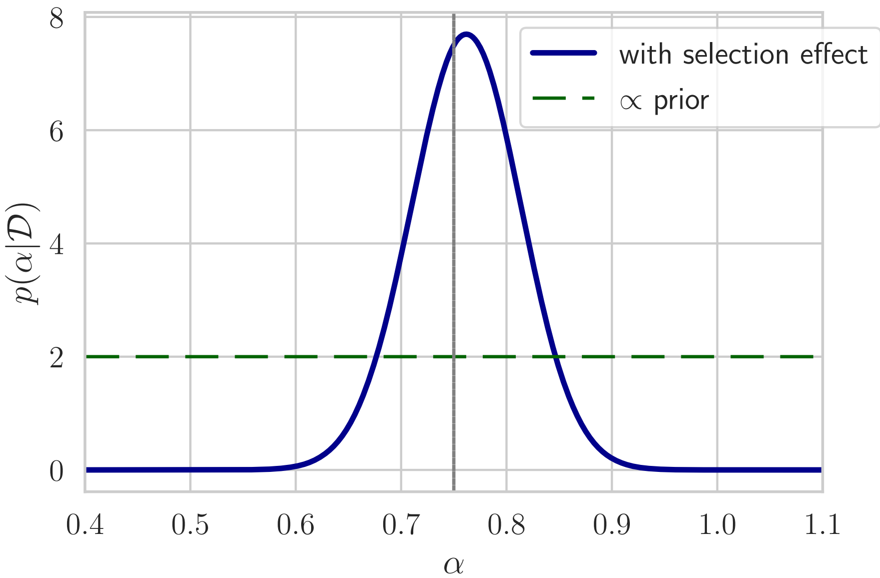

Figure 3.4: *Result of Bayesian inference on mock data for α alone (the power of the first mass). The solid gray line indicates the fiducial value.*

Results for several parameters

In order to test several parameters, we perform a MCMC (see appendix A) to get the results partially shown in fig. 3.5. We use the priors and the fixed values of table 3.3.

Inferred parameter	H_0	Ξ_0	λ	α	m_l	m_h
Type of prior	flat	flat	flat	flat	flat	flat
Range	$(20, 140)$	$(0.1, 10)$	$(-15, 10)$	$(0, 10)$	$(2, 20)$	$(20, 200)$
True value	67.74	1.0	3.0	0.75	5.0	45.0

Fixed parameter	n	β	σ_l	σ_h
Value	1.91	0	0.1	0.1

Table 3.3: *Table of priors and fixed values of parameters used on mock data.*

We can see in fig. 3.5 that our Bayesian inference works very well on mock data to recover the fiducial values of simulated data. This mock test shows us that:

- Bayesian hierarchical inference using the black hole mass gap is a technique that works to find the values of hyperparameters of GWs, particularly cosmological parameters;

- With $\mathcal{O}(5000)$ GW events (corresponding to $\mathcal{O}(5\text{ yrs})$ of detections with advLIGO/advVirgo detectors at largest sensitivity), dark sirens alone can constrain the value of the Hubble constant at $\sim 20\%$. In ref. [11], the authors quote a value of the error of 2.9% for the Hubble parameter, but this value is obtained for $H(z = 0.8)$ by minimising the relative error on $H(z)$ with respect to z.

- We observe some degeneracies between parameters, for example between H_0 and Ξ_0, indeed they are proportional:
$$H_0 = \frac{z}{d_{\mathrm{L}}^{\mathrm{EM}}} = \frac{z\Xi(z)}{d_{\mathrm{L}}^{\mathrm{GW}}}. \tag{3.7}$$
Another degeneracy is given by Ξ_0 and λ (or H_0 and λ, but H_0 and Ξ_0 are themselves proportional): a larger λ implies a larger value for the merger rate $\mathcal{R}(z)$ at any given redshift. So if λ is overestimated, then the total number of events N is overestimated, thus to explain the number of GWs detections, a smaller horizon of detection in the z-space is needed. From eq. (3.7) we see that a smaller redshift horizon, corresponds to a higher Ξ_0. A smaller redshift at fixed distance should also correspond to a smaller H_0 that we do not observe. Maybe there is another effect we did not think about and that explains the increase of H_0 with the increase of λ or maybe the degeneracy between H_0 and Ξ_0 is dominant.

  A third degeneracy is given by H_0 and m_h that are inversely proportional: the inference uses the increase of mass with redshift to determine the redshift of the source. If the source-masses are heavier, then the detected mass are less redshifted at a given distance, thus H_0 is smaller (and vice versa).

- Since we are interested in constraining cosmological parameters, *we must perform inferences on all parameters*, both cosmological and astrophysical parameters, because of the degeneracies between them.

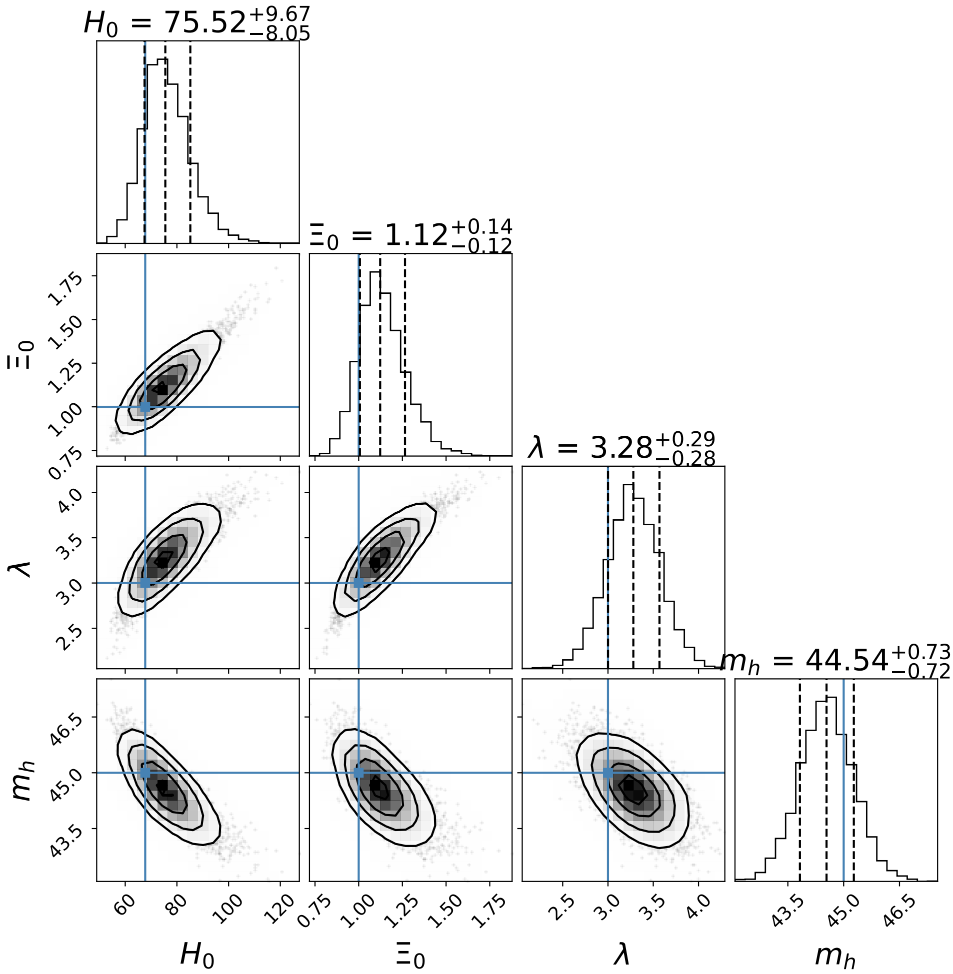

Figure 3.5: *Corner plot of the* partial *results of Bayesian inference on the mock data of ref. [11] (5 years of observation with advLIGO at design sensitivity). Results are given at 68% C.L. Blue lines indicate the fiducial values.*

3.2.2 Simulated data with modified GWs propagation

Until now, we used mock data for which modified propagation of GWs is not taken into account. Even if we know that our inference works well to find the values of parameters in cosmology, it is useful to test if the modified propagation of GWs (more especially the parametrisation (Ξ_0, n)) can be measured from GWs detections by using the black hole mass gap. Furthermore, if it can be measured, we need to check if the measurement is possible with current detectors.

In order to obtain such mock data, we sample the mass and redshift populations. For the masses, we use the broken power-law mass population function (see section 1.6), that is given for the first mass by:

$$p_{\rm pop}(m_1|\alpha_1, \alpha_2, m_{\rm min}, \delta_m, m_{\rm max}, b) \propto \begin{cases} m_1^{-\alpha_1}\ \mathcal{S}(m_1|m_{\rm min}, \delta_m) & \text{if } m_{\rm min} < m_1 < m_{\rm break}; \\ m_1^{-\alpha_2}\ \mathcal{S}(m_1|m_{\rm min}, \delta_m) & \text{if } m_{\rm break} < m_1 < m_{\rm max}; \\ 0 & \text{otherwise,} \end{cases} \tag{3.8}$$

where

$$m_{\rm break} = m_{\rm min} + b(m_{\rm max} - m_{\rm min}). \tag{3.9}$$

and

$$\mathcal{S}(m|m_{\rm min}, \delta_m) = \begin{cases} 0 & \text{if } m < m_{\rm min}; \\ [f(m - m_{\rm min}, \delta_m) + 1]^{-1} & \text{if } m_{\rm min} \leq m < m_{\rm min} + \delta_m; \\ 1 & \text{if } m \geq m_{\rm min} + \delta_m, \end{cases} \tag{3.10}$$

for the function:

$$f(m', \delta_m) = \exp\left(\frac{\delta_m}{m'} + \frac{\delta_m}{m' - \delta_m}\right). \tag{3.11}$$

While for the mass ratio $q \equiv m_2/m_1$, we get:

$$p_{\rm pop}(q|\beta, m_{\rm min}, m_1) = \begin{cases} q^{\beta} & \text{if } m_{\rm min} < m_2 < m_1; \\ 0 & \text{otherwise.} \end{cases} \tag{3.12}$$

For the redshift population, we use the simple power-law:

$$p(z|R_0, \lambda_z) \equiv \mathcal{R}(z) = R_0(1+z)^{\lambda_z}. \tag{3.13}$$

We use the values given in table 3.4. The used value of Ξ_0 is chosen in order to have modified GWs propagation and n is chosen at a typical value (see table 3.1).

From a sampled triplet $\{m_1, m_2, z\}$ we compute the detected SNR in a given detector, that is associated with a source of a BBH with masses m_1 and m_2 at a redshift z (see appendix B). If the SNR is larger than 8, then the sample $\{m_1, m_2, z\}$ is taken as a detection. The SNR depends on the luminosity distance, the cosmology intervenes when we convert the redshift into the luminosity distance: $d_{\rm L} = d_{\rm L}(z, H_0, \Xi_0, n, \Omega_{\rm m,0}, w_{\rm DE})$. We use detected simulations for five years of a detector of advanced LIGO at design sensitivity. To do this, we start from the normalised differential rate of formation of BBHs $\mathrm{d}\mathcal{N}(N, \Lambda)/\mathrm{d}\theta = N p_{\rm pop}(\theta|\Lambda)$. In this normalisation, the bias function $\alpha(\Lambda)$ is given by (see ref. [62] for a demonstration):

Parameter	R_0	λ_z	α_1	α_2	β	δ_m	$m_{\rm min}$	$m_{\rm max}$	b
Value	25 [Gpc^{-3} yr^{-1}]	2	1.6	5.6	1.4	4.8	4.0 [M$_\odot$]	90 [M$_\odot$]	0.40

Parameter	H_0	$\Omega_{\rm m,0}$	$w_{\rm DE}$	Ξ_0	n
Value	67.74 [km s^{-1} Mpc^{-1}]	0.3075	-1	1.20	2

Table 3.4: *Table of the used values to simulate mock data with modified gravitational wave propagation.*

$$\alpha(\Lambda) = \int_{\mathcal{D}>\text{threshold}} \mathcal{L}(\mathcal{D}|\theta) p_{\rm pop}(\theta|\Lambda)\ {\rm d}\theta {\rm d}\mathcal{D}, \tag{3.14}$$

and if we generate $N_{\rm draw}$ triplets θ_j from a distribution $p_{\rm draw}(\theta_j)$, to obtain $N_{\rm obs}$ detections, eq. (3.14) becomes at first approximation (see ref. [62]):

$$\alpha(\Lambda) \approx \frac{1}{N_{\rm draw}} \sum_{j=1}^{N_{\rm obs}} \frac{p_{\rm pop}(\theta_j|\Lambda)}{p_{\rm draw}(\theta_j)}. \tag{3.15}$$

While to find the number of events N we marginalise the differential formation rate over θ:

$$N = \int \frac{{\rm d}\mathcal{N}(N,\Lambda)}{{\rm d}\theta}\ {\rm d}\theta. \tag{3.16}$$

Since this mock data is simulated from the broken power-law mass distribution eqs (3.8) to (3.12), and from the simple power-law redshift distribution eq. (3.13), the posterior $p(\Lambda|\mathcal{D})$ is given by eq. (3.5) with $\mathscr{P}(\theta|\Lambda)$ given by eq. (3.6), where $p_{\rm pop}(m_1, m_2|\vec{\lambda}_{\rm BBH})$ is given by eqs (3.8) to (3.12).

Bayesian hierarchical inference is performed on this mock data with the priors and fixed values shown in table 3.5.

Inferred parameter	H_0	$\Omega_{\rm m,0}$	Ξ_0	R_0	λ_z
Type of prior	Gaussian*	Gaussian*	flat	flat-in-log	flat
Range	67.74 ± 0.6774*	0.3075 ± 0.003075*	$(0.1, 10)$	$(10^{-1}, 10^3)$	$(-10, 10)$

* A Gaussian prior on a range $X \pm \Delta X$ means a normal distribution $\mathcal{N}\left(X, \Delta X^2\right)$.

Inferred parameter	α_1	α_2	β	δ_m	$m_{\rm min}$	$m_{\rm max}$	b
Type of prior	flat	flat	flat	flat	flat	flat	flat
Range	$(-4, 12)$	$(-4, 12)$	$(-4, 12)$	$(0, 10)$	$(2, 10)$	$(30, 100)$	$(0, 1)$

Fixed parameter	$w_{\rm DE}$	n
Value	-1	2

Table 3.5: *Table of priors and fixed values of parameters used on mock data, for modified gravitational waves propagation.*

Results of this inference are partially shown in fig. 3.6. We can observe:

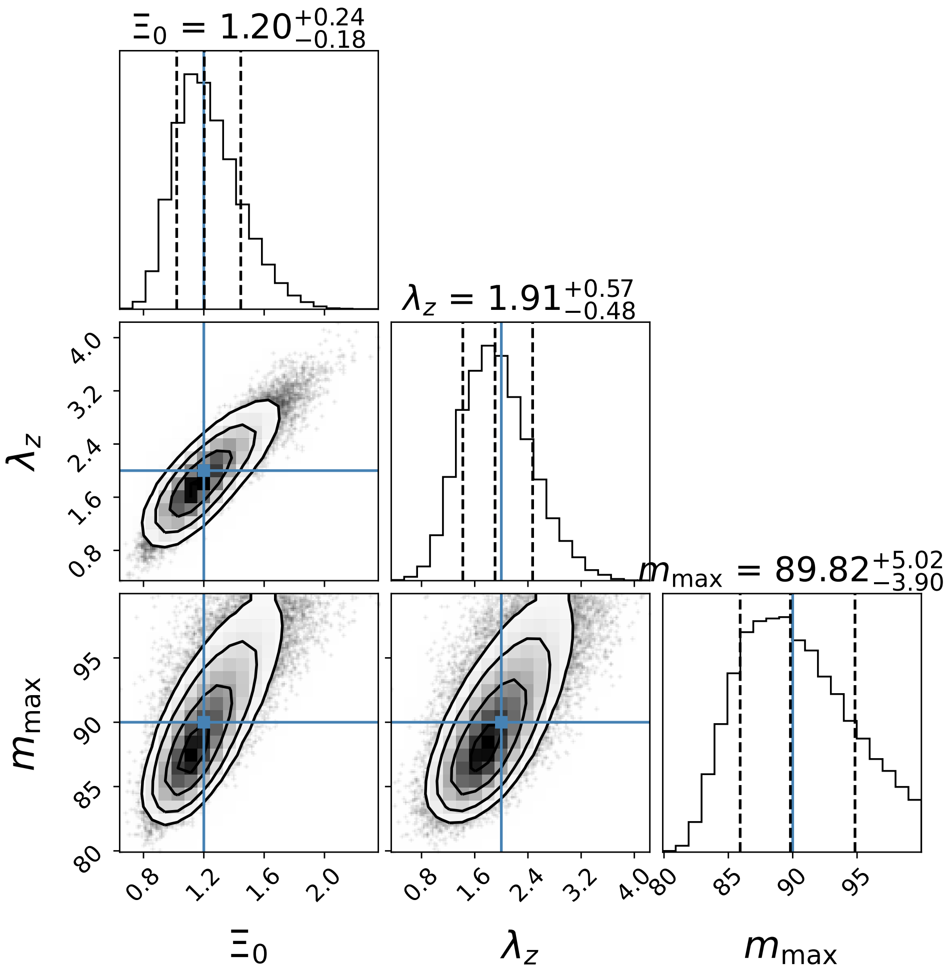

Figure 3.6: *Corner plot of the* partial *results of Bayesian inference on the mock data with modified gravity (5 years of observation with advLIGO at design sensitivity). Results are given at 68% C.L. Blue lines indicate the fiducial values.*

- Hierarchical inference constrains the value of Ξ_0 at $\sim 30\%$ on 5 years of observation by LVC at design sensitivity: *dark sirens alone could be able to distinguish between some modified gravity theories and GR in 5 years of data*;
- There are degeneracies, *e.g.* for Ξ_0 and λ_z. As mentioned above, cosmological parameters and astrophysical parameters cannot be constrained separately but must be inferred by the same inference.

3.3 LVC data

We saw in the previous section that hierarchical Bayesian inference on dark sirens with a mass gap alone works well to constrain values of cosmological and astrophysical parameters. We are here interested in analysing actual LVC data. All these computations were done on the UNIGE clusters *Yggdrasil* and *Baobab* [72].

3.3.1 Presentation of the catalogs

The GWs catalogs GWTC-1 [3] and GWTC-2 [4] are composed of the events detected by the two advLIGO and the advVirgo detectors during the runs O1 (only advanced LIGO; between

September 2015 and January 2016), O2 (between January and August 2017) and O3a (between April and September 2019). At the time of the project, the results of run O3b (between November 2019 and March 2020, with KAGRA as a fourth detector) are not publicly available. Fig. 3.7 shows the past and planned near future timeline of the ground-based interferometers.

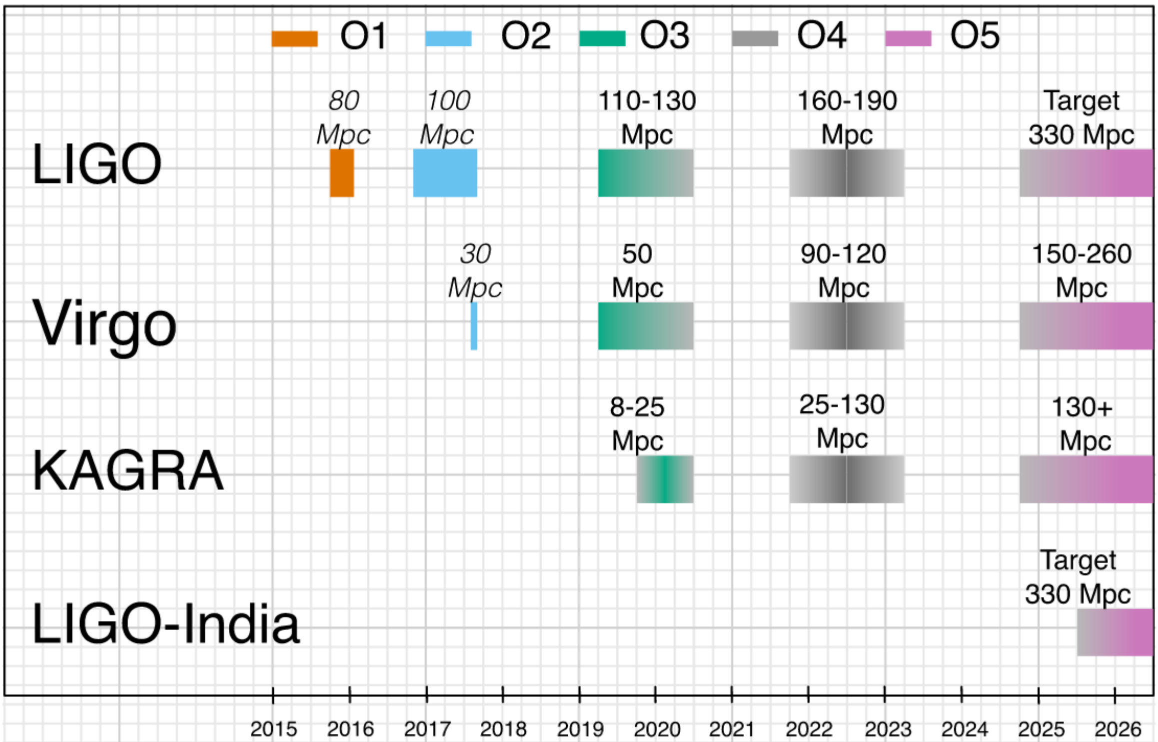

Figure 3.7: *Past and planned future timeline for the ground-based GWs detectors. This timeline was produced in 2020 and comes from ref. [73].*

These catalogs contain events from BBHs mergers, BH–NS mergers and BNSs mergers: there are 50 events. Masses of the events are shown in fig. 1.10 by blue dots. We exclude 6 events: GW170817, GW190425, GW190426_152155, GW190719_215514, GW190814, GW190909_114149, because either they involve one or two neutron stars (or maybe a very light BH) or because the 68% C.I. on their SNR is below 8. Furthermore, one event, GW190521 does not fit well the population models. Let us see why.

GW190521

The event GW190521 was caused by the merge of a BBH of masses $m_1 = 95.3^{+28.7}_{-18.9}$ $M_\odot$ and $m_2 = 69.0^{+22.7}_{-23.1}$ $M_\odot$ at a (GW) luminosity distance $d_L = 3.92^{+2.19}_{-1.95}$ Gpc. It formed a $163^{+39.2}_{-23.5}$ $M_\odot$ BH [4]. The heavier BH of the source is the heavier known "stellar-mass" BH, and in particular it lies in the *black hole mass gap* with a large probability. A few hypotheses have been put forward to explain this $\mathcal{O}(100)$ $M_\odot$ BH, and among others:

- ref. [57] suggests that it is a primordial black hole (that are not concerned by the mass gap);
- it is also possible that this BH is itself a second generation BH, caused by the previous coalescence of two astrophysical BHs;

- the interpretation of the detected signal could be wrong: ref. [74] finds by using a different prior on the masses, that the signal can be explained by the merge of a roughly 170 $M_\odot$ BH with a 16 $M_\odot$ BH, hence the heavier BH could be a second generation BH and the light one, an astrophysical BH (it was maybe a trinary BH). Ref. [75] is even more exotic: it suggests that a $15-50$ $M_\odot$ disc orbiting a 50 $M_\odot$ spinning BH can produce high-amplitude GWs by the deformation of the disc, and such a system at 100 Mpc would produce a signal similar to GW190521.

These hypotheses have in common that GW190521 does not hold in the stellar origin BHs mass population that we use. As we will see in the next subsection, taking into account GW190521 or not, changes the median values and the 68% C.I. of the parameters. It is particularly visible for Ξ_0 whose median is < 1 by taking into account GW190521, and > 1 by neglecting it.

3.3.2 Results for GWTC-1 and GWTC-2

To apply our hierarchical inference on data of GWTC-1 and GWTC-2, we use the mass population function given by the broken power-law, see eqs (3.8) to (3.12); while for the merger rate, we use the astrophysical rate:

$$p(z|R_0, \alpha_z, \beta_z, z_p) \equiv \mathcal{R}(z) = R_0 C_0 \frac{(1+z)^{\alpha_z}}{1+\left(\frac{1+z}{1+z_p}\right)^{\alpha_z+\beta_z}}, \tag{3.17}$$

where $C_0(z_p, \alpha_z, \beta_z) = 1 + (1+z_p)^{-\alpha_z-\beta_z}$ sets $\mathcal{R}(0) = R_0$. The parameter z_p corresponds to the redshift of the peak of star formation.

We use the broken power-law mass population model, as does LVC, because it fits very well the observed events [58] and because we rely on the mass gap. The astrophysical merger rate is better than a simple power-law merger rate: it takes into account that the merger rate should go to 0 when z goes to infinity (first stars formed at redshift $z \sim 6$, so no merger of stellar BHs can be observed for a higher redshift), and the fact that star formation had a peak at redshift $z_p \sim 2$.[1]

The hyperparameters are then:

$$\lambda_{\rm cosmo} = \{H_0, \Omega_{\rm m,0}, w_{\rm DE}, \Xi_0, n\} \tag{3.18}$$
$$\lambda_{\rm BBH} = \{\alpha_1, \alpha_2, \beta, \delta_m, m_{\rm min}, m_{\rm max}, b\} \tag{3.19}$$
$$\lambda_{\rm merger} = \{R_0, \alpha_z, \beta_z, z_p\}. \tag{3.20}$$

The hyperposterior $p(\Lambda|\mathcal{D})$ is then given by eq. (3.5) with:

$$\begin{aligned}\mathscr{P}(\theta|\Lambda) \propto & \frac{4\pi\, T_{\rm obs}\, p_{\rm pop}(m_1, q|\vec{\lambda}_{\rm BBH})\, u^2(z^*|\lambda_{\rm cosmo})}{\pi(m_1,m_2)\, \pi(d_{\rm L})\, \pi(\Theta)\, \left[E(z^*|\lambda_{\rm cosmo})\, s'(z^*|\lambda_{\rm cosmo})\, u(z^*|\lambda_{\rm cosmo}) + s(z^*|\lambda_{\rm cosmo})\right]} \\ & \times \left(\frac{c}{H_0}\right)^2 R_0 C_0 \frac{(1+z)^{\alpha_z-3}}{1+\left(\frac{1+z}{1+z_p}\right)^{\alpha_z+\beta_z}}.\end{aligned} \tag{3.21}$$

We can decide to constrain all parameters at the same time, using a flat (or flat-in-log) prior for each parameter, but doing so does not give yet good enough results: the credible intervals

[1] The current detections of GWs have a redshift from far inferior to $z_p \sim 2$ (for events of GWTC-2, $z_{\rm max} \approx 1$ [4]), so the simple power-law is not a bad approximation for the moment.

are large and the MCMC chains are very slow to converge (see appendix A). More data would be necessary to obtain exploitable results. We leave this aspect for a future work, maybe after the release of the events of the LIGO/Virgo/KAGRA collaborations, run O3b.

We then choose to apply more narrow priors for the cosmological parameters H_0 and $\Omega_{m,0}$: we use their median *Planck* 2018 [69] values as priors, see table 3.6. We already explained that we must vary every parameter in order to obtain exploitable results. However it is possible to use a tight prior for some parameters, as H_0 or $\Omega_{m,0}$ if we assume that this previous measurement is correct. This is what we do here by using the *Planck* median values. With more data, it could be possible to *not use* the *Planck* priors. Table 3.6 presents the priors we used.

Inferred parameter	H_0	$\Omega_{m,0}$	Ξ_0	n
Type of prior	Gaussian*	Gaussian*	flat	flat
Range	$67.66 \pm 0.42^*$	$0.311 \pm 0.056^*$	$(0.1, 10)$	$(0, 10)$

* A Gaussian prior on a range $X \pm \Delta X$ means a normal distribution $\mathcal{N}\left(X, \Delta X^2\right)$.

Inferred parameter	R_0	α_z	β_z	z_p
Type of prior	flat-in-log	flat	flat	flat
Range	$(10^{-1}, 10^3)$	$(-15, 15)$	$(0, 15)$	$(0, 4)$

Inferred parameter	α_1	α_2	β	δ_m	$m_{\min}$	$m_{\max}$	b
Type of prior	flat	flat	flat	flat	flat	flat	flat
Range	$(-4, 12)$	$(-4, 12)$	$(-4, 12)$	$(0, 10)$	$(2, 10)$	$(30, 100)$	$(0, 1)$

Fixed parameter	w_{DE}
Value	-1

Table 3.6: *Table of priors and fixed values of parameters used to analyse the GW data of GWTC-1 and GWTC-2.*

Figure 3.8 shows some posteriors we obtain using hierarchical Bayesian inference of dark sirens with the black hole mass gap, with and without taking into account the event GW190521. The median and 68% C.L. values are given in table 3.7.

We can see in fig. 3.8 that taking into account GW190521 disrupts the results (with respect to the same inference but without GW190521). Since GW190521 has a very large mass, to fit the population model, it would need to be highly redshifted. This explains a larger value of H_0 and/or a smaller value of Ξ_0 (for the same reason as above when we do not take into account the selection effects). It is then normal to observe a smaller value for Ξ_0 in order to explain this large mass (when we perform the inference also on H_0 we observe that H_0 becomes larger, but it is not statistically decisive). Let us consider the case where we neglect GW190521 in fig. 3.9 and where we include GW190521 in fig. 3.10.

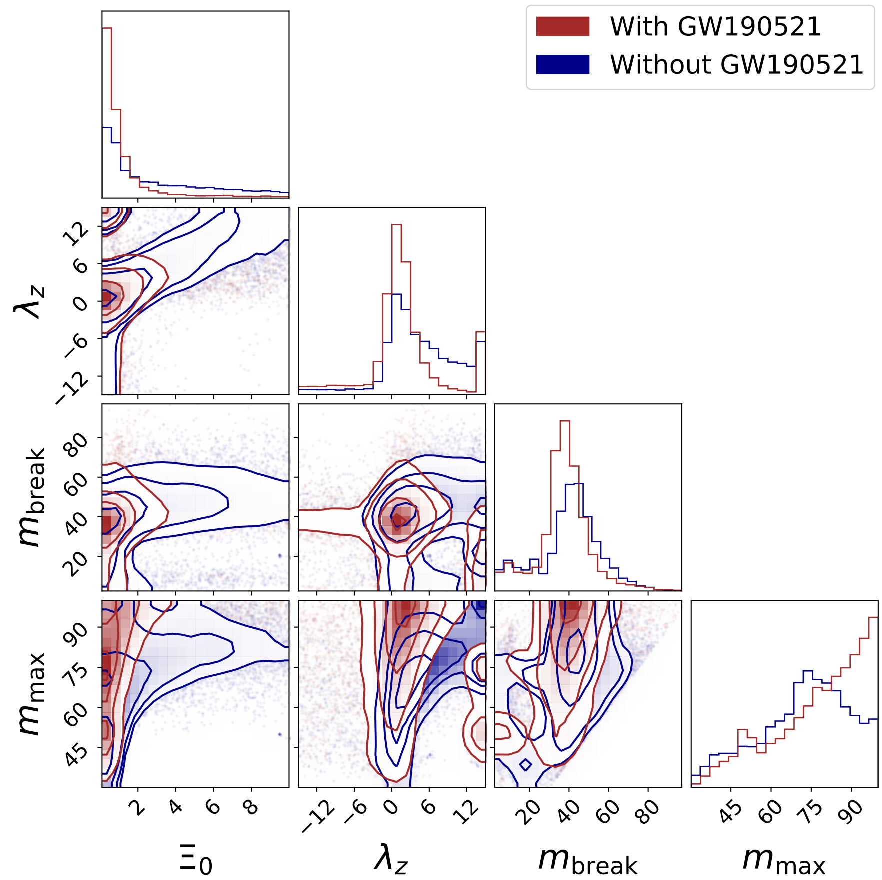

Figure 3.8: *Corner plot of the* partial *results of Bayesian inference on the GWTC-1 and GWTC-2 catalogs.*

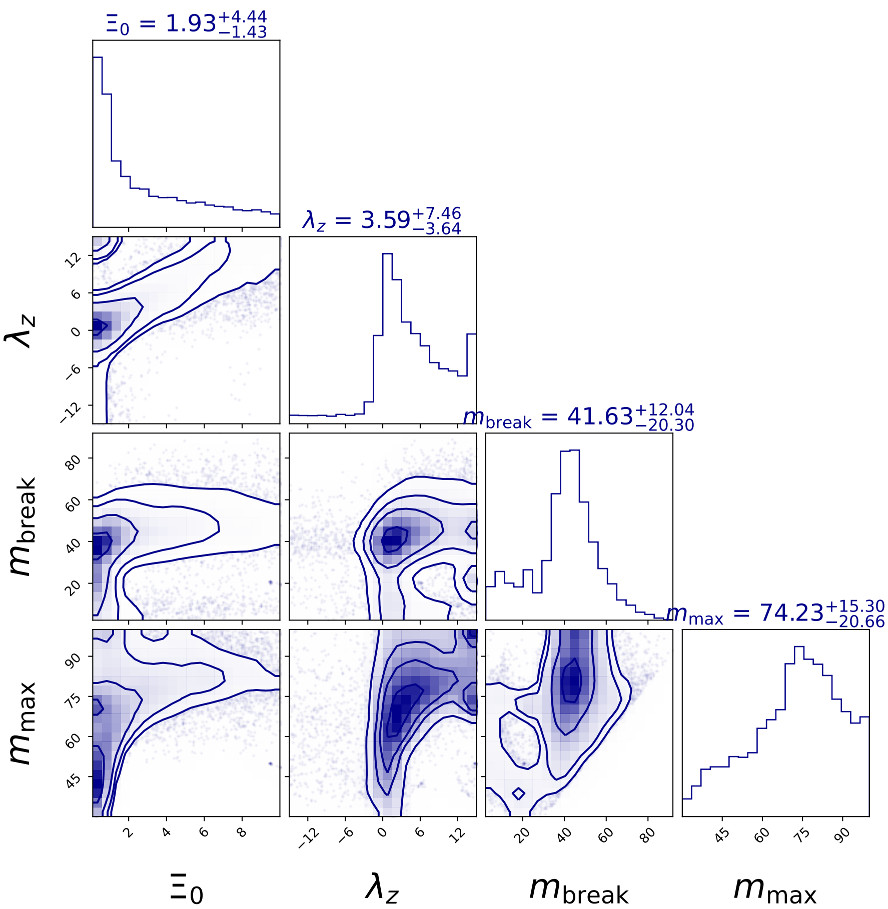

Figure 3.9: *Corner plot of the* partial *results of Bayesian inference on the GWTC-1 and GWTC-2 catalogs without GW190521.*

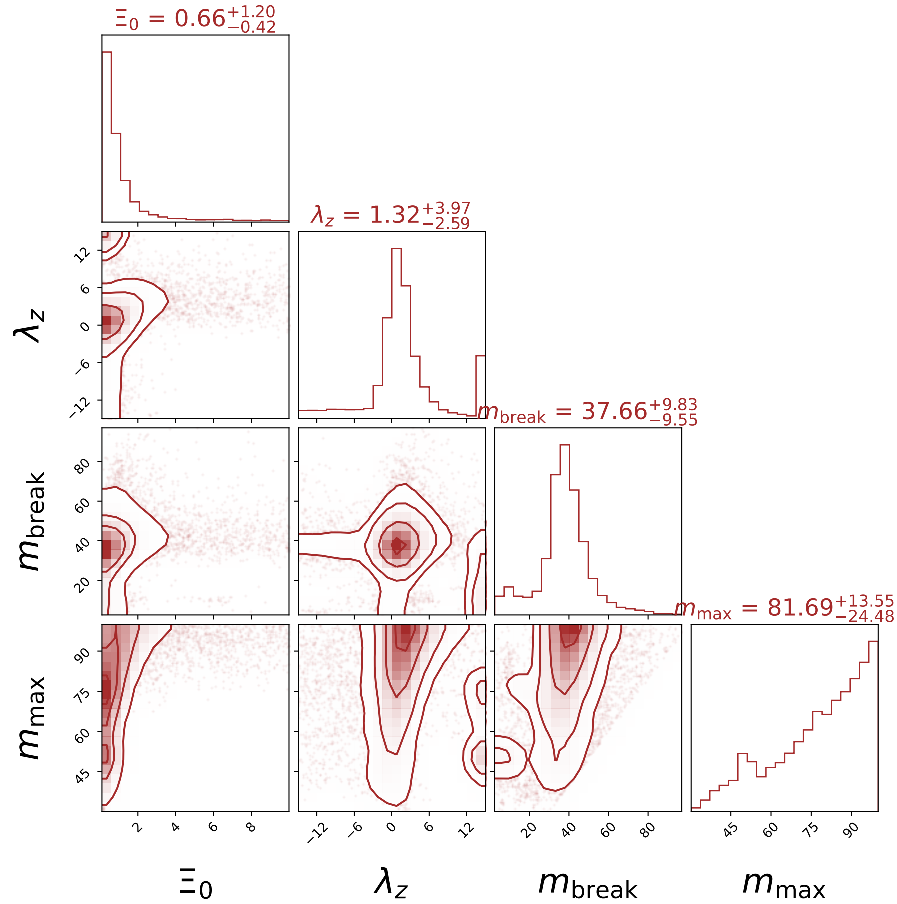

Figure 3.10: *Corner plot of the* partial *results of Bayesian inference on the GWTC-1 and GWTC-2 catalogs with GW190521.*

The MCMC chains we present in the corner plot fig. 3.8 do not have fully converged according to the autocorrelation time criteria (see appendix A). However, as discussed in section A.4, the criteria of convergence by a chain 50 times longer than the autocorrelation time is quite arbitrary: our chains are approximately 25 times longer than the autocorrelation time (after more than 20 days of computations on the UNIGE clusters *Yggdrasil* and *Baobab*). Furthermore the width of the credible intervals divided by the median value of the parameters do not change anymore when adding more steps to the chains. For these reasons we can consider that the chains have reached the value of the parameters at 68% credible level.

However we can also observe than some chains seem to be stuck far from the others, for example for the parameter α_z (both with and without GW190521).

Since the credible intervals are too large, it is not possible to conclude yet about the precise value of parameters, and in particular it is not possible to distinguish between modified gravities and GR. Ignoring GW190521, we obtain a value of Ξ_0 that is consistent with other works that use another technique (in particular correlations between GWs sources and galaxies in ref. [10]):

$$\Xi_0 = 1.93^{+4.44}_{-1.43} \text{ (at 68\% C.L. for a flat prior on } (0.1, 10)), \tag{3.22}$$

while taking into account GW190521 gives a different value:

$$\Xi_0 = 0.66^{+1.20}_{-0.42} \text{ (at 68\% C.L. for a flat prior on } (0.1, 10)). \tag{3.23}$$

Results we obtained for the astrophysical, merger rate and cosmological hyperparameters are summarised in table 3.7.

In ref. [12], a similar inference for the modified GW propagation is performed, with the c_M parametrisation (see subsection 1.5.3), and taking into account the event GW190521. The author obtains a value $c_\mathrm{M} = -3.2^{+3.4}_{-2.0}$ (see also table 3.1). A negative value of c_M corresponds to a value of $\Xi_0 < 1$. This being consistent with our value (3.23), that takes into account GW190521. But we find that the value of Ξ_0 is highly changed if we neglect the single event GW190521.

3.4 Summary

Bayesian hierarchical inference of dark sirens using the black hole mass gap is powerful to constrain values of cosmological and astrophysical parameters.

Yet the credible intervals are pretty large with respect to the mean values, however they go as the inverse of the square root of the number of events. We also show on mock data that 5 years of observation by advLIGO/advVirgo/KAGRA network at design sensitivity would constrain the value of Ξ_0 at $\sim 30\%$. It would then be possible to distinguish between GR and some modified gravity theories within 5 years of observation, just by using GWs.

Table 3.7 summarises the preliminary values we obtain.

To obtain the results of table 3.7, we choose to fix H_0 and $\Omega_{\mathrm{m},0}$ to their *Planck* median value [69]. However it is of course possible to use flat priors for these two parameters. In this configuration, the convergence of the MCMC chains is very slow (because the number of GW events is small) but bounds can be found on the values of H_0 and $\Omega_{m,0}$. We leave it for a future work.

Parameter	Ξ_0	n	R_0	α_z	β_z	z_p
With GW190521	$0.66^{+1.20}_{-0.42}$	$3.94^{+4.11}_{-3.06}$	$14.65^{+14.27}_{-8.58}$	$1.32^{+3.97}_{-2.59}$	$4.88^{+6.76}_{-4.04}$	$2.40^{+1.21}_{-1.32}$
Without GW190521	$1.93^{+4.44}_{-1.43}$	$4.04^{+4.27}_{-3.09}$	$28.86^{+72.53}_{-17.79}$	$3.59^{+7.46}_{-3.64}$	$6.60^{+5.67}_{-5.22}$	$2.26^{+1.15}_{-1.39}$

Parameter	α_1	α_2	β	δ_m	$m_{\min}$	$m_{\max}$	b
With GW190521	$1.78^{+0.58}_{-0.63}$	$5.79^{+2.97}_{-2.98}$	$1.64^{+1.76}_{-1.20}$	$4.56^{+2.86}_{-2.89}$	$4.10^{+1.29}_{-1.31}$	$81.69^{+13.55}_{-24.48}$	$0.44^{+0.18}_{-0.12}$
Without GW190521	$1.84^{+0.64}_{-0.61}$	$5.34^{+3.53}_{-3.61}$	$1.67^{+1.61}_{-1.16}$	$4.92^{+3.05}_{-3.20}$	$4.10^{+1.29}_{-1.29}$	$74.23^{+15.30}_{-20.66}$	$0.53^{+0.23}_{-0.20}$

Table 3.7: *Summary of the results we obtain for the astrophysical, merger rate and cosmological parameters. At 68% C.L., for the priors given in table 3.6. R_0 has unit of $Gpc^{-3}yr^{-1}$; m_{min} and m_{max} have unit of $M_\odot$.*

Conclusions

During this project we applied hierarchical Bayesian inference on standard dark sirens together with assumptions about the shape of the mass population of binary black holes, in order to constrain the values of parameters, especially modified gravity parameters.

This method works very well, as can be seen by testing it on mock data: the fiducial values of parameters are recovered at $\mathcal{O}(10\%)$ with $\mathcal{O}(1\,000)$ detections. However the method can be improved without much difficulties: we did not consider spins of the sources, it could be added in a future work to increase the accuracy. Yet, the number of observations is small $\mathcal{O}(50)$ so that the credible intervals are big enough to hide the effects of the spins on the waveforms. Another improvement that is possible consists in using dark sirens together with the standard sirens with electromagnetic counterpart or together with a galaxy catalog. These different methods are complementary and can be used together to improve the accuracy of the constraints. The results can also be improved by considering another BBHs mass population that would fit better the detections: other models are proposed by LVC (see ref. [54]). We can also consider that some sources are not part of the stellar origin BHs: ref. [57] considers that some detected BHs are of primordial type.

Because of the small number of detections, it is not possible for the moment to use them to solve the Hubble tension nor to choose between GR or some modified gravity theory. Since the credible intervals go approximately as $1/\sqrt{N_{\text{obs}}}$, it is possible to roughly estimate the number of detections that is needed to decide between GR or a modified gravity. To do this, let us consider the 68% credible interval on the value of Ξ_0. With $\mathcal{O}(50)$ detections, we have $\Delta\Xi_0/\Xi_0 \sim 300\%$. With $\mathcal{O}(5\,000)$ detections (five years of observation for the advanced LIGO, advanced Virgo and KAGRA network at design sensitivity), the credible errors would be of $\mathcal{O}(30\%)$. (This value is indeed consistent with the value we obtained by testing the method on mock data.) To have a measurement of Ξ_0 accurate at 5% we would need $\mathcal{O}(10^5)$ detections, while for an accuracy at the level of the percent we would need $\mathcal{O}(10^6)$ detections.

With current ground-based interferometers these numbers of detections are enormous. But next generation of detectors is planned for the mid-2030s. Not exhaustive list of (in development) third generation detectors includes LISA (that is a space detector), LIGO Voyager, *Cosmic Explorer* (CE) and the *Einstein telescope* (ET) [7]. ET and CE have a similar noise power spectrum and in particular will have the good resolution to detect mergers of astrophysical BHs (see fig. 5 of ref. [76]). These detectors will observe together with future detectors of gamma-ray bursts and will be able to detect $\mathcal{O}(10^2)$ standard sirens with EM counterpart each year [7], providing a measurement of H_0 or of Ξ_0 at the percent level. However the BH–BH detection rate will be of order $10^5 - 10^6$ per year for ET [7]. This rate corresponds to the number of dark sirens we need to estimate at 5% or 1% the value of Ξ_0 by using the black hole mass gap. Order of one year of observation with ET will allow us to constrain at the percent level the value of Ξ_0 by using only dark sirens.

Appendix A

Markov chain Monte Carlo methods

Contents

We saw in chapter 2 (page 47) that we have very large integrals (more precisely integrals with a large dimension d) to evaluate in order to calculate our posterior distributions. It is of course unthinkable to resolve these equations analytically. We then need to do it numerically.

In this appendix, we introduce the numerical method we use in the present work: Markov chain Monte Carlo (or "MCMC"). This technique is now a very used numerical method in many domains of physics (for example to determine the average magnetisation in an Ising model [77]) and of applied mathematics (for example to decipher a substitution cipher by only knowing the language in which it is written [78]). It was also the technique used in subsection 2.2.3. For a very complete introduction, see *e.g.* ref. [79].

A.1 Monte Carlo algorithm

Our goal is to evaluate numerically the integral of a (supposed C^∞) function, let us say: $\int_a^b f(x)\,\mathrm{d}x$. We could use a Riemann sum to approximate the integral [77]:

$$I = \int_a^b f(x)\,\mathrm{d}x \approx \left(\frac{b-a}{N}\right)\sum_{j=0}^{N-1} f\left(a + \frac{j(b-a)}{N}\right) = I_N, \tag{A.1}$$

the approximation is quite good for one dimension: the error goes as the inverse of N

$$|I - I_N| \sim \frac{1}{N}, \tag{A.2}$$

but when the integral has d dimensions, the error goes as:

$$|I^{(d)} - I_N^{(d)}| \sim \frac{1}{N^{1/d}}, \tag{A.3}$$

thus, to have a 1% error on the value of the integral, one has to use a grid with $\sim 100^d$ points on it. This grows exponentially and is then totally unuseful when $d \gtrsim 10$, regardless of the computer.

The Monte Carlo methods use chance[1] to evaluate in a very accurate way an integral. Let us see how.

To evaluate the integral of eq. (A.1), we can rewrite I as:

$$I = \int_a^b f(x)\ \mathrm{d}x = \int_a^b \frac{f(x)}{\mathsf{P}(x)}\ \mathsf{P}(x)\ \mathrm{d}x, \tag{A.4}$$

with P a (yet undefined) probability distribution function and $\mathsf{P}(x) \neq 0, \forall x$. The goal is now to generate N samples of the pdf $\mathsf{P}(x)$, and to evaluate the function (f/P) on the samples $\{x_i\}_{i=1}^N$, then to take the arithmetic mean of the values:

$$\frac{1}{N}\sum_{i=1}^{N} \frac{f(x_i)}{\mathsf{P}(x_i)} = \left(\frac{f}{\mathsf{P}}\right)_N . \tag{A.5}$$

The strong law of large numbers says that this mean converges (almost surely) to the expected value μ [60]:

$$\mathsf{P}\left\{\lim_{N\to\infty}\left(\frac{f}{\mathsf{P}}\right)_N = \mu\right\} = 1, \tag{A.6}$$

with:

$$\mu = \mathbb{E}\left[\frac{f}{\mathsf{P}}\right] \equiv \int_a^b \frac{f(x)}{\mathsf{P}(x)}\ \mathsf{P}(x)\ \mathrm{d}x \tag{A.7}$$

$$= \int_a^b f(x)\ \mathrm{d}x = I. \tag{A.8}$$

With the central limit theorem one can show that the standard deviation between the partial mean $(f/\mathsf{P})_N$ and μ goes as $1/\sqrt{N}$. So as soon as $d > 2$, the Monte Carlo algorithm is more accurate than the Riemann sum for the same N.

We write the Monte Carlo integration as:

$$\int_{\mathscr{D}} f(x)p(x)\ \mathrm{d}x = \frac{1}{N}\sum_{i=1}^{N} f(x_i)\ |_{\ x_i\ \sim\ p(x)}. \tag{A.9}$$

Example A.1: The famous basic example of Monte Carlo algorithm is a technique to measure π ($\approx 3.14159\cdots$). One draws a circle into a square of known side's length. The goal is to use hazard to compute the integral of the disc's surface in units of the known square surface. One just have to throw tokens on the drawing with a flat probability. The surface of the disc is then just the ratio of the number of tokens in the circle by the total number of thrown tokens (when this number goes to infinity).[2,3]

[1] This class of algorithms takes its name from the Monte Carlo Casino (see also Las Vegas and Atlantic City algorithms: Monte Carlo are always fast and probably correct, Las Vegas are always correct and probably fast, while Atlantic City are probably correct and probably fast).

[2] We can see a link with the Buffon's needle problem.

[3] It is also interesting to note that this definition of Monte Carlo algorithms lies in a frequentist view of statistics.

A.2 Markov chains

In order to apply a Monte Carlo method, we then need to generate samples of the probability distribution function $\mathsf{P}(x)$. A well-used technique consists in using a Markov chain [78]. We then talk about a Markov chain Monte Carlo method. (The definitions come from ref. [80].)

Definition A.1: A process is a variation with time of the state of a certain system. It is written: $(N_t)_{t\in\mathbb{R}_+}$. $\lozenge$

Definition A.2: (Stochastic process) A process whose course depends on chance and for which probabilities for some courses are given. $\lozenge$

Let $X_0, X_1, \cdots, X_n$ be a series of random variables with values in a countable set S. X is a stochastic process and P its law.

Definition A.3: The process X is a *Markov chain* if it has the Markov property:

$$\mathsf{P}(X_n = s_n \mid X_0 = s_0, X_1 = s_1, \cdots, X_{n-1} = s_{n-1}) = \mathsf{P}(X_n = s_n \mid X_{n-1} = s_{n-1}), \tag{A.10}$$

for every $n \geq 1$ and with $s_0, s_1, \cdots, s_n \in S$. $\lozenge$

Definition 3 means that if the state at the n-th step of a process only depends on the state of the process at the $(n-1)$-th step, then this process is a Markov chain.

In the case of discrete variables, one can represent a Markov chain as a matrix K [78], with elements $K_{ij} \equiv K(x,y) \geq 0$, such that $\sum_y K(x,y) = 1, \forall x$. Each matrix element $K(x,y)$ represents the probability to go from a state x to a state y:

$$K(x,y) = \mathsf{P}(X_1 = y|X_0 = x), \tag{A.11}$$

and if one wants the probability $\mathsf{P}(X_2 = z|X_0 = x)$, one has to sum on the different values of X_1, hence:

$$\mathsf{P}(X_2 = z|X_0 = x) = \sum_y K(x,y)\ K(y,z), \tag{A.12}$$

and so on. Equation (A.12) is just the matrix product. Then, by writing K_n, the matrix of the probabilities $\mathsf{P}(X_n = y|X_0 = x)$, we simply get:

$$\mathrm{K}_n = \mathrm{K}_1^n. \tag{A.13}$$

In the following, we will consider only symmetric Markov matrices, *i.e.* $K(x,y) = K(y,x)$, and thus, the probability to go from state x to state y is the same as the probability to go from state y to state x. If we also write $\pi_n(x)$ with $\pi_n(x) \geq 0$, $\sum_x \pi_n(x) = 1$ the probability to be in the state $X_n = x$ (so after n steps of the chain), we get:

$$\pi_{n+1}(y) = \sum_x \pi_n(x)\ K(x,y). \tag{A.14}$$

Some Markov chains (actually all the Markov chains we are interested in here) have a *stationary distribution*, $\lim_{n\to\infty} \pi_n(x) = \mathcal{P}(x)$, with $\mathcal{P}(x) \geq 0$, $\sum_x \mathcal{P}(x) = 1$ and for which:

$$\sum_x \mathcal{P}(x)\ K(x,y) = \mathcal{P}(y), \tag{A.15}$$

($\mathcal{P}$ is a left (row) eigenvector of the matrix K with eigenvalue 1). This means that from any starting state x, the probability to be at the state y after n steps (for n large enough) is close to the stationary distribution $\mathcal{P}(y)$.

It is easy to go from the discrete variables to the continuous ones by transforming the sums into integrals and the Markov matrix K into an operator.

A.3 The Metropolis–Hastings algorithm

The Metropolis–Hastings (or often just "Metropolis") algorithm (Nicholas Metropolis *et al.*, 1950s, then generalised by Wilfred Hastings, 1970) is one of the most used MCMC method.

Let $\mathcal{X}$ be a finite state space and $\mathcal{P}(x)$ a probability on $\mathcal{X}$. The goal is to have a sample of the distribution $\mathcal{P}$. The Metropolis algorithm transforms a Markov matrix J into a new Markov matrix K with stationary distribution $\mathcal{P}$ that we want to sample. The algorithm is given by [78]:

$$K(x,y) = \begin{cases} J(x,y) & \text{if } x \neq y, A(x,y) \geq 1; \\ J(x,y)\ A(x,y) & \text{if } x \neq y, A(x,y) < 1; \\ J(x,y) + \sum_{\{z|A(x,z)<1\}} J(x,z)(1 - A(x,z)) & \text{if } x = y. \end{cases} \tag{A.16}$$

In eq. (A.16), the $A(x,y)$ is the acceptance ratio, defined by:

$$A(x,y) = \frac{\mathcal{P}(y)J(y,x)}{\mathcal{P}(x)J(x,y)}, \tag{A.17}$$

A is then not a Markov matrix.

The algorithmic interpretation of eqs (A.16) and (A.17) is the following [81]:

1. Start from a random point x ;
2. Propose a candidate point y, coming from a proposal distribution $J(x,y)$ (J is a Markov matrix) ;
3. Evaluate the posterior at the candidate point y: $\mathcal{P}(y)$, and accept y with probability:
$$\alpha = \min\left(\frac{\mathcal{P}(y)\ J(y,x)}{\mathcal{P}(x)\ J(x,y)}, 1\right); \tag{A.18}$$
4. If the candidate point y is accepted, then we add it to the chain. Otherwise we add x to the chain ;
5. Go back to 2.

Let us have a few comments. On step 2, for the proposal distribution J, one can use a Gaussian distribution of mean x and of known standard deviation σ. The distribution can also be symmetric (*i.e.* $J(x,y) = J(y,x)$) in the case of the Metropolis algorithm (the asymmetry was later introduced by Hastings). Then in point 3, in the case of a "true" Metropolis algorithm (J being symmetric), eq. (A.18) simplifies to:

$$\alpha_{(\text{sym.})} = \min\left(\frac{\mathcal{P}(y)}{\mathcal{P}(x)}, 1\right). \tag{A.19}$$

To accept the candidate point y with that probability α, one can pick a random number u in $[0, 1)$ and accept the candidate if $u < \alpha$, otherwise the candidate is rejected. We can see from eq. (A.19) that if $\mathcal{P}(y) \geq \mathcal{P}(x)$, then $\alpha = 1$ and thus the candidate is always accepted. But if $\mathcal{P}(y) < \mathcal{P}(x)$ (and even if $\mathcal{P}(y) \ll \mathcal{P}(x)$), α is non zero.

This possible acceptance of a point y worst than the previous point x (in the sense that $\mathcal{P}(y) < \mathcal{P}(x)$) can seem counter productive, but its goal is to avoid to the chain to be stuck in a local maximum $x_{\text{l.m.}}$ of the distribution $\mathcal{P}$. Indeed if $x_{\text{l.m.}}$ is a local maximum, and if any candidate point with a posterior probability less than the starting point is accepted, then the chain is stuck forever in this local maximum (supposing there is no higher (local) maximum close enough to $x_{\text{l.m.}}$ to be raised in one step). By allowing a "worst" point to be chosen, the chain can move out of a local maximum to reach the global maximum. And when the chain is at the global maximum, it can leave the maximum for a few steps, but will reach it again with probability 1 after a few steps (since it is the maximum of $\mathcal{P}$).

We often call points 3 and 4 of the Metropolis–Hastings algorithm the "Metropolis test".

Another easy way to reduce the "local maximum" risk: we generally run a few Markov chains in parallel (see section A.5).

A.4 Convergence of the chains

We saw in the previous sections that the MCMC algorithm is an amazing idea to evaluate integrals. But there is a subtle point: how to know when the Markov chain has converged? As a reminder, we saw that the distribution $\mathcal{P}$ is correctly sampled by the fact that:

$$\lim_{n \to \infty} \pi_n(x) = \mathcal{P}(x), \tag{A.20}$$

so, with an infinite number of steps (hence with an infinite time of computation), the result of the MCMC is "correct" (with probability 1). But eternity is a long time. The aim of this section is to define a $n_{\text{conv.}}$, such that $\forall n \geq n_{\text{conv.}}$: "$n = \infty$".

First thing to know: except in some very easy cases in which $\mathcal{P}$ can be known from other techniques, it is impossible to determine in an accurate way the value of $n_{\text{conv.}}$. However, there exists many convergence tests to check if the chains already have enough steps to trust the convergence to be true or not. All these tests are necessary conditions to the convergence but sadly no test is a sufficient condition [82].[4]

Here we introduce only the statistical tests of convergence we use (it is the one recommended in the Python package `emcee`'s online documentation [64]). The review [82] presents a much longer list of tests of convergence. This test is a graphical test on the length of the Markov chain. To measure this length, we introduce the autocorrelation time τ_f as the parameter that quantises the difference between the MCMC decrease of the error and the Gaussian decrease of the error:

$$\sigma^2_{\text{Gauss.}} = \frac{1}{N}\text{Var}_{p(x)}[f(x)] \quad \text{vs.} \quad \sigma^2_{\text{MCMC}} = \frac{\tau_f}{N}\text{Var}_{p(x)}[f(x)]. \tag{A.21}$$

This parameter τ_f depends on the function f, it then needs to be estimate through statistical methods during the MCMC. It can be interpreted as being the number of steps that the chain needs to "forget" where it started.

[4] This is why we sometimes read that Monte Carlo algorithms are always fast and probably correct.

Empirical tests show that a chain with a number of steps larger than $50\tau_f$ can be trusted as having converged [64]. Of course this limit is pretty arbitrary. If the number of steps is less than $50\tau_f$, but the results do not change anymore by adding more steps, we can also say that the chain has converged.

A.5 The software `emcee`

In this master's project, we use the Python package `emcee` [64, 66] to realise our MCMCs. This software is of course not the only one that implements a MCMC, and a few different algorithms are used.

`emcee` does not use a Metropolis–Hastings (MH) algorithm, but rather uses a "stretch move" ensemble method (it is describes in ref. [66], in which other references for more information can be found). This algorithm is significantly better than MH (in the sense that is is faster, with a smaller autocorrelation time).

In the stretch move algorithm, there is an ensemble of W walkers that evolve simultaneously. And the proposal position (as for step 2 of MH) of the walker w for a time $n+1$ depends on the positions of the $W-1$ other walkers.

Explicitly, if we want to propose a new position for the walker w being at position $X_w(n)$, we randomly choose another walker j ($j \neq w$) and the new *proposed* position is:

$$Y = X_j + Z\left[X_w(n) - X_j\right], \tag{A.22}$$

where Z is a random variable drawn from a distribution $g(Z)$ and where X_j is the position of the walker j at the moment of the test (since w and j are randomly chosen, they not necessarily at the same time).

At this step, a test is done (see step 3 of MH). We compute:

$$q = \min\left(1; Z^{N-1}\frac{\mathcal{P}(Y)}{\mathcal{P}\left(X_k(n)\right)}\right), \tag{A.23}$$

and we accept the proposed position Y with probability q (see step 4 of MH). Then we do this algorithm for each walker. And we start again.

Appendix B

Computation of the selection bias function α

Contents

The selection bias function α (sometimes called β) was derived in subsection 2.2.2 using the so-called "bottom-up derivation". Another equivalent derivation, called "top-down", is also given in ref. [13]. In this appendix, we show how to compute the function α.

The function of the selection bias, α, is given by eq. (2.28):

$$\alpha(\Lambda) = \int p_{\text{det}}(\theta)\ p_{\text{pop}}(\theta|\Lambda)\ \mathrm{d}\theta. \tag{B.1}$$

We have to be careful here: $p_{\text{det}}(\theta)$, the probability that a GW produced by a BBH with parameters θ is detected, is not normalised to unity over θ's: $\int p_{\text{det}}(\theta)\ \mathrm{d}\theta \neq 1$. It is easy to understand if we take the extreme example of a detector that cannot detect any GW, then $p_{\text{det}}(\theta) = 0, \forall\theta$.[1]

However, $p_{\text{pop}}(\theta|\Lambda)$ is a well normalised probability distribution function (on the $\theta \in \mathscr{D}$):

$$\int_{\mathscr{D}} p_{\text{pop}}(\theta|\Lambda)\ \mathrm{d}\theta = 1. \tag{B.2}$$

B.1 The probability of detection

Let us first see how to compute the probability of detection $p_{\text{det}}(\theta)$.

[1] It is not because Initial LIGO did not detect any GW that $p_{\text{det}}(\theta) = 0, \forall\theta$: indeed, it could have detected GWs coming from events whose frequency of occurrence is less than one per decade. The probability $p_{\text{pop}}(\theta|\Lambda)$ is then also important to predict the number of detections.

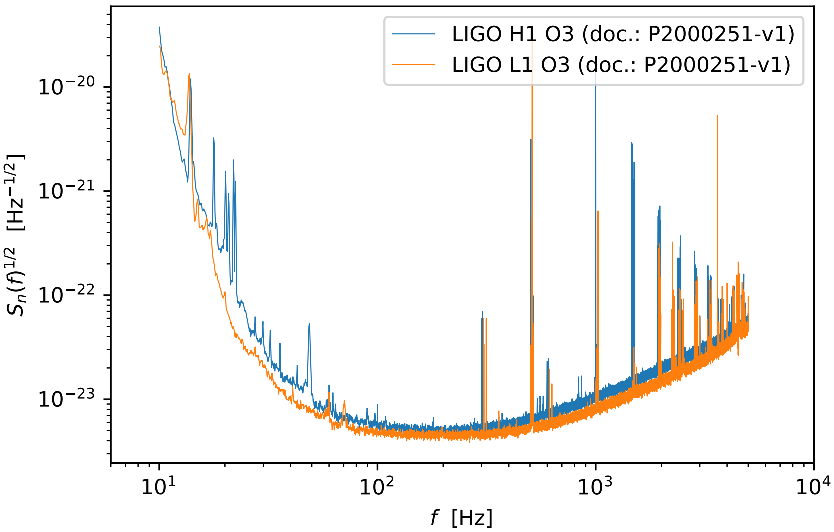

Figure B.1: *Plot of the power spectrum densities for the detector LIGO O3 of Hanford, Washington (H1) and of Livingston Parish, Louisiana (L1), data come from the LVC public document* `P2000251-v1` *[83].*

As we already said in subsection 2.2.2 (eqs. (2.30) and (2.31)), in GW astronomy, a signal-to-noise ratio (SNR) greater or equal to 8 in the second loudest detector is a good approximation to the actual pipelines for a detection:

$$p_{\rm det}(\theta) \equiv p_{\rm det}^{\rm exp}(\theta) = \Theta\left(\mathrm{SNR}(\theta) - 8\right), \tag{B.3}$$

where $\Theta(x)$ is the Heaviside step-function:

$$\forall x \in \mathbb{R}, \quad \Theta(x) = \begin{cases} 0 & \text{if} \quad x < 0; \\ 1 & \text{if} \quad x \geq 0. \end{cases} \tag{B.4}$$

It is then necessary to compute the signal-to-noise ratio associated to the parameter θ in order to obtain the probability of detection $p_{\rm det}(\theta)$. As in ref. [59], we call the SNR ρ. It is related to the inner product of the waveform $h_\theta(f)$ (see subsection 1.1.3 and *e.g.* refs [8, 59]):

$$\rho^2 = \langle h_\theta(f) | h_\theta(f) \rangle, \tag{B.5}$$

where $h_\theta(f)$ is the Fourier transform of the GW signal, and where the inner product is defined by:

$$\langle a(f) | b(f) \rangle \equiv 2 \int \frac{a(f) b^*(f) + a^*(f) b(f)}{S_n(f)} \, \mathrm{d}f, \tag{B.6}$$

with $S_n(f)$ the power spectrum density (PSD) of the detector. Figure B.1 shows PSDs for the LIGO O3 detectors. As one could guess from the latter equation, the more sensitive the detector, the smaller its PSD. The PSD is the capacity of the detector to detect some frequencies of GWs. For ground-based detectors (all the detectors we have yet), it is generally limited on the small frequencies by the seismic wall ($\sim 10 - 20$ Hz) and on the high frequencies by the Nyquist frequency (which is one half of the sampling frequency of the signal, it is a purely technological bound) [59].

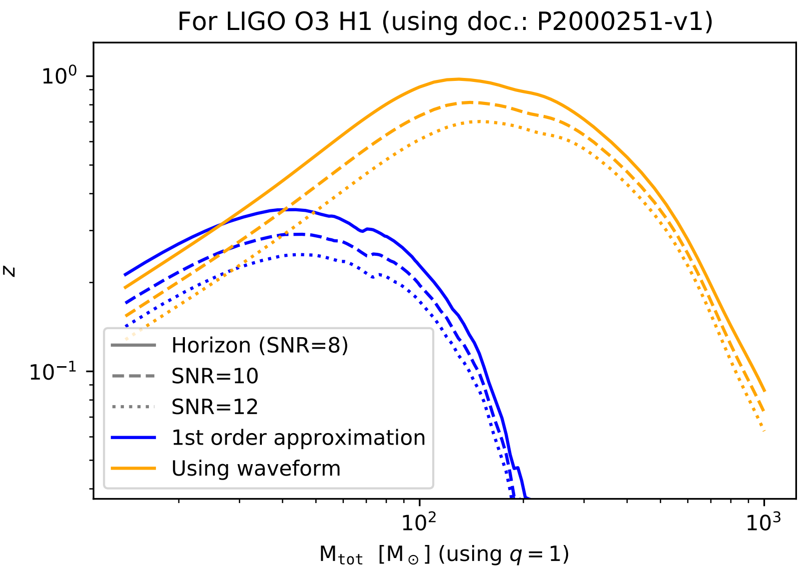

Figure B.2: *Plot of the horizons of detection for a LIGO O3 detector comparing the post-Newtonian approximation (eq. (B.7)) to the numerical computation of the waveform (using ref. [84]). The PSD comes from ref. [83].*

The waveform is a complicated function to compute, but at the lowest order of the post-Newtonian expansion (see subsection 1.1.2 and *e.g.* refs [8, 10, 59]), we can work with easy analytical equations. We need to suppose that the GW source is a BBH without any spins and with almost equal masses (hence, the multipolar emission mode with $m = l = 2$, the quadrupole, dominates). This scenario is quite good, especially at low masses (see fig. B.2) for the inspiral phase (so without taking into account the merge nor the ringdown, see fig. 1.1).

In this approximation and for one single detector, we have:

$$\rho^2 = \frac{5}{6} \frac{[G\mathcal{M}_\mathrm{c}]^{5/3}\ w^2(\alpha,\delta,\iota,\psi)}{c^3 \pi^{4/3}\ d_\mathrm{L}^2} I_{7/3}(\mathcal{M}_\mathrm{tot}), \tag{B.7}$$

with

$$w^2(\mathrm{RA},\mathrm{dec},\iota,\psi) = F_+^2(\mathrm{RA},\mathrm{dec},\psi)\left(\frac{1+\cos^2\iota}{2}\right) + F_\times^2(\mathrm{RA},\mathrm{dec},\psi)\cos^2\iota, \tag{B.8}$$

and

$$I_{7/3}(\mathcal{M}_\mathrm{tot}) = \int_{f_\mathrm{min}}^{f_\mathrm{insp}(z)} \frac{f^{-7/3}}{S_n(f)}\,\mathrm{d}f, \tag{B.9}$$

where f_insp is the frequency at the end of the inspiral phase of the BBHs orbits. In the case of a circular orbit, one has:

$$f_\mathrm{insp}(z) \approx 4.4\ \mathrm{kHz}\ \frac{\mathrm{M}_\odot}{\mathcal{M}_\mathrm{tot}(z)}, \tag{B.10}$$

with $\mathcal{M}_\mathrm{tot} = (1+z)M_\mathrm{tot} = (1+z)(m_1+m_2)$ being the redshifted total mass (*i.e.* the measured total mass in the *detector frame*) and with $\mathcal{M}_\mathrm{c} = (1+z)M_\mathrm{c} = (1+z)[(m_1 m_2)^{3/5}/M_\mathrm{tot}^{1/5}]$ being the redshifted chirp mass. RA is the right ascension (also denoted α), dec the declination (also denoted δ), ι the orbital orientation (the angle between the line of sight and the normal to the orbital plane of the source) and ψ the polarisation.

In eq. (B.7), we can note that the luminosity distance squared appears at the denominator of the SNR squared. Therefore $\rho \propto d_{\rm L}^{-1}$ (a result that we will need below) and $\rho \propto (S_n(f))^{-1}$. In the case of modified gravity, this distance is the GW luminosity distance: $d_{\rm L}^{\rm GW}$, see subsection 1.5.2. In eq. (B.8) we can also note that w takes its values in $[0,1]$.

At this post-Newtonian approximation, we have a clear distinction in the SNR between the extrinsic $(\mathrm{RA}, \mathrm{dec}, \iota, \psi)$ and the intrinsic $(m_1, m_2, d_{\rm L})$ parameters. We can then rewrite ρ such that:

$$\rho = w(\mathrm{RA}, \mathrm{dec}, \iota, \psi) \cdot \rho_{\rm opt}(m_1, m_2, d_{\rm L}), \tag{B.11}$$

where $\rho_{\rm opt}$ means *optimally oriented SNR*, since it corresponds to the maximal value that ρ can take (when the source is located just over the detector with its orbit's plane parallel to the detector plane [57], then: $w = 1$). To compute the SNR of a source with $m_1, m_2, d_{\rm L}$ and with a given orientation, we just have to use the optimal oriented SNR function $\rho_{\rm opt}$ evaluated at the parameters $m_1, m_2, d_{\rm L}$, and then multiply it by the function w of the source orientation with respect to the detector.

If we suppose that the intrinsic and extrinsic parameters are independent, we re-write $\alpha(\Lambda)$ with θ explicit [59]:

$$\begin{aligned}\alpha(\Lambda) = \int & p_{\rm det}(\mathrm{RA}, \mathrm{dec}, \iota, \psi, m_1, m_2, d_{\rm L})\ p_{\rm pop}(\mathrm{RA}, \mathrm{dec}, \iota, \psi, m_1, m_2, d_{\rm L}|\Lambda) \\ & \qquad \mathrm{d}(\mathrm{RA}, \mathrm{dec}, \iota, \psi, m_1, m_2, d_{\rm L}) \qquad \text{(B.12)} \\ = \int & p_{\rm pop}(m_1, m_2, d_{\rm L}|\vec{\lambda}_{\rm BBH}, R_0, \gamma) \\ & \times \left\{ \int p_{\rm pop}(\mathrm{RA}, \mathrm{dec}, \iota, \psi)\ p_{\rm det}(\mathrm{RA}, \mathrm{dec}, \iota, \psi, m_1, m_2, d_{\rm L})\ \mathrm{d}(\mathrm{RA}, \mathrm{dec}, \iota, \psi) \right\} \mathrm{d}(m_1, m_2, d_{\rm L})\,, \qquad \text{(B.13)}\end{aligned}$$

where we write $\mathrm{d}(x, y, z, \cdots)$ as a short notation for the infinitesimal hypervolume element of the coordinates $x, y, z, \cdots$. Let us look at the integral between the braces:

$$\begin{aligned}&\int p_{\rm pop}(\mathrm{RA}, \mathrm{dec}, \iota, \psi)\ p_{\rm det}(\mathrm{RA}, \mathrm{dec}, \iota, \psi, m_1, m_2, d_{\rm L})\ \mathrm{d}(\mathrm{RA}, \mathrm{dec}, \iota, \psi) && \text{(B.14)}\\ &\quad = \int p_{\rm pop}(\mathrm{RA}, \mathrm{dec}, \iota, \psi)\ \Theta\left(\rho(\mathrm{RA}, \mathrm{dec}, \iota, \psi, m_1, m_2, d_{\rm L}) - \rho_{\rm thr}\right)\ \mathrm{d}(\mathrm{RA}, \mathrm{dec}, \iota, \psi) && \text{(B.15)}\\ &\quad = \int p_{\rm pop}(\mathrm{RA}, \mathrm{dec}, \iota, \psi)\ \Theta\left(w\rho_{\rm opt} - \rho_{\rm thr}\right)\ \mathrm{d}(\mathrm{RA}, \mathrm{dec}, \iota, \psi) && \text{(B.16)}\\ &\quad = \int p_{\rm pop}(\mathrm{RA}, \mathrm{dec}, \iota, \psi)\ \Theta\left(w - \frac{\rho_{\rm thr}}{\rho_{\rm opt}}\right)\ \mathrm{d}(\mathrm{RA}, \mathrm{dec}, \iota, \psi)\,, && \text{(B.17)}\end{aligned}$$

where we call $\rho_{\rm thr}$ the threshold signal-to-noise ratio. In our case, and for one detector, we take $\rho_{\rm thr} = 8$.

To evaluate eq. (B.17), we choose the orientation *prior* to be isotropic: $p_{\rm pop}(\mathrm{RA}, \mathrm{dec}, \iota, \psi) =$ const., it is then possible to evaluate the integral by taking a sampling of $p_{\rm pop}(\mathrm{RA}, \mathrm{dec}, \iota, \psi)$ and to evaluate w on each sample. Those points w_i represent a pdf: $p(w)$. Equation (B.17) then becomes:

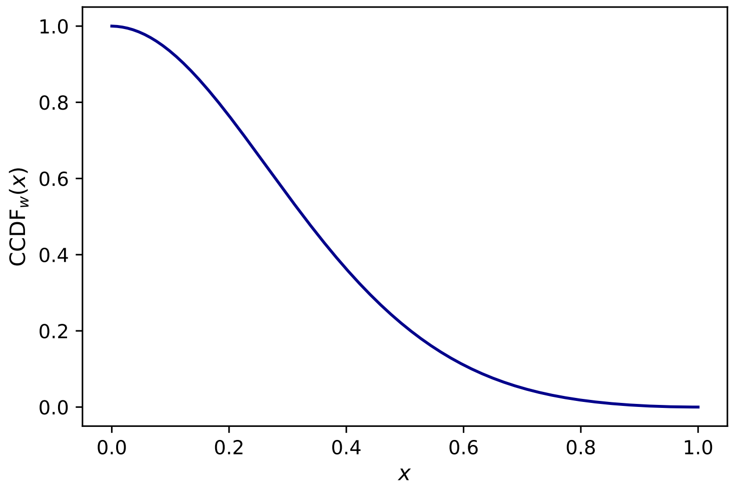

Figure B.3: *Plot of CCDF*$_w(x)$ *as a function of* x *as approximated in ref. [85]. We can see that CCDF*$_w(0.33) \approx 0.5$, *hence we need an optimal SNR of* $\approx 8/0.33 \approx 24$ *to detect half of the events.*

$$(\text{B.17}) = \int_{\rho_\text{thr}/\rho_\text{opt}}^{1} p(w)\ \mathrm{d}w = 1 - \text{CDF}_w\left(\frac{\rho_\text{thr}}{\rho_\text{opt}}\right), \tag{B.18}$$

with $\text{CDF}_w(x)$ the *cumulative distribution function* of w. The function α is then:

$$\alpha(\Lambda) = \int p_\text{pop}(m_1, m_2, d_\text{L}|\Lambda)\ \left[1 - \text{CDF}_w\left(\frac{\rho_\text{thr}}{\rho_\text{opt}}\right)\right]\ \mathrm{d}m_1\ \mathrm{d}m_2\ \mathrm{d}d_\text{L}. \tag{B.19}$$

One minus the cumulative distribution function is also called the *complementary cumulative distribution function*, denoted $\text{CCDF}_w(x)$ $(= 1 - \text{CDF}_w(x))$.

The sampling w_i and then the integral of the pdf $p(w)$ can be done numerically (by doing a MCMC), but ref. [85] has already evaluated this integral, by considering that RA, cos(dec), $\cos\iota$ and ψ are uniformly distributed (the uniform distribution on the *cosines* of the angles and not on the angles themselves seems strange (maybe because the observable is $\cos\iota$ and ι not directly?), but it does not change a lot the curve). By doing so, they obtain the following parametrisation of the cumulative distribution function (for one detector) (see eq. (A2) of ref. [85]):

$$\text{CCDF}_w(x) = a_2[(1-x)^2] + a_4[(1-x)^4] + a_8[(1-x)^8] + (1 - a_2 - a_4 - a_8)[(1-x)^{10}], \tag{B.20}$$

with $a_2 = 0.374222$, $a_4 = 2.04216$ and $a_8 = -2.63948$, $\forall x \in [0,1]$. This function is plotted in fig B.3.

Hence, the only thing we need to compute is the *optimally oriented* SNR, $\rho_\text{opt}(m_1, m_2, d_\text{L})$. To do so, we can use the post-Newtonian approximation (eq. (B.7)) or directly a numerical computation of $h_\theta(f)$ (in this work we use the numerical computation of ref. [84]). Since ρ varies as d_L^{-1}, we can evaluate only ρ_opt on a grid of masses m_1 and m_2 at a fixed distance, let us say d^*, and we compute:

$$\rho_\text{opt}(m_1, m_2, d_\text{L}) = \rho_\text{opt}(m_1, m_2, d^*)\ \cdot\ \frac{d^*}{d_\text{L}}. \tag{B.21}$$

Figure B.4 shows the *detectable* fraction of events at a redshift $z = 0.1$ for the detector advanced LIGO at designed sensitivity, using the Python package `pycbc.psd` [86].

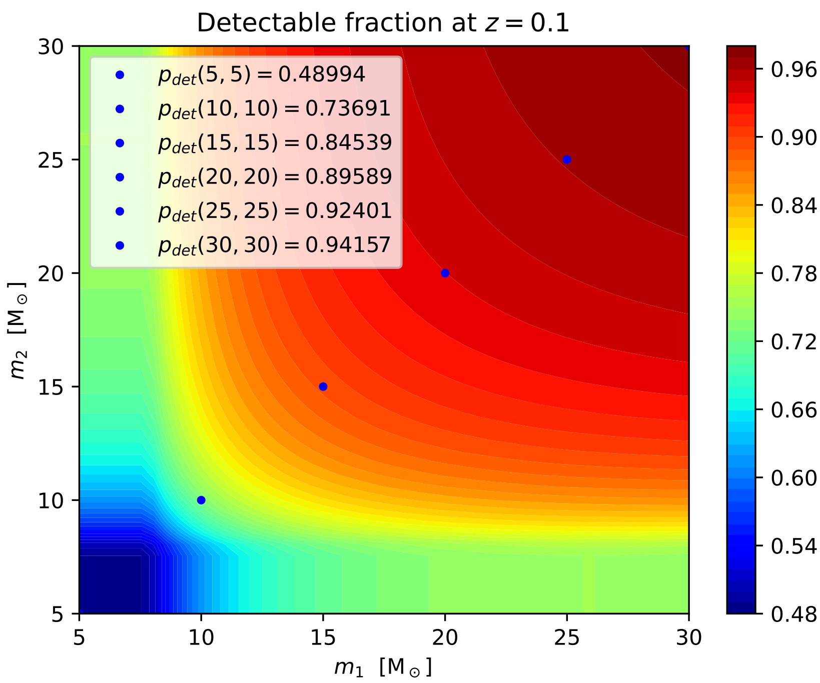

Figure B.4: *Plot of* detectable *events at a redshift* $z = 0.1$ *for advanced LIGO, using the analytical PSD* `pycbc.psd.analytical.aLIGODesignSensitivityP1200087` *[86].*

B.2 The function α

In the previous section, we saw the probability of detection of a GW generated by a source with parameters θ. But for the function $\alpha(\Lambda)$, we are interested in the detectability of the hyperparameter Λ. We then have to multiply the probability of detection, $p_{\rm det}(\theta)$ by the probability that a source with parameters θ exists (and then to integrate over the θ's). This probability of population depends on the hyperparameter Λ.

To obtain the probability of population of the extrinsic parameters $p_{\rm pop}(m_1, m_2, d_{\rm L}|\Lambda)$, we recall that in section 2.4.1, we saw how to obtain $p_{\rm pop}(m_1^z, m_2^z, d_{\rm L}|\Lambda)$. We can just use again Jacobians to transform $p_{\rm pop}$ from a dependence on m_i^z to a dependence on m_i.

Now it is possible to use a Monte Carlo integration to evaluate $\alpha(\Lambda)$, and eq. (B.19) becomes:

$$\alpha(\Lambda) = \frac{1}{n_s}\sum_{i=1}^{n_s} \mathrm{CCDF}_w\left(\frac{\rho_{\rm thr}}{\rho_{\rm opt}(m_1^i, m_2^i, d_{\rm L}^i)}\right) \Big|_{\, m_1^i, m_2^i, d_{\rm L}^i \,\sim\, p_{\rm pop}(m_1, m_2, d_{\rm L}|\Lambda)}. \tag{B.22}$$

Since the dependence in the parameter Λ is in the population pdf $p_{\rm pop}(m_1, m_2, d_{\rm L}|\Lambda)$, it is necessary to sample this function at each value of Λ that is tested by our Bayesian hierarchical inference.

References

[1] Mancarella, Michele; Genoud-Prachex, Edwin & Maggiore, Michele. *In writing.* 2021.

[2] Abbott, B.P. *et al.* (LIGO/Virgo collaborations). "Observation of Gravitational Waves from a Binary Black Hole Merger". *Physical Review Letters*, Volume 116, 11 February 2016. `arXiv:1602.03837v1 [gr-qc]`.

[3] Abbott, B.P. *et al.* (LIGO/Virgo collaborations). "GWTC-1: A Gravitational-Wave Transient Catalog of Compact Binary Mergers Observed by LIGO and Virgo during the First and Second Observing Runs". *Physical Review X*, Volume 9, 4 September 2019. `arXiv:1811.12907v3 [astro-ph.HE]`.

[4] Abbott, R. *et al.* (LIGO/Virgo collaborations). "GWTC-2: Compact Binary Coalescences Observed by LIGO and Virgo During the First Half of the Third Observing Run". *Physical Review X*, Volume 11, 9 June 2021. `arXiv:2010.14527v3 [gr-qc]`.

[5] Abbott, B.P. *et al.* (LIGO/Virgo collaborations). "A gravitational-wave standard siren measurement of the Hubble constant". *Nature*, Volume 551, 16 October 2017. `arXiv:1710.05835v1 [astro-ph.CO]`.

[6] Abbott, B.P. *et al.* (LIGO/Virgo collaborations, *Fermi* Gamma-ray Burst Monitor and INTEGRAL). "Gravitational Waves and Gamma-Rays from a Binary Neutron Star Merger: GW170817 and GRB 170817A". *The Astrophysical Journal Letters*, Volume 848, Number 2, 16 October 2017. `arXiv:1710.05834v2 [astro-ph.HE]`.

[7] Maggiore, Michele *et al.* "Science Case for the Einstein Telescope". *Journal of Cosmology and Astroparticle Physics*, Volume 2020, Volume 3, 24 March 2020. `arXiv:1912.02622v4 [astro-ph.CO]`.

[8] Maggiore, Michele. *Gravitational Waves, Volume I: Theory and Experiments.* Oxford University Press, Oxford, 2008. ISBN: 978-0-19-857074-5.

[9] Belgacem, Enis; Dirian, Yves; Foffa, Stefano & Maggiore, Michele. "Modified gravitational-wave propagation and standard sirens". *Physical Review D*, Volume 98, 13 July 2018. `arXiv:1805.08731v3 [gr-qc]`.

[10] Finke, Andreas; Foffa, Stefano; Iacovelli, Francesco; Maggiore, Michele & Mancarella, Michele. "Cosmology with LIGO/Virgo dark sirens: Hubble parameter and modified gravitational wave propagation". [Submitted on 29 Jan 2021] `arXiv:2101.12660v2 [astro-ph.CO]`.

[11] Farr, Will M.; Fishbach, Maya; Ye, Jiani & Holz, Daniel E. "A Future Percent-Level Measurement of the Hubble Expansion at Redshift 0.8 With Advanced LIGO". *The Astrophysical Journal Letters*, Volume 883, number 2, 1 October 2019. `arXiv:1908.09084v2 [astro-ph.CO]`.

[12] Ezquiaga, Jose María. "Hearing gravity from the cosmos: GWTC-2 probes general relativity at cosmological scales". 11 April 2021. `arXiv:2104.05139 [astro-ph.CO]`.

[13] Mandel, Ilya; Farr, Will M. & Gair, Jonathan R. "Extracting distribution parameters from multiple uncertain observations with selection biases". *Monthly Notices of the Royal Astronomical Society*, Volume 486, Issue 1, 28 March 2019. arXiv:1809.02063v2 [physics.data-an].

[14] Straumann, Norbert. *General Relativity, With Applications to Astrophysics*. Springer, Berlin, 2004. ISBN: 3-540-21924-2.

[15] Kunz, Martin. "General Relativity, version 2019". Lecture notes, Université de Genève, 2019. Available at: http://fiteoweb.unige.ch/~kunzm/lectures/gr_2019.pdf.

[16] Jetzer, Philippe. "Applications of General Relativity in Astrophysics and Cosmology". Lecture notes (written by Felix Hähl), Universität Zürich, 2017, last update 2019 by Tobias Baldauf and Raymond Angélil. Available at: https://cutt.ly/Kb8NVux.

[17] Jetzer, Philippe. "Advanced Topics in General Relativity and Gravitational Waves". Lecture notes (written by Simone S. Bavera), Universität Zürich, 2017. Available at: https://cutt.ly/rb8VrgH.

[18] Durrer, Ruth. "General Relativity". Lecture notes, Université de Genève, 2002, last update 2016. Available at: http://fiteoweb.unige.ch/~durrer/courses/relaE.pdf.

[19] Durrer, Ruth. "Advanced Topics in General Relativity". Lecture notes, Université de Genève, 2019. Available at: http://fiteoweb.unige.ch/~durrer/courses/GRadv_v2.pdf.

[20] Moore, Thomas A. *A General Relativity Workbook*. University Science Book, Mill Valley, CA, 2013. ISBN: 978-1-891389-82-5 (French translation by Richard Taillet, De Boeck Supérieur, Louvain-la-Neuve, 2014).

[21] Maggiore, Michele. *Gravitational Waves, Volume II: Astrophysics and Cosmology*. Oxford University Press, Oxford, 2018. ISBN: 978-0-19-857089-9.

[22] Damour, Thibault. "Thibault Damour – Gravitational Waves and Binary Systems". "Les cours de l'IHÉS", crash course in four lectures, given at the *Institut des Hautes Études Scientifiques* in 2016. Available at: http://y2u.be/qYong_D4VUI (1/4); http://y2u.be/xZL3MZ6Fx-U (2/4); http://y2u.be/TCa34HbuLvg (3/4) and http://y2u.be/6RgL3hrG1wU (4/4).

[23] Weisberg, Joel M. & Taylor, Joseph H. "Relativistic Binary Pulsar B1913+16: Thirty Years of Observations and Analysis". [Submitted on 7 July 2004] arXiv:astro-ph/0407149v1.

[24] Damour, Thibault. "Gravitational Waves and Binary Black Holes". *Séminaire Poincaré*, XXII: pages 1–51, 3 December 2016. Available at: http://www.bourbaphy.fr/damourgrav.pdf.

[25] "LIGO Lab | Caltech | MIT". LIGO official website. Available at: https://www.ligo.caltech.edu/.

[26] "Virgo Website". Virgo official website. Available at: https://www.virgo-gw.eu/.

[27] "KAGRA Large-scale Cryogenic Graviationai [*sic*] wave Telescope Project". KAGRA official website. Available at: https://gwcenter.icrr.u-tokyo.ac.jp/en/.

[28] "LIGO's interferometer | LIGO Lab | Caltech". LIGO official website. No date, no author. Available at: https://www.ligo.caltech.edu/page/ligos-ifo (accessed 10 July 2021).

[29] Moore, Christopher J.; Cole1and, Robert H. & Berry, Christopher P. L. "Gravitational-wave sensitivity curves". *Classical and Quantum Gravity*, Volume 32, Number 1, 8 December 2014. `arXiv:1408.0740v2 [gr-qc]`.

[30] Abbott, R. *et al.* (LIGO/Virgo/KAGRA collaborations). "Observation of Gravitational Waves from Two Neutron Star–Black Hole Coalescences". *The Astrophysical Journal Letters*, Volume 915, Number 1, 29 June 2021. `arXiv:2106.15163v1 [astro-ph.HE]`.

[31] Dodelson, Scott. *Modern Cosmology*. Academic Press, *An Imprint of Elsevier*, San Diego, 2003. ISBN: 978-0-12-219141-1.

[32] Baumann, Daniel. "Cosmology". Lecture notes, Universiteit van Amsterdam, no date. Available at: `https://bit.ly/3eVENov`.

[33] "NED results for object MESSIER 031". NASA/IPAC Extragalactic Database. Available at: `https://cutt.ly/7b6g2dm` (accessed 23 May 2021).

[34] Schutz, Bernard F. "Determining the Hubble constant from gravitational wave observations". *Nature*, Volume 323, 25 September 1986.

[35] Thrane, Eric & Talbot, Colm. "An introduction to Bayesian inference in gravitational-wave astronomy: parameter estimation, model selection, and hierarchical models". *Publications of the Astronomical Society of Australia*, Volume 36, 11 March 2019. `arXiv:1809.02293v8 [astro-ph.IM]`.

[36] Chen, Hsin-Yu; Fishbach, Maya & Holz, Daniel E. "A two per cent Hubble constant measurement from standard sirens within 5 years". *Nature*, Volume 562, 17 October 2018. `arXiv:1712.06531v2 [astro-ph.CO]`.

[37] Fishbach, Maya *et al.* "A standard siren measurement of the Hubble constant from GW170817 without the electromagnetic counterpart". *The Astrophysical Journal Letters*, Volume 871, Number 1, 22 January 2019. `arXiv:1807.05667v2 [astro-ph.CO]`.

[38] Soares-Santos, Marcelle *et al.* (DES collaboration and LIGO/Virgo collaborations). "First Measurement of the Hubble Constant from a Dark Standard Siren using the Dark Energy Survey Galaxies and the LIGO/Virgo Binary–Black-hole Merger GW170814". *The Astrophysical Journal Letters*, Volume 876, Number 1, 26 April 2019. `arXiv:1901.01540v2 [astro-ph.CO]`.

[39] Palmese, Antonella *et al.* "A statistical standard siren measurement of the Hubble constant from the LIGO/Virgo gravitational wave compact object merger GW190814 and Dark Energy Survey galaxies". *The Astrophysical Journal Letters*, Volume 900, Number 2, 7 September 2020. `arXiv:2006.14961v3 [astro-ph.CO]`.

[40] You, Zhi-Qiang; Zhu, Xing-Jiang; Ashton, Gregory; Thrane, Eric & Zhu, Zong-Hong. "Standard-siren Cosmology Using Gravitational Waves from Binary Black Holes". *The Astrophysical Journal*, Volume 908, number 215, 25 February 2021. `arXiv:2004.00036 [astro-ph.CO]`.

[41] Haster, Carl-Johan. "Pi from the sky – A null test of general relativity from a population of gravitational wave observations". [Submitted on 11 May 2020] `arXiv:2005.05472v1 [gr-qc]`.

[42] Ezquiaga, Jose María & Zumalacárregui, Miguel. "Dark Energy in Light of Multi-Messenger Gravitational-Wave Astronomy". *Frontiers in Astronomy and Space Sciences*, 21 December 2018. `arXiv:1807.09241v2 [astro-ph.CO]`.

[43] Belgacem, Enis; Dirian, Yves; Finke, Andreas; Foffa, Stefano & Maggiore, Michele. "Gravity in the infrared and effective nonlocal models". *Journal of Cosmology and Astroparticle Physics*, Volume 2020, Number 4, 8 April 2020. arXiv:2001.07619v1 [astro-ph.CO].

[44] Belgacem, Enis; Dirian, Yves; Foffa, Stefano & Maggiore, Michele. "Gravitational-wave luminosity distance in modified gravity theories". *Physical Review D*, Volume 97, 31 May 2018. arXiv:1712.08108v4 [astro-ph.CO].

[45] Belgacem, Enis *et al.* "Testing modified gravity at cosmological distances with LISA standard sirens". *Journal of Cosmology and Astroparticle Physics*, Volume 2019, July 2019. arXiv:1906.01593v2 [astro-ph.CO].

[46] Mancarella, Michele. *Consistency tests of the Universe and cosmic relics.* PhD thesis, Université Paris-Saclay, 27 June 2017. Available at: https://tel.archives-ouvertes.fr/tel-01613859.

[47] Belgacem, Enis; Dirian, Yves; Foffa, Stefano & Maggiore, Michele. "Nonlocal gravity. Conceptual aspects and cosmological predictions". Proceedings of the 53rd *Rencontres de Moriond*: Cosmology; 17–24 March 2018, La Thuile, Aosta Valley, Italy; edited by Étienne Augé, Jacques Dumarchez and Jean Trân Thanh Vân. Pages 203-206. Available at: http://moriond.in2p3.fr/Proceedings/2018/Moriond_Cosmology_2018.pdf.

[48] Tolley, Andrew J. "Theories of Modified Gravity". Proceedings of the 52nd *Rencontres de Moriond*: Gravitation; 25 March – 1 April 2017, La Thuile, Aosta Valley, Italy; edited by Étienne Augé, Jacques Dumarchez and Jean Trân Thanh Vân. Pages 209-216. Available at: http://moriond.in2p3.fr/Proceedings/2017/Moriond_Gravitation_2017.pdf.

[49] Sobral Blanco, Daniel & Lombriser, Lucas. "Exploring the self-tuning of the cosmological constant from Planck mass variation". [Submitted on 3 Dec 2020] arXiv:2012.01838v2 [gr-qc].

[50] Maggiore, Michele & Mancarella, Michele. "Nonlocal gravity and dark energy". *Physical Review D*, Volume 90, 7 July 2014. arXiv:1402.0448v2 [hep-th].

[51] Maggiore, Michele. "Phantom dark energy from nonlocal infrared modifications of general relativity". *Physical Review D*, Volume 89, 18 February 2014. arXiv:1307.3898v3 [hep-th].

[52] Dirian, Yves; Foffa, Stefano; Kunz, Martin; Maggiore, Michele & Pettorino, Valeria. "Nonlocal gravity and comparison with observational datasets. II. Updated results and Bayesian model comparison with ΛCDM". *Journal of Cosmology and Astroparticle Physics*, Volume 2016, Number 5, 31 May 2016. arXiv:1602.03558v2 [astro-ph.CO].

[53] Adam, R. *et al.* (Planck collaboration). "*Planck* 2015 results I. Overview of products and scientific results". *Astronomy & Astrophysics*, Volume 594, 20 September 2016.

[54] Abbott, R. *et al.* (LIGO/Virgo collaborations). "Population Properties of Compact Objects from the Second LIGO–Virgo Gravitational-Wave Transient Catalog". *The Astrophysical Journal Letters*, Volume 913, Number 1, 19 May 2021. arXiv:2010.14533v2 [astro-ph.HE].

[55] Mastrogiovanni, Simone *et al.* "Cosmology in the dark: On the importance of source population models for gravitational-wave cosmology". 30 March 2021. arXiv:2103.14663v2 [gr-qc].

[56] "Masses in the Stellar Graveyard – LIGO". Available at: https://media.ligo.northwestern.edu/gallery/mass-plot (accessed 11 July 2021).

[57] De Luca, Valerio; Franciolini, Gabriele; Pani, Paolo & Riotto, Antonio. "Bayesian evidence for both astrophysical and primordial black holes: mapping the GWTC-2 catalog to third-generation detectors". *Journal of Cosmology and Astroparticle Physics*, Volume 2021, Number 5, 3 May 2021. `arXiv:2102.03809v2 [astro-ph.CO]`.

[58] Abbott, B.P. *et al.* (LIGO/Virgo collaborations). "Binary Black Hole Population Properties Inferred from the First and Second Observing Runs of Advanced LIGO and Advanced Virgo". *The Astrophysical Journal Letters*, Volume 882, Number 2, 9 September 2019. `arXiv:1811.12940v4 [astro-ph.HE]`.

[59] Vitale, Salvatore; Gerosa, Davide; Farr, Will M. & Taylor, Stephen R. "Inferring the properties of a population of compact binaries in presence of selection effects". [Submitted on 10 July 2020] `arXiv:2007.05579v3 [astro-ph.IM]`. Chapter of *Handbook of Gravitational Wave Astronomy* (Eds. C. Bambi, S. Katsanevas and K. Kokkotas; Springer, Singapore, 2021). 1st version under the name "One, No One, and One Hundred Thousand – Inferring the properties of a population in presence of selection effects", by S. Vitale.

[60] `(fr)` Appel, Walter. *Mathématiques pour la physique* et les physiciens. H&K, Paris, 2002 (5th edition: 2017). (American edition: *Mathematics for Physics and Physicists*, Princeton University Press, Princeton, 2007.) ISBN: 978-2-35141-039-4.

[61] Hájek, Alan. "Interpretations of Probability". *Stanford Encyclopedia of Philosophy*. 21 October 2002, last revision on 28 August 2019. Available at: `https://plato.stanford.edu/entries/probability-interpret/` (accessed 11 July 2021).

[62] Farr, Will M. "Accuracy Requirements for Empirically Measured Selection Functions". *Research Notes of the American Astronomical Society*, Volume 3, Number 5, May 2019. `arXiv:1904.10879v1 [astro-ph.IM]`.

[63] Mastrogiovanni, S.; Haegel, L.; Karathanasis, C.; Magaña Hernandez, I.; & Steer, D. A. "Gravitational wave friction in light of GW170817 and GW190521". *Journal of Cosmology and Astroparticle Physics*, Volume 2021, Number 2, 23 February 2021. `arXiv:2010.04047v2 [gr-qc]`.

[64] "emcee — emcee 3.0.2 documentation". Online documentation of the Python package `emcee`. Available at: `https://emcee.readthedocs.io/en/stable/#`.

[65] Fuhrmann, Christoph; Harney, Hanns Ludwig; Harney, Klaus & Müller, Andreas. "On the Gaussian Approximation to Bayesian Posterior Distributions". [Submitted on 1 Dec 2020] `arXiv:2012.00748v1 [math.ST]`.

[66] Foreman-Mackey, Daniel; Hogg, David W.; Lang, Dustin & Goodman, Jonathan. "emcee: The MCMC Hammer". *Publications of the Astronomical Society of the Pacific*, Volume 125, Number 925, 25 February 2013. `arXiv:1202.3665v4 [astro-ph.IM]`.

[67] Foreman-Mackey, Daniel. "corner.py: Scatterplot matrices in Python". *The Journal of Open Source Software*, Volume 1, number 2, 8 June 2016. Available at: `https://joss.theoj.org/papers/10.21105/joss.00024`.

[68] "Gravitational Wave Open Science Center". GWTC-2 Data Release Documentation. First release: October 28, 2020. Added notes about 2nd PE release: March 9, 2021. Available at: `https://www.gw-openscience.org/GWTC-2/` (accessed 11 July 2021).

[69] Aghanim, N. *et al.* (Planck collaboration). "*Planck* 2018 results. VI. Cosmological parameters". *Astronomy & Astrophysics*, Volume 641, 11 September 2020. `arXiv:1807.06209v3 [astro-ph.CO]`.

[70] Mortsell, Edvard; Goobar, Ariel; Johansson, Joel & Dhawan, Suhail. "The Hubble Tension Revisited: Additional Local Distance Ladder Uncertainties". [Submitted on 17 Jun 2021] arXiv:2106.09400v1 [astro-ph.CO].

[71] Farr, Will. "PISNLineCosmography". GitHub: https://github.com/farr/PISNLineCosmography.

[72] "High Performance Computing - eResearch - UNIGE". Baobab & Yggdrasil official website. Available at: https://www.unige.ch/eresearch/en/services/hpc/.

[73] "Observing Capabilities – LIGO/Virgo Public Alerts User Guide 16 documentation". Update: 2020. Available at: https://emfollow.docs.ligo.org/userguide/capabilities.html (accessed 6 July 2021).

[74] Nitz, Alexander H. & Capano, Collin D. "GW190521 May Be an Intermediate-mass Ratio Inspiral". *The Astrophysical Journal Letters*, Volume 907, Number 1, 15 January 2021. arXiv:2010.12558v3 [astro-ph.HE].

[75] Shibata, Masaru; Kiuchi, Kenta; Fujibayashi, Sho & Sekiguchi, Yuichiro. "Alternative possibility of GW190521: Gravitational waves from high-mass black hole-disk systems". *Physical Review D*, Volume 103, 25 March 2021. arXiv:2101.05440v2 [astro-ph.HE].

[76] Rosati, Piero *et al.* "Synergies of THESEUS with the large facilities of the 2030s and guest observer opportunities". [Submitted on 19 Apr 2021] arXiv:2104.09535v2 [astro-ph.IM].

[77] Giamarchi, Thierry; Iucci, Anibal & Berthod, Christophe. "Introduction to Many Body physics". Lecture notes, Université de Genève, 2008–2013. Available at: https://dqmp.unige.ch/giamarchi/local/people/thierry.giamarchi/pdf/many-body.pdf.

[78] Diaconis, Persi. "The Markov chain Monte Carlo revolution". *Bulletin of the American Mathematical Society*, Volume 46, Number 2, April 2009, Pages 179–205. Available at: https://www.ams.org/journals/bull/2009-46-02/S0273-0979-08-01238-X/.

[79] Krauth, Werner. Statistical Mechanics*: Algorithms and Computations*. Oxford Master Series in Statistical, Computational, and Theoretical Physics. Oxford University Press, Oxford, 2006. ISBN: 978-0-19-851535-7.

[80] (fr) Velenik, Yvan. "Probabilités et Statistique". Lecture notes, Université de Genève, 12 December 2018. Available at: https://www.unige.ch/math/folks/velenik/cours.html.

[81] Trotta, Roberto. "Bayesian Methods in Cosmology". (Lecture notes for the 44th Saas Fee Advanced Course on Astronomy and Astrophysics.) [Submitted on 5 Jan 2017] arXiv:1701.01467 [astro-ph.CO].

[82] Sinharay, Sandip. "Assessing Convergence of the Markov Chain Monte Carlo Algorithms: A Review". *Educational Testing Service, Princeton, NJ*, March 2003. (Research Reports.) Available at: https://www.ets.org/Media/Research/pdf/RR-03-07-Sinharay.pdf.

[83] "LIGO Document P2000251-v1". Online LVC public documentation. Available at: https://dcc.ligo.org/LIGO-P2000251/public.

[84] Gerosa, Davide. "gwdet: Detectability of gravitational-wave signals from compact binary coalescences". Python script `gwdet.py`, available on the author's GitHub: https://github.com/dgerosa/gwdet.

[85] Dominik, Michal *et al.* "Double Compact Objects III: Gravitational-Wave Detection Rates". *The Astrophysical Journal*, Volume 806, Number 2, 23 June 2015. arXiv:1405.7016v2 [astro-ph.HE].

[86] "pycbc.psd package". Online documentation of the Python package `PyCBC`. Available at: https://pycbc.org/pycbc/latest/html/index.html.